Neural correlates of action effects anticipation– towards ecological more relevant paradigms

Dissertation

for the award of the degree

"Doctor rerum naturalium" (Dr.rer.nat.)

of the Georg-August-Universität Göttingen

within the doctoral program Systems Neuroscience

of the Georg-August University School of Science (GAUSS)

submitted by

Zurna Ahmed

from Karachi, Pakistan

Göttingen, 2022

Thesis Committee

Prof. Dr. Alexander Gail (Supervisor)
Sensorimotor Group, Cognitive Neuroscience Laboratory, German Primate Center – Leibniz Institute for Primate Research, Göttingen

Prof. Dr. Stefan Treue
Cognitive Neuroscience Laboratory, German Primate Center – Leibniz Institute for Primate Research, Göttingen

Prof. Dr. Annekathrin Schacht
Affective Neuroscience and Psychophysiology, Georg-Elias-Müller Institute of Psychology, Göttingen

Members of the Examination Board

Reviewer: Prof. Dr. Alexander Gail
Sensorimotor Group, Cognitive Neuroscience Laboratory, German Primate Center – Leibniz Institute for Primate Research, Göttingen

Second Reviewer: Prof. Dr. Stefan Treue
Cognitive Neuroscience Laboratory, German Primate Center – Leibniz Institute for Primate Research, Göttingen

Further members of the Examination Board

Prof. Dr. Annekathrin Schacht
Affective Neuroscience and Psychophysiology, Georg-Elias-Müller Institute of Psychology, Göttingen

Prof. Dr. Alexander Ecker
Neural Data Science Group, Institute of Computer Science, Göttingen

Prof. Dr. Julia Fischer
Cognitive Ethology Laboratory, German Primate Center – Leibniz Institute for Primate Research, Göttingen

Dr. Caspar Schwiedrzik
Perception and Plasticity Junior Research Group, Cognitive Neuroscience Laboratory, Göttingen

Date of the oral examination: 7th December 2022

Acknowledgements

It is my humble opinion that intention of written words is rather controlled by the recipient than by those attempting to express themselves. Paradoxically, it is within the same nature, in which the beauty of literature, music and lyrics lies; as those who want to see positivity and lightness, have endless tools at hand.

As this thesis would have never been what it turned out to be without the beautiful souls I was fortunate enough to work with, interact with and create never-to-be-forgotten memories,

I want to use

my voice,

my face,

my gestures

and body language

to express the immense gratitude, I carry within me. Any foolish attempts without these additional tools are destined to fail.

Those of you who had an impact on me and this work, you already know.

As of now, I leave you with this:

Appreciation is a wonderful thing: It makes what is excellent in others belong to us as well.

- *Voltaire.*

Table of Content

Part I

General Introduction

Chapter 1

General Introduction

We primates, human and non-human, are remarkable masters of our environment. As we come to the world we learn to adapt to and produce changes very quickly and intuitively. This ability is acquired so fast and spontaneously, that we hardly bother to question it. Behind the seemingly simplest interaction with our surrounding complex brain computations are in process. Even when we are performing an action as simple as reaching towards an object, for instance, our brain needs to represent the hand and its target in relation to one another. To do so, it needs to integrate multiple representations from different modalities such as the visual and proprioceptive information (Cohen & Andersen, 2002; Colby, 1998; Crawford et al., 2011; Rizzolatti & Luppino, 2001). Lastly, this integrated internal model needs to be continuously updated in real time and within hundreds of milliseconds. We realize what an incredible machine our brain is only when, in face of lesion or pathology, performing the simplest action becomes almost impossible.

Needless to say, real-live interactions are not limited to simple, single hand reaches but come with a much bigger repertoire including full-body behaviors (Berger et al., 2020, Voloh et al., 2020; 2022). Take for example interacting with a tree branch, an action that can be easily observed both from children and monkeys in the wild. Whether a branch is stiff or flexible can make a big difference, since it will define the subset of potential successful interactions that we can have with it. In other words, if we want to pick a fruit or climb a tree, we have to be able to predict whether pulling on a branch will make it give in, or if it will resist our pressure and weight.

It becomes clear, at this point, that a successful interaction with one's environment requires not only to represent the hand and its target, but also an additional piece of information: we should know the effect (will the branch hold or give in, if I pull it) of our action (pulling a branch) before we even perform the said action. A leading theory in the field of system neuroscience states that we are constantly representing the intended effects of our actions and comparing them to the actual effects thereby creating an internal model (Francis and Wonham, 1976, Kawato and Wolpert,1998; Shadmehr and Krakauer, 2008; Stavisky et al., 2017). This type of representation does not only come in handy when cherry-picking, but it is crucial for survival. When being chased by a predator, for example, a monkey able to anticipate which branches of a tree will hold his weight will have more chances to escape unharmed.

This thesis is motivated by investigating the neural correlates of action effect anticipation during action planning while working towards ecologically more relevant paradigms.

In the following introduction I will first provide an overview of the existing literature, introducing the controversial debate of action effect anticipation and its potential role during action planning. The evidence collected so far focuses mainly on human behavioral data. Therefore, I will next provide a short overview of the frontoparietal reach network of rhesus macaques and explain why it can be considered as the best candidate to investigate the neural correlates of action effect anticipation during action planning. As we want to move towards the understanding of ecologically more relevant behaviors, which imply unrestrained full-body behaviors, I will provide a short overview of the current state-of-the art of experimental setups in systems neuroscience for free behaviors in rhesus macaques. At last I will describe in more detail the aim of my thesis and give a brief overview of the chapters.

Ideomotor theory versus internal simulation of selected motor program

In daily life we perform actions to produce meaningful changes in our environment. How action effects are represented during action execution has been studied in depth. Concepts of predictive coding (O'Neil and Schultz, 2018, Kok and Lange, 2015) and of prediction error (Matsumoto et al., 2007; Abe and Lee, 2011; Zarr and Brown, 2016), which describes a mismatch between the expected action effect and actual action effect have been established. By now we have a better grasp on how these mechanisms can be exploited for motor adaptation (Wise et al., 1998; Mandelblat-Cerf, 2009; Stavisky et al., 2017), which are then leveraged for BMI appliances (Velliste et al., 2008; Chase et al., 2012; Golub et al., 2015). This understanding of action effects after and during movement execution have been put into the theoretical framework of the so-called internal model (Francis and Wonham, 1976, Kawato and Wolpert,1998). In short, the internal model hypothesizes that we are constantly comparing the desired action effects with the actual action effect to control our actions.

While we assume we have a basic understanding of action effects during and after movement execution, the role of action effect anticipation during action planning remains an open question. Since decades scientists have been debating various theories and the potential role of action effect anticipation during action planning. In this process two lines of ideas emerged.

The German root first established by Johann Friedrich Herbart (1816) hypothesized that our minds have no idea about our body and therefore sensations must be connecting both. He formulated the idea that therefore actions are already initiated through the idea of intentional behavior. These bidirectional connections can be learned during learning phases in which actions are associated with their effects. He further theorized that the driving force for this mechanism is the "self-preservation of soul" meaning, the soul is only in balance

when expected action effects match the actual action effects. He also developed the concept of joint “sensorimotor organ” implying that sensory and motor substrates are not separated. Lotze agreed with the proposed thesis and formulated his own view (1852). He conceptualized that we can create an action but we cannot accomplish that action by ourselves. There is a necessity of linking our will with the mechanics required to change our body. We have a control over this link only by the means of connecting the movement to the aim of our consciousness by creating a psychic state. The soul would not be able to move the body, if there would not be the psychic state, in which two independent motifs to move the body coincide and spontaneously teach effect and movement to the soul (Lotze, 1852). Later on, Harless (1861) considered the ideomotor principle as the fundamental mechanisms of intentional behaviors. The ideomotor theory constitutes that the bare anticipation of action effects is sufficient to activate the relevant motor program. Harless claimed that before a movement can be initiated on a voluntary basis, we must have experienced the sensory consequences. Therefore, the primary prerequisite of a voluntary movement is the intense sensation of the action effect even though it is not entirely effecting the movement itself (Harless, 1861).

At around the same time the English root was establishing its own concepts. The English route was mainly focused on involuntary movements at first, which are elicited by specific perceptions like cerebral reflex (e.g. in hydrophobic patients, Laycock, 1845). In the context of parapsychological phenomena (e.g. table turning, pendulum.), Carpenter linked the ideo-motor terminology to physiology (1852) and claimed that ideomotor movements can only exist when the will is not in control due to occult manipulation.

Later on, in 1890, both roots were combined by William James. He stated that a distinction between sensory and motor cells has no fundamental significance as all cells are motor. He also stipulated the ideomotor theory and provided the definition that the bare anticipation of action effects is sufficient to activate the underlying motor program. He concluded consciousness has no role prior to action but is rather a gatekeeper and blocks unwanted immediate responses. It was later proposed (Greenwald, 1970; Shin et al., 2010) to introduce the terminology ‘ideomotor mechanism’, which implies that when stimulus-response-effect chain is repeatedly experienced, it creates a “conditioned anticipatory image of response feedback”. So in other words ‘motor command is exhaustively coded with the intrinsic feedback that it aims to produce’ (Shin et al., 2010).

Already in 1913 a strongly contradicting view emerged criticizing the ideomotor theory. Thorndike (1913) openly criticized the concept of the ideomotor theory based on the claim that the majority of cases, which have been shown as a potential evidence for the ideomotor theory, can be also seen as purely habit creation and that these cases often required the subjects to perform the action in order to get the action-effect association established in the first place therefore making the action effect anticipation not essential for movement.

Also in modern psychology these opposing views remain. The ideomotor theory has been backed up by several behavioral studies in humans, in which learned association between keypresses and a subsequent visual or auditory stimulus was presented as an action effect resulting in either congruent or incongruent action effects (Paelecke and Kunde, 2007; Janczyk and M., Kunde, 2010). Additionally, effort was made to extract the temporal involvement of anticipated action effects by using a Psychological Refractory Period (PRP) paradigm. PRP underlies the assumption one action only be selected at a given time and only processes before and after action selection can run in parallel. In other words action selection creates a bottleneck in information processing (Pashler, 1984). This temporal bottleneck can be titrated by using a two-choice task, in which the stimulus onset asynchrony (SOA) for the second choice task is varied in time resulting in slower or faster reaction times. If action effect anticipation is part of the action selection stage, this bottleneck should be measurable by slower reaction times during short SOAs (Paelecke and Kunde, 2007).

However, also opposing views of Thorndike have been backed up by behavioral studies in humans. They claim that action effect anticipation can only be made use of after the motor program has been selected not before action execution (Pfister et al., 2010; Ziessler et al., 2011). In these studies, a flanker paradigm was used. Subjects had to learn the relationship between a letter presented in the center of the screen (stimulus) and the required keypress associated with it (response). At the same time a letter was shown on the left and right side next to the central letter (response effect). This way the participant learned to expect certain flanked letters given a specific stimulus (compatible response and response effect association). During the testing phase the stimulus letter was presented together with either compatible (expected) or incompatible (unexpected) flanked letters. Reaction times were measured with the underlying hypothesis that compatible flankers would confirm the selected response and therefore improve reaction times and incompatible flankers would interrupt the selected response resulting in slower reaction times. Additionally, they varied the timing of flanked letters similar to the PRP paradigm by presenting the flankers either before or with the stimulus hypothesizing that if action effects play a role prior to motor program selection, this should activate the motor program already in advance and result in shorter reaction times than when shown with the stimulus letter simultaneously.

Detailed discussion on one crucial point remains short. Not all action effect types are identical. In line with existing literature (Ziessler et al., 2012; Liu et al., 2019) we hypothesize there are at least two categories of action effects: exogenous and endogenous (Fig. 1). The criticism raised by Thorndike is valid for exogenous types of action effects. These action effects are arbitrary learned associations between stimulus, response and effects. They are categorized as exogenous as they are introduced from the outside and not necessarily intrinsically motivated. In other words, if an action is performed after a stimulus presentation, the task can be performed correctly without any involvement of the action effects. The response is solely dependent on the stimulus and the action effect can only confirm or contradict the expected action effects. This is true for both types of commonly

used paradigms to address action effect anticipation during action planning (PRP and flanker paradigm) as the effects have no influence on the correct or incorrect response. On the other hand, it has been hypothesized that endogenously generated action effects might play a different role during action planning (Ziessler et al., 2012; Liu et al., 2019). These types of action effects are immediately linked to the response and therefore time-continuous. The action effect here plays a crucial role in determining whether or not one`s response is correct or incorrect (matching the desired goal or not). Therefore, they might be intrinsically motivated. A paradigm along this line has been introduced by a computer based avatar task (Wirth et al., 2015). In this two-choice task, participants had to first respond to an auditory stimulus by pressing one of the two keys with their left hand. In the second task participants controlled an avatar via a computer mouse. The aim was to bring the avatar to the correct portal (left or right). Different stimuli for the action effect indicated in each trial whether the portals would bring the avatar to the actual location or to the opposite direction, requiring the participant to move the avatar to the opposite portal. The timing of presenting the action effect of the second task was varied. Based on the participants reaction times and the continuous trajectory analysis the authors conclude that action effect anticipation is involved in response selection during planning providing additional evidence in line with the ideomotor theory. However, the exact role whether action effects are involved before or only after response selection remains open. Any evidence on single neuron level remains missing. For this we suggest recording in the frontoparietal reach network of rhesus macaques (*m. mulatta*) using a novel paradigm, which creates endogenous action effects.

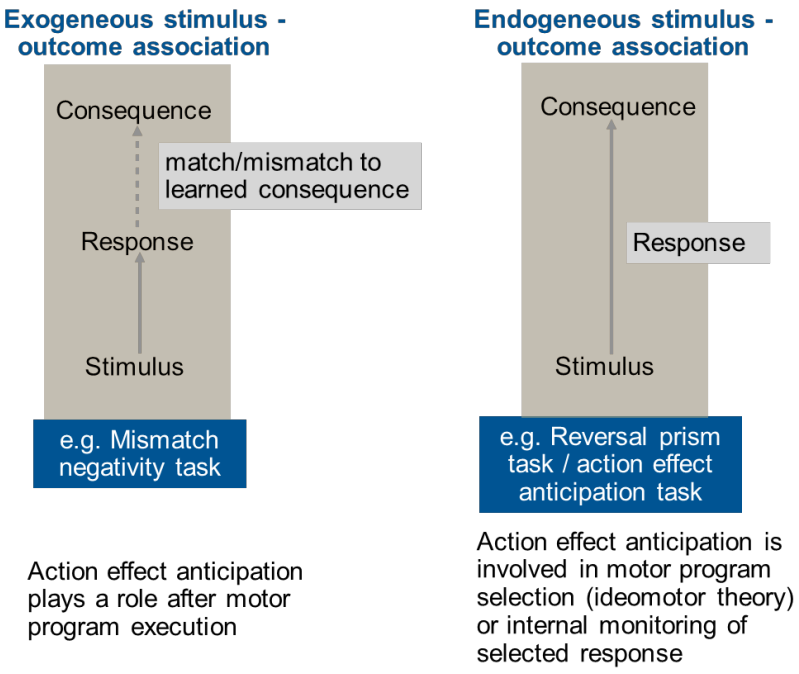

Figure 1: Schematics based on existing ideas in literature of the two action effect (action consequence) categories. Left panel – exogenous stimulus outcome association: Information about a stimulus is sufficient to perform a correct response, e.g. in a mismatch negativity task. Only after the response selection a compatible or incompatible action consequence is presented,

which can either confirm or violate the anticipated action effect. However, it does not have any influence on the correctness of response selection. Right panel – endogenous stimulus-outcome association: Information about a stimulus provides only part of the knowledge needed to select the correct response. The actual action consequence is crucial to select the correct response.

The frontoparietal reach network

Rhesus macaques are widely used to address systems neuroscience questions on a single neuron level. While we are still in the process of understanding the precise functional roles of various brain areas, many studies have been conducted to provide evidence to allow some basic assumptions. One of which is the brain areas primary motor cortex (M1), dorsal premotor cortex (PMd) and the parietal reach region (PRR) form the so-called frontoparietal reach network (Fig.2), which is involved in computing visually guided voluntary goal-directed movements (Andersen & Cui, 2009; Graziano & Cooke, 2006; Rizzolatti & Luppino, 2001; Colby & Goldberg, 1999; Kurata, 1991; Snyder et al., 1997;Colby & Duhamel, 1991; Fellemann & Van Essen, 1991; Andersen et al., 1990).

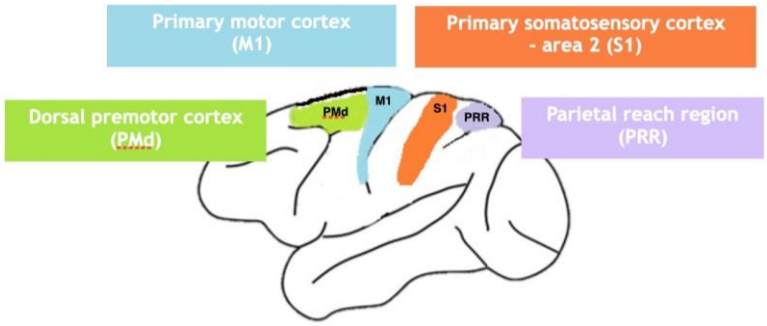

Figure 2: Location of brain areas primary motor cortex (M1), dorsal premotor cortex (PMd) and parietal reach region (PRR), which together form the frontoparietal reach network. Additionally, the primary somatosensory cortex (S1) is marked.

The primary motor cortex (M1) is considered to be involved in motor execution rather than in higher level motor planning (Crammond &Kalaska, 2000; Georgopoulos et al., 1982; Kalaska & Crammond, 1992). M1 encodes intrinsic parameters of motor movements like velocity, which can be successfully decoded for BMI (Velliste et al., 2008; Collinger et al., 2013; Wodlinger et al.,2014; Rajangam et al., 2016).

The dorsal premotor cortex (PMd) has bidirectional connections with the parietal reach network (Johnson 1996, Kurata 1991, Marconi 2001, Pandya & Kuypers 1969, Wise et al 1997). It is additionally known to be involved in action planning for reach movements (Crammond und Kalska, 1994, 2000, Wise und Mauritz 1985, Gail and Andersen, 2006). Ohbayahsi and colleagues (2016) demonstrated by using inactivation methods that PMd might reflect memory guided movement plans.

The parietal reach region consists of 4 subregions, the medial intraparietal area (MIP), dorsal part of the parieto-occipital area (PO), medial dorsal parietal area (MDP) and V6a (Snyder et al 2000). While investigating reach related neural encoding, studies focus on MIP (Andersen and Cui, 2009). They showed that neurons in area PRR are selective for arm movements (Andersen and Buneo, 2002; Snyder et al., 2000). Desjmurget and colleagues (2009) showed that when applying electrical stimulation in humans, it triggers the desire to move instead of the movement. Existing studies conclude that PRR is involved in planning of reach movement despite its physical location being close to visual areas.

Neurons of the frontoparietal reach network are spatially tuned to arm movement direction (Georgopoulos, 1982;1986; Kalaska et al., 1983). In other words, neurons have a preferred movement direction. When the arm movement (physical movement) is performed towards the preferred direction, these neurons increase their firing rate. When the physical movement is performed in the opposite direction, neurons do not increase their firing rate significantly.

The somatosensory cortex (S1) area 2 is known for its proprioceptive representation during reach-related activity (Jennings et al., 1983; Kaas et al., 1979; London and Miller, 2013). Recently it has been identified that the neural activity of S1 not only correlates with hand translation (Weber et al., 2011; London et al., 2011; London and Miller, 2013) but also with the whole arm reach (Chowdhury et al., 2020). Additionally neurons in S1 represent the arm state differently during passive and active movements (Chowdhury et al., 2020).

While the literature on neural evidence for time-continuous (endogenous) action effect anticipation is sparse, there are few existing studies there proposing the involvement of the frontoparietal reach network.

An EEG study using visual action effects comparing event related potentials (ERPs) found evidence that M1 might be the driving source for action effect prediction (Hughes and Waszak, 2011). Pilacinski and colleagues (2018) performed a study using fMRI. They conclude that PMd initially represents the action plan on the basis of the desired sensory outcome and only later shifts to the motor program. At last, in single neuron rhesus macaque study by Kuang and Gail (2016), in which the monkey performed a center out pro-anti reach task with and without reversal prism glasses, concludes anticipated visual sensory consequences of the intended movement are encoded in PRR.

Current state-of-the-art of experimental setups for freely moving rhesus macaques

Most of the established concepts presented up to now are studies, which were conducted in conventional chair -seated setup often with head or even eye fixation. All of the existing, behavioral studies in humans in the context of action effect anticipation were performed in a chair seated setup involving single arm reaches or keypresses. From real life scenarios we

know that most of our interactions are not limited to one arm reach nor to sitting but go beyond these behaviors. How the existing behavioral findings generalize towards more complex interactions remains unknown. The neural underpinning of action effect anticipation in a more dynamic environment is missing entirely up to date. There is already some evidence that conventional studies using structured trials might come with the risk of over interpretation. Aflalo and Graziano, 2007, recorded a free arm movement in 3D space while the animal was chair seated. Direction was determined by connecting the start and endpoint of a single reach and calculating the azimuth and elevation angles. They tested the explained variance based on directional tuning with the result of 8 percent. When the identical model was applied on a subset of arm movement, which are typical for classical center-out reach tasks (Zhang and Barash, 2000; Gail and Andersen, 2006), the explained variance increased to 42%.

In the past years with the recent technological advances, new approaches are introducing neural recordings in an experimentally controlled setup for free rhesus behaviors. Existing setups with wireless neural recordings in freely moving macaques have provided first neural evidence of walking on a treadmill (Foster et al., 2014), reward-based decision making processes (Shahidi et al., 2021) ,single unit selectivity for different reach and walk-and-reach movements in the frontoparietal reach network (Berger et al., 2020) and neural correlates of social behaviors (Testard, Trembaly et al., 2023) These setups with neural recordings are limited in size and suited for short range full body movements.

To push the limitations further, novel approaches are building large scale setups to allow the monkeys to elicit more complex behaviors, which go beyond sitting and walking. The main focus of these studies to date has been precise markerless video based motion tracking (Bala et al., 2020) and to characterize the behaviors (Voloh et al., 2021; 2022). Remarkably few studies have attempted to leverage these goal directed full body behaviors towards combining them with neural recordings mainly in the context of navigation (: Voloh et al., 2023; Manea et al., 2023; Maisson et al., 2022; Mao et al., 2021). How to leverage the opportunity to make the animals elicit a variety of full body behavior, which are experimentally induced and to use this continuous data to demonstrate the suitability for systems neuroscience remains a challenge up to date.

Aim of the thesis

Despite the long-standing debate about the role of action effect anticipation during planning, there is no evidence on single neuron resolution in the frontoparietal reach network up to date. The role of action effect anticipation when going beyond chair seated single hand reaches has not been studied so far.

This thesis is motivated by two research questions. First, what are the neural correlates of action effect anticipation during planning in a static, highly controlled environment and second, how do these correlates change in a dynamic, ecologically more relevant environment? To address these questions this thesis contains five original manuscripts. The contributions for each individual chapter are noted below.

Chapter 2 describes a novel, step-by-step tutorial to custom-design and custom-fit cranial implants to individual skull and brain of rhesus macaques based on MRI and CT scans. This tutorial, complemented with a GitHub repository and video tutorials, is suited for novice users, who have no prior CAD experience therefore enabling scientists to design their own implants to their specific needs. This chapter is published in *eNeuro.*

Chapter 3 is a manuscript providing the first single neuron evidence in the frontoparietal reach network for action effect anticipation during action planning using a novel action effect anticipation (AEA) paradigm. The results describe a 2-fold role of action effect anticipation. They are involved in motor program selection, which is in line with the ideomotor theory, but also during the internal simulation of the selected motor program before execution. Based on our findings and in line with existing literature we propose a possible extension of the theoretical internal model towards the planning stage.

Chapter 4 describes the interactive device B-PRIME, which we designed and programmed for Suppl. Chapter 1 and Chapter 5. This was necessary as existing haptic devices are rather simple and therefore not suited for a direct translation of the AEA paradigm.

Chapter 5 presents a novel, highly modular large-scale experimental environment for ecologically more relevant behaviors in rhesus macaques called the Exploration Room (ExR) to expand the repertoire of action and the action effects associated with them towards the goal of increasing ecological validity. In this manuscript, we demonstrate that the ExR is suited for systems neuroscience research by reproducing trial-based behaviors as well continuous exploration. We present how existing challenges can be overcome by providing examples of i) how to make the animals elicit a variety of complex behaviors without human interference and ii) how to analyze the continuous behaviors with established neuroscience analysis methods.

Chapter 6 summarizes and discusses the results from chapters 2 to 5.

Part II

Original Manuscripts

Universal guide for skull extraction and custom-fitting of implants to continuous and discontinuous skulls

Zurna Ahmed, Naubahar Agha, Attila Trunk, Michael Berger, Alexander Gail

ZA, NA, MB and AG conceptualized the design, ZA, AT and NA designed the methodology, ZA wrote the manuscript, AG, MB and NA edited the manuscript.

(published in *eNeuro*: https://doi.org/10.1523/ENEURO.0028-22.2022)

Neural correlates of action effect anticipation during action planning in the frontoparietal reach network

Zurna Ahmed, Lukas Amann, Alexander Gail

ZA and AG designed the experiment; ZA collected the data; ZA and LA analyzed the data; ZA, LA and AG interpreted the data; ZA and LA wrote the manuscript; AG edited the manuscript.

B PRIME - an interactive haptic device for controlled, free behaviors in rhesus macaques

Zurna Ahmed, Naubahar Agha, Alexander Gail

ZA, NA and AG conceptualized the device; ZA and NA designed the device; ZA wrote the software; ZA wrote the manuscript; AG edited the manuscript.

The Exploration Room (ExR) – a novel environment for large scale, neurophysiological testing of natural behavior in systems neuroscience

Zurna Ahmed, Irene Lacal, Matthias Nuske, Richard Vogg, Neda Shahidi, Florentin Wörgötter, Alexander Ecker, Alexander Gail

ZA, IL, NS and AG designed the setup; ZA, IL and AG designed the experiment; ZA and IL collected the data; ZA, IL, RV, MN FW and AE analyzed the data; ZA, IL, RV and MN wrote the manuscript; AG edited the manuscript

Supplementary Chapter: Switch from egocentric to allocentric reference frame in ecologically more relevant interactions in rhesus macaque

Zurna Ahmed, Lukas Amann, Alexander Gail

ZA and AG designed the experiment; ZA collected the data; ZA and LA analyzed the data; ZA, LA and AG interpreted the data; ZA and LA wrote the manuscript; AG edited the manuscript.

Chapter 2

Universal guide for skull extraction and custom-fitting of implants to continuous and discontinuous skulls

This Manuscript was published in eNeuro.
doi: 10.1523/ENEURO.0028-22.2022

Novel Tools and Methods

Universal Guide for Skull Extraction and Custom-Fitting of Implants to Continuous and Discontinuous Skulls

Zurna Ahmed,[1,2] Naubahar Agha,[1] Attila Trunk,[1] Michael Berger,[4] and Alexander Gail[1,2,3]

https://doi.org/10.1523/ENEURO.0028-22.2022

[1]German Primate Center, Cognitive Neuroscience Laboratory, 37077, Göttingen, Germany, [2]Faculty of Biology and Psychology, University of Göttingen, 37073, Göttingen, Germany, [3]Bernstein Center for Computational Neuroscience, 37073, Göttingen, Germany, and [4]Laboratory of Neural Systems, The Rockefeller University, 10065, New York, NY

Abstract

Intracranial neurophysiological recordings require chronic implants to provide transcranial access to the brain. Especially in larger animals, which participate in experiments over extended periods of time, implants should match the skull curvature to promote osseointegration and avoid tissue and bacterial ingress over time. Proposed CAD methods for designing implants to date have focused on naive animals with continuous and even skull surfaces and calculate Boolean differences between implant and skull surface to fit the implant to the skull curvature. However, custom-fitting by calculating the difference fails, if a discontinuous skull surface needs to be matched. Also, the difference method does not allow designs with constant material thickness along the skull curvature, e.g., to allow fixed screw lengths. We present a universal step-by-step guide for custom-fitting implants which overcomes these limitations. It is suited for unusual skull conditions, like surface discontinuities or irregularities and includes virtual bending as a process to match skull surfaces while maintaining implant thickness. We demonstrate its applicability for a wide spectrum of scenarios, ranging from complex-shaped single-pieced implants to detailed multicomponent implant systems built on even or discontinuous skull. The guide uses only a few software tools and the final virtual product can be manufactured using CNC milling or 3D printing. A detailed description of this process is available on GitHub including step-by-step video instructions suitable for users without any prior knowledge in CAD programming. We report the experience with these implants over several years in 11 rhesus monkeys.

Significance Statement

Chronic implants are essential for intracranial neurophysiological recordings. In this study, we show how to custom-design and custom-fit such implants for rhesus monkeys (*Macaca mulatta*). Different to existing approaches, our procedure is not limited to even skull surfaces but can be applied to discontinuous or irregular surfaces. It furthermore presents a description of virtual implant bending to match the skull curvature while maintaining implant thickness. The final virtual product can be manufactured using CNC milling or 3D printing. In contrast to previous studies, this guide is suited for users without any prior expertise in CAD programming using our step-by-step video instructions.

Introduction

Cranial implants are essential for invasive brain neurophysiology in nonhuman primates and other animals. For example, headposts are routinely used to stabilize the animal's head and chamber implants are used to protect craniotomies, which provide access to the brain for intracortical electrophysiological recordings (Evarts, 1968a,b; Adams et al., 2011). With an increasing variety of available

Received January 22, 2022; accepted April 26, 2022; First published May 31, 2022.

The authors declare no competing financial interests.

Author contributions: Z.A., N.A., M.B., and A.G. designed research; Z.A., N.A., and A.T. performed research; Z.A. analyzed data; Z.A. and A.G. wrote the paper.

neurophysiological recording and stimulation techniques, there is a growing demand to custom-design implants and to custom-fit them to the individual animal. These include advanced chamber designs for semi-chronic adaptive multielectrode arrays (Galashan et al., 2011; Dotson et al., 2017; Ferrea et al., 2018) or chronic electrode arrays with wireless recording (Schwarz et al., 2014; Berger et al., 2020).

Because of the requirements that cranial implants in systems neuroscience are often specific to a recording technique or a project-specific experimental setting, ready-to-go commercial solutions are mostly not available and out-sourcing of the implant design can be expensive and time consuming. Since affordable or even free tools for computer-aided design (CAD) became powerful and production with different materials via 3-dimensional (3D) or CNC milling became easier to access, more and more labs invest into their own CAD-based implant construction.

Previous studies have focused on surgery planning (Gardiner and Toth, 1999; McAndrew et al., 2012) and explain how to extract a 3D skull model from anatomic computer tomography (CT) or magnetic resonance imaging (MRI) scans. The model is then used to physically bend an originally nonmolded implant to conform to the skull curvature (Lanz et al., 2013; Overton et al., 2017). Such two-step procedure allows the user to start out with a simpler, nonmolded ("standard") implant which is easier to produce, e.g., on a three-axis instead of five-axis milling machine, because of surfaces which only curve along one dimension. Compared with fitting standard implants to the skull during surgery, the existence of a 3D skull model allows shorter surgery times as the fitting is done before surgery. Yet, physical fitting might prevent from an optimal fit and increase chances of implant failure because of tissue growth between implant and bone. Also, postproduction physical bending can weaken the implant materials and is discouraged for certain metal materials (e.g., titanium) or not possible for plastic materials [e.g., polyetheretherketon (PEEK)].

Newer studies have been focusing on methods that allow 3D implant matching to the skull curvature before its manufacturing (Johnston et al., 2016) using software like Blender (https://www.blender.org/) or SolidWorks (Dassault Systèmes SolidWorks Corporation) for invasive implants (Chen et al., 2017; Blonde et al., 2018) and other noninvasive methodologies, e.g., EEG (Sandhaeger et al., 2019). The resulting implants can be produced using CNC milling or 3D printing. Openness to different production pipelines gives large flexibility in the choice of material. This way, implants can be built that are sturdy, yet small and light-weight, or even radiotranslucent, for compatibility with different imaging techniques.

Previous methods in neuroscience research focused on first-time implantations with smooth skull surfaces that cannot be used for animals with discontinuous skull characteristics (Mulliken et al., 2015; Chen et al., 2017; Blonde et al., 2018). The latter might, for example, result from previous surgical procedures. Studies on human reconstructive surgery, on the other hand, have tried to reconstruct skulls with a hole caused by a previous trauma. Existing approaches mirror the image of the contrahemispheric skull and calculates the difference between the original skull with hole and the mirror image extracting the missing part of the skull for reconstruction (Ming-Yih et al., 2002; Singare et al., 2009). However, this method assumes perfect symmetry and is not applicable if the skull defects affect both hemispheres.

We present an approach to overcome shortcomings of existing methods. First, our guide enables custom-fitting of implants for animals with unusual skull conditions, such as discontinuities or irregularities on the skull surface. Second, our guide is universal as it is applicable to variable implant designs, including a description of how to virtually bend implants to fit the skull curvature thus allowing to maintain the thickness of the implant even after custom-fitting. Our guide provides a complete process description for customized implant design from skull extraction using imaging data to the final design of the implant in a production-ready file format. Outsourcing of the CAD fitting process to external companies is not necessary while the result of the process can be used for in-house or external production. Final CAD models can be produced by CNC-milling or 3D-printing methods in a large choice of materials. Our extensive tutorial, including step-by-step video tutorials, allows researchers without prior CAD experience to design custom implants. The given examples in this guide are focused on but not limited to nonhuman primates.

In the following, we will describe how to extract 3D models of the brain and skull followed by the implant design procedure for three categories of implants. To demonstrate the functionality especially for discontinuous skulls, we present its application on a skull containing prior craniotomies by designing a multicompartment chamber covering the craniotomies. In the end, we will give an overview of the manufacturing processes and file formats.

Materials and Methods

A step-by-step written tutorial guide with corresponding video tutorials for each step, example CAD models and implants can be found on https://github.com/ZuAh/Custom-fitting-of-implants as Extended Data. References to the Extended Data Tutorial (EDT) will follow the format "EDT 0–1" to indicate chapter (0: "skull extraction") and processing step (1).

The study was supported by the European Commission in the context of the Plan4Act consortium (http://plan4act-project.eu; EC-H2020-FETPROACT-16732266 WP1) and the German Research Foundation (http://www.dfg.de) in the context of the Research Units 1847 and 2591 and the Collaborative Research Consortium 1528 "Cognition of Interaction".

Acknowledgments: We thank Klaus Heisig and Sina Plümer for helpful discussions with implant design and technical support. We thank Daniela Lazzarini and Sina Plümer for performing MRI- and CT-scans.

Correspondence should be addressed to Zurna Ahmed at zahmed@dpz.eu.

https://doi.org/10.1523/ENEURO.0028-22.2022

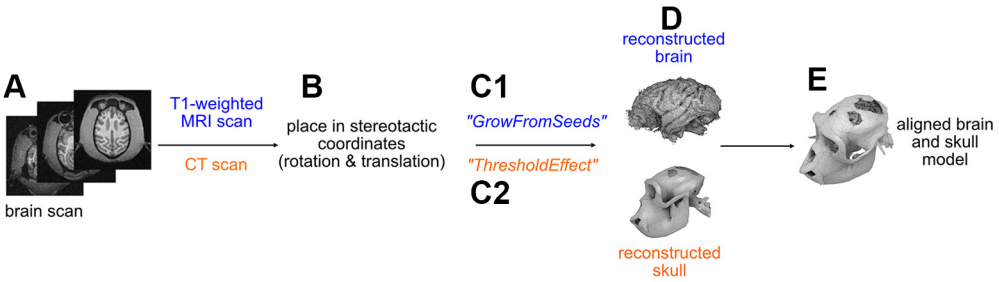

Figure 1. Brain and skull extraction from brain scans using 3D slicer. An example of a discontinuous skull is shown for demonstration purposes. ***A***, T1-weighted Magnetic Resonance Imaging (MRI) scan scan was used for brain extraction, Computed Tomography (CT) scan for skull extraction. ***B***, The scans are first rotated and translated until they are aligned according to the Horsley–Clarke stereotactic coordinates. ***C***, Depending on the scan type, either the more manual function "GrowFromSeeds" or automatic function "ThresholdEffect" is used to extract the brain and skull (***D***), respectively. ***E***, Extracted brain and skull models are aligned and used for further implant planning and designing.

Skull and brain extraction and locating regions of interest (ROIs)

While the focus of this step-by-step guide is implant design and customization, we will still give a short overview of how to extract a 3D skull and brain model, since this is used as the basis for implant fitting.

We use CT and MRI to extract the 3D skull and brain models, respectively (Fig. 1*A*,*D*). For DICOM image processing we use 3D Slicer (https://www.slicer.org), an open-source software available for Microsoft Windows, Apple Mac OS X and Linux OS. T1-weighted scan is used to extract the brain (see below). The MRI scan could be used for skull reconstruction as well, but we preferably use CT scans if available because of faster scanning and ease of use in software flow. CT scans have to be aligned with MRI scans, if implant placement depends on the neuroanatomy of the brain. Image alignment can either be done in 3D Slicer using the Transformation module or in a separate CAD program. We used Fusion 360 (Autodesk). CT and MRI imaging data types require their own specific extraction steps described in the following.

Before planning the surgery, the scans are placed in Horsley–Clarke stereotactic coordinates (Fig. 1*B*). In 3D Slicer, we used translation and rotation to create a head-centered Horsley–Clarke coordinate system by identifying five points via cranial landmarks: one point in each ear channel (external auditory bony meatus), which may be additionally indicated by a fiducial marker from the stereotactic frame during the scan, if a monkey was placed in such; one point below each eye marking the inferior orbital edge (infraorbital margin). The fifth point is defined as the equidistant point between the two ear channels and serves as the origin. The scans are translated and rotated until the origin point has the value 0 in a set of three orthogonal coordinate planes and all five stereotactic points are aligned on the horizontal plane.

To extract the skull by using a CT scan, we use the built-in threshold method of 3D Slicer "ThresholdEffect" (Fig. 1*C1*). This function selects all voxels in the source volume within a range of the signal intensity. The range is modified until the entire skull surface is detected while skull irrelevant voxels are rejected by the algorithm. The 3D skull model can be generated afterward using the selected voxels (EDT 0–1).

To extract the skull and brain if a T1-weighted MRI scan is available, we use a technique which requires more manual steps (Fig. 1*C2*). For 3D slicer (version 4.8.1-S4) the extension named "FastGrowCut" needs to be installed. In newer versions, starting from 4.10.1, this extension is integrated in the main software and is called "GrowFromSeeds," which is a multilabel segmentation method. In this approach, seeds are placed by the expert viewer in the region of the skull or brain, respectively. Different seeds can be planted for different tissue types in parallel; for example, one seed type for brain and one for skull. The algorithm detects the skull and the brain separately, such as that one model for each seed type is generated. To verify whether the correct areas were detected, it is important to control the tissue separation in the individual slices. If necessary, additional seeds can be placed or suboptimal seeds removed to improve the skull and brain extraction (EDT 0–2).

To plan the coordinates of the implant on the skull if the position of the implant depends on the brain anatomy, we first identify the coordinates of the brain ROI. We use anatomic landmarks and a brain atlas (Saleem and Logothetis, 2012) to locate the ROI in stereotactic coordinates. We mark the coordinates of ROIs in the 3D skull model by using "MarkUps" and determine the position of the implant on the skull, e.g., by projecting the ROI position in the brain to the surface of the skull along the stereotactic Z-dimension. Another possibility of determining the implant position, especially when targeting deeper brain regions and aiming for surface-normal implant positioning, is the open software package Planner (Ohayon and Tsao, 2012). We mark the stereotactic points (origin, ear bars and eye bars) to allow placements of the models in a stereotactic coordinate even after export to a CAD program for implant designing. These marks can additionally be used for alignment of the skull and brain models, if they were obtained from different sources (e.g., an MRI scan for brain extraction, a CT scan for skull extraction). This can be necessary, if the MRI scan is for instance not sufficiently clear to extract the skull model in its details.

We export the extracted 3D brain and skull models in the STereoLitography format (.STL file; EDT 0–3). This file format can be used for 3D printing of physical brain and skull models, as well for importing to CAD programs for the following skull-fitting implant design procedure (EDT 1–1). Before printing, it is recommended to clean up, and if necessary, cut the 3D skull model for better printing quality. We use, for example, the freeware Meshmixer (https://www.meshmixer.com/) for cutting and Meshlab (https://www.meshlab.net/) for quick .STL viewing.

To allow below procedure of implant fitting based on a continuous representation of the skull surface, we create a 3D surface in NURBS (nonuniform rational B-splines) format out of the extracted 3D skull model using Rhinoceros 6 (Robert McNeel and Associates). This is necessary as the .STL format of the original imported extracted 3D skull prevents the use of the fitting tools described in this guide.

For this, first, we create a fine mesh using the parameters "Spacing," which is the space between the individual mesh points, "AutoSpacing," which enables Rhinoceros to identify the spacing automatically and "AutoDetectMaxDepth," which detects the depth, can be adjusted (EDT 1–2). A sufficient mesh is created once it covers all relevant parts of the skull surface to a degree of detail that is required for skull reconstruction depending on the skull condition. For all our designed implants the automatic "AutoSpacing" and "AutoDetectMaxDepth" with a "Spacing" of 5 was sufficient. Then the mesh is converted in a 3D NURBS surface using "Drape," which is described in more detail in "implant design and fitting" (EDT 1–2).

In the next section, we will describe the implant design processes for this most typical case of a naive skull being prepared for a first-time implantation. Below, we will return to the topic of skull extraction and reconstruction in the case of more complex surgical situations, e.g., bone discontinuities because of prior surgeries.

Implant design and fitting

This guide can be used to design various types of implants (Fig. 2). As an example, for a single-compartment implant, we will show how to create a headpost implant (Fig. 2*B*). This design is characterized by a central pin (the "post") extruding vertically from a base. Multiple "legs" build the base and extrude horizontally along the surface of the skull. The legs need to fit the curvature of the skull, but at the same time keep their thickness along the entire length ("virtual bending"), such that bone screws fit exactly the holes in the legs.

As an example for a multicompartment implant, we describe how to create a chamber with different interior elements suitable for chronic array recordings with wireless transmission (Fig. 2*C*). One single chamber surrounds and protects a large-scale craniotomy with chronic implanted arrays in multiple brain ROIs while giving enough space for array connectors and adaptors to hold the wireless transceiver. The elements are molded to the skull surface without constraints by the thickness of the material ("virtual cutting").

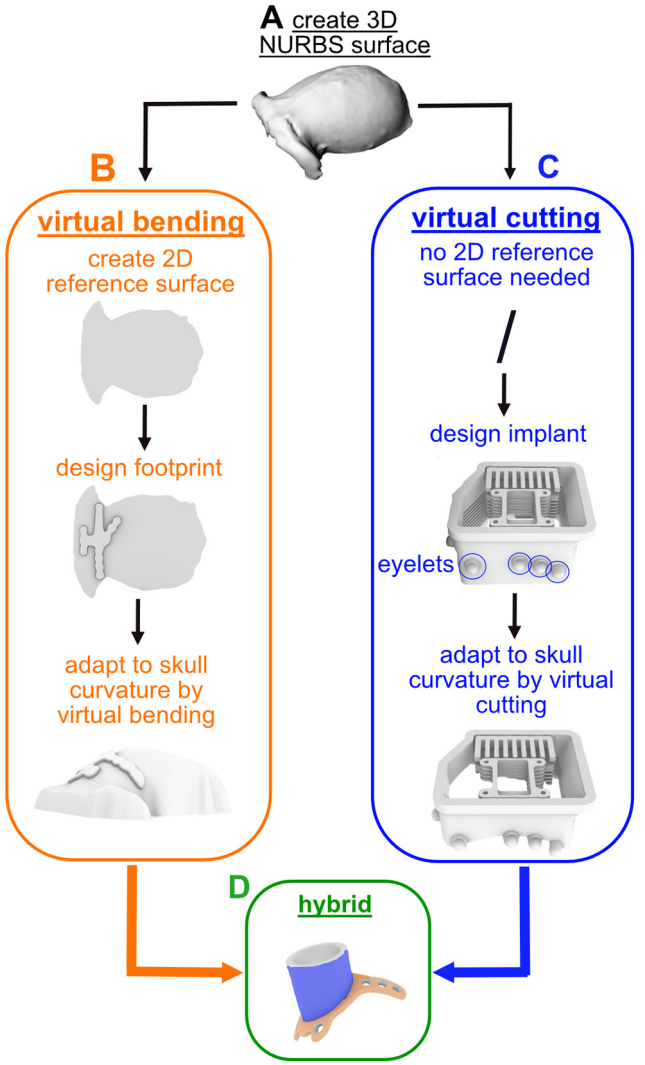

Figure 2. Overview of presented implant types and their individual custom-fitting approaches. ***A***, 3-dimensional (3D) skull surface in NURBS format reconstructed from the extracted 3D skull surface acquired from a CT scan. ***B***, Virtual bending (orange), After creating a 2-dimensional (2D) reference surface the to-be-matched implant part is designed and extruded. It is then virtually bent before completion, which implies the thickness of headpost "legs" (perforated metal strips) is maintained while fitting them to skull curvature. ***C***, Virtual cutting (blue), The lower end of large-scale "chamber" (enclosure with lid) together with the placed eyelets are fitted to the skull curvature such that remaining height matches desired specification. The example shows a wireless recording chamber with additional interior elements to hold a circuit board and multiple electrode array connectors (Berger et al., 2020). ***D***, Hybrid (green), Example of a standard chamber to access single brain ROI with legs for mounting; this design combines virtual bending (orange) and cutting (blue).

Finally, we describe how to design a standard chamber encircling a small craniotomy and having legs for screwing the implant directly to the skull, similar to the headpost (Fig. 2*D*). This demonstrates an implant design which combines cutting and bending (hybrid design).

The focus of the article is on the digital workflow of designing and custom-fitting the implants to curved surfaces, and will follow below. Since some steps in this guide depend on geometric properties of the implants (e.g., cutting or bending), we first briefly describe the main implant features to give an impression of the scope of implants dealt with.

For implant fitting by virtual bending or cutting we used the software Rhinoceros. For designing of extended chambers, we used Fusion 360, which was because of convenience based on prior user expertise and not a necessity. However, the fitting of all proposed implant types was done using Rhinoceros only.

For animals with preexisting cranial implants, e.g., a headpost, the persistent implants need to be part of the 3D skull model such that additional implants, e.g., a chamber, can be designed respecting the constraints of the preexisting implant. Ideally, this planning is done for all implants together based on imaging data recorded before first implantation to take all planned implants' positions and their physical dimensions into account. If not all planned implants are implanted within the same surgery, it is recommended to perform a second CT scan close before custom-fitting the second implant. With this, changes in skull surface that developed since the first implantation, e.g., bone growth in reaction to the primary implants, can be accounted for, possibly allowing a better fit of the to-be-added implant(s). However, depending on which material was used for the first implant, this follow-up imaging data can contain artefacts potentially limiting the precision of the skull extraction procedure. While ceramic screws and plastic materials polylactide (PLA) and PEEK allow nearly artifact-free imaging, titanium and ferromagnetic materials (e.g., stainless steel) cause substantial and strong artefacts in MRI, and CT, scans, respectively.

Implants with maintained thickness, virtual bending

Headposts are common in nonhuman primate research to stabilize the animal's head position and thereby allow precise measurements of eye movements or applying sensitive neurophysiological probes, e.g., semi-chronic microelectrodes. A common headpost design used in our lab consists of a central transcutaneous post surrounded by four subcutaneous perforated metal strips ("legs") at its base that are custom-fitted to the skull curvature (Fig. 2*B*) for better osseointegration. The implant is fixed to the skull by titanium screws through the holes in the legs, equivalent to titanium strips used in cranioplasty. To maintain the thickness of these legs is important as the self-tapping cortical screws have predefined length and should fit the combined thickness of implant material plus skull to provide implant stability while avoiding transcranial protrusion of the screws.

We achieve constant thickness of skull-fit cranial implants by "virtual bending" (Fig. 2*B*). We used the software Rhinoceros for designing the headpost. It offers a useful built-in tool for the bending process. Rhinoceros can also be used for designing the implants itself, which we did in this example.

In the first step, we create a 2D reference plane corresponding to the 3D reconstructed skull, which is converted automatically by Rhinoceros into a 3D NURBS surface format (EDT 1–4 to 1–6). The footprint of the implant is then designed on the virtual 2D reference plane (EDT 1–7). Projecting the outline of the 3D skull model onto this plane helps for planning the layout and leg positions. Once the 2D footprint is finalized, the 2D implant sketch is extruded vertically to create an unmolded 3D version of the implant (EDT 1–7). To remove sharp edges, the function "fillet edges" is used (EDT 1–7).

In the second step, the legs are molded by using the FlowAlongSrf function of Rhinoceros (EDT 8). We selected the extruded footprint as an object to flow along a surface. The previously generated 2D reference plane is used as the "base surface" while the 3D NURBS surface is referred to as the "target surface."

It is important to select corresponding edges or corners on both surfaces to keep the location of the implant. Additionally, it is helpful to place the 2D surface in front of the 3D NURBS surface, otherwise Rhinoceros can confuse the location and instead of bending on top of the skull try to match it from underneath.

Following, screw holes are added. The diameter of the holes is 3 mm to fit the 2.7-mm cortical screws of 6–8 mm in length (6–8 mm, Synthes), which will be used during the surgery to screw the implant to the bone. A counter bore with 45° inclination is virtually added to the holes for later embedding the screw heads (EDT 1–11). It is important not to introduce the screw holes and counter bores before the bending step, as otherwise they will be deformed during the bending because of the non-zero material thickness and thereby would lose their functionality.

In the final step, the transcutaneous post is designed. It consists of an elliptic cylinder which is 14 mm high and has a large diameter of 12.7 mm and a small diameter of 8 mm (exemplary size used in our laboratory). The shape of this post and its top end is adapted to fit the counterpart, which will be specific to the experimental setup. In the example shown here, the top consists of a circular cylinder which has a diameter of 6.8 mm and a height of 6 mm and will later be threaded by hand. To round the post edges on the top and to combine it with the bottom part, the "fillet edges" function is used with a radius of 1 mm.

After fitting, the customized implant is placed on the originally extracted 3D skull to verify the fit, location, and angle of the implant (EDT 1–14).

Extended chambers, virtual cutting

Extended chambers for chronic implantation might protect craniotomies that span several brain ROIs, and can additionally contain interior constructions for holding electronic equipment for wireless recordings (Berger et al., 2020). As an example, we designed a set of multiple components (Fig. 2*C*): (1) a biocompatible chamber that encircles the craniotomy and houses array connectors and other components; (2) a connector holder that allows for easy positioning of the electrode array connectors and protecting the connectors and cables against mechanical

stress during the surgery; (3) a circuit board holder to attach additional electronic components; (4) various-sized protective caps covering the chamber while containing different wireless headstages and components.

We use "virtual cutting" for such chamber implants, as they do not need virtually bend legs but still require the bottom part to follow the skull curvature while dimensions and angles toward the top part are preserved. Virtual cutting achieves custom-fitting by calculating the Boolean difference between the implant's bottom and the skull surface. We exemplify this procedure with a chamber-like implant containing additional interior elements (Fig. 2*C*).

In the first step, as above, unmolded 3D versions of all implant components are designed first. We used Fusion 360 for the example presented here, but any other CAD program including Rhinoceros is suited depending on experience, convenience and preference (EDT 2–1). If not originally designed in Rhinoceros, we export all parts that need molding to the skull surface to Rhinoceros using the Initial Graphics Exchange Specification (.IGES) format (EDT 2–4).

In the second step, we import the 3D reference skull surface created in Rhinoceros as described in the section about skull extraction above [Skull and brain extraction and locating regions of interest (ROIs)]. The implant components are arranged and placed on the 3D skull surface using the landmarks of the skull. While placing the virtual implant it is pushed through the skull far enough such that the whole lower circumference intersects with the skull and that at the same time the desired implant height remains above skull level. The latter can be measured using either the "Distance" or "Length" command in Rhinoceros (EDT 2–5). For this, the original implant needs to be design high enough; in fact, it might be easiest to design it significantly higher than actually needed, since it will be cut anyway.

In the third step, we use the command "BooleanDifference" and select the implant as the target to subtract from and the 3D NURBS surface as the target to subtract with (EDT 2–6). After fitting, we placed the customized implant on the originally extracted 3D skull to verify the fit, location, and height of the implant.

Depending on the way the implant is mounted to the skull, additional design features will be necessary. If the implant is going to be embedded into acrylic dental cement, furrows along the surface help to improve mechanical stability because of the form-fitting of the cement flowing into the furrows (EDT 2–7). If the implant should be directly screwed to the bone, instead, eyelets (single-holed "mini-legs") can be added to the outer surfaces (EDT 2–2 and 2–3; Fig. 2*C*). When creating such eyelets, it is helpful to place them as close as possible to the expected elevation of the skull curvature. This is achieved by placing the eyelets horizontal midline approximately on the skull surface such that half of the eyelet is sticking inside the skull.

Hybrid implants, virtual cutting and bending

Standard cylindrical cranial chambers typically encircle small craniotomies, e.g., to target one brain area. We here add custom-fitted legs with constant thickness (equivalent to the ones of the headpost) to the cylindrical center part to demonstrate a hybrid design (Fig. 2*D*). The lower end of the cylindrical part follows the skull curvature, while the top of it preserves specific dimensions and angles for mechanical adapters (e.g., to hold recording devices) that should not be distorted by bending.

As a first step, the legs are designed in a process that is equivalent to what is described above, Implants with maintained thickness, virtual bending.

In a second step, the 3D cylinder is designed, in our case with a diameter of 24 mm and height of 30 mm (EDT 3–1). The cylinder is placed on top of the molded legs. We then temporarily remove the legs and push the chamber into the skull model, equivalent to above, Extended chambers, virtual cutting. By calculating the Boolean difference, the cylinder bottom part is fitted to the skull curvature (EDT 3–2). This fitted top part is then placed on the legs and pulled through them until a protrusion of around 1–2 mm on the bottom side of the implant is reached (EDT 3–3). With this (optional) protrusion, the bottom part of the implanted cylinder will be protruding slightly into the craniotomy. Such protrusion of the implant into the craniotomy allows easier centering of the implant on the cranial opening, can help to achieve a better seal between implant and bone and additional mechanical stability, and also can prevent later closure of the craniotomy by bone growth. As the last designing step, the implant is placed on the originally extracted 3D skull to verify fit, location, and angle.

Skull reconstruction based on discontinuous or uneven skull

As key feature, our guide is suitable for designing implants for skulls with preconditions, e.g., discontinuous or uneven skulls. Difficulties in reconstructing 3D skull surfaces with standard techniques can result from unevenness because of excessive bone growth in response to other nearby implants which have been implanted earlier. As part of the osseointegration such bone growth can be stimulated, leading to elevated bone structures on the skull. Skull discontinuities, e.g., left-over skull openings from previous craniotomies, are an additional challenge for implant fitting. Advanced implant fitting techniques should allow, first, discontinuities to be digitally reconstructed and the original shape of the skull to be approximated as best as possible for fitting an implant to areas of the skull that contains bone protrusions or holes with softer tissue. Second, the technique should allow discontinuities to be taken into consideration for designing the implant, e.g., for placing screw holes on top of solid bone structures only and avoiding the open patches. Extra time and effort may be needed to reconstruct the skull and brain when preexisting implants on the animal's skull produce scanning artefacts that extend to the part of the skull targeted for implantation.

To virtually reconstruct a discontinuous skull as continuous surface, first, a 2D reference plane is created out of the original 3D surface extracted from the imaging data. This reference plane still contains the discontinuities so

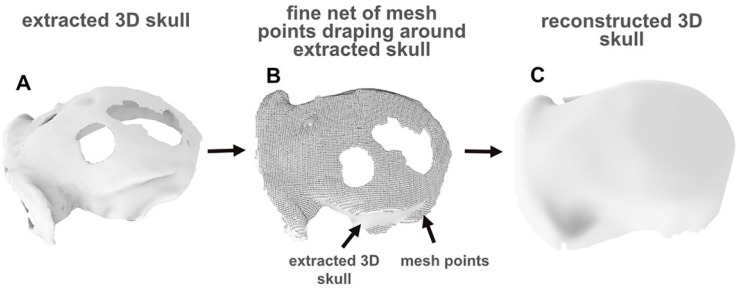

Figure 3. Overview of 3D skull reconstruction for discontinuous or uneven skull surfaces. ***A***, Discontinuous skull with holes reconstructed from CT scan. ***B***, A fine mesh is created out of the originally extracted 3D skull model. All mesh points, which represent the discontinuity, are manually removed. ***C***, Afterwards the mesh is reconverted into a 3D (NURBS) surface.

that they can be taken into account when designing the implant, e.g., placing screw holes outside the discontinuous regions (EDT 4–6).

In case of an uneven skull (Fig. 3*A*), reasonably simple implant design might be prevented because the unevenness requires matching of the implant to sharp edges on the skull. This can require the implants to have low-radius concavities, which are difficult to manufacture. Therefore, smoothing out of the unevenness might be required and would later during surgery have to be complemented with corresponding smoothing of the actual bone structure.

Importantly, both the filling of discontinuities and smoothing of unevenness need to be done in a way such that the shape of the other parts of the skull are maintained in their details as much as possible. This is needed to guarantee an appropriate implant match to the actual skull curvature during surgery. We achieve this, after importing the 3D model into Rhinoceros (EDT 1–1), by creating a fine mesh (EDT 1–2) which represents the 3D skull model. We then remove only the single mesh points that are created in the region of the discontinuity or unevenness resulting in a clean mesh point cloud (Fig. 3*B*). Finally, we convert the mesh into a 3D NURBS surface by using “MeshPatch” (EDT 1–2) and “Drape” (EDT 1–3; Fig. 3*C*).

In contrast to other common smoothing algorithms, our approach allows removing the discontinuity or unevenness in a targeted fashion, i.e., without changing the overall skull surface outside the discontinuous region that would result from general smoothing.

We exemplify the skull reconstruction procedure by designing a headpost and an extended chamber implant for chronic microelectrode implants in an animal with multiple, partly widespread presurgical discontinuities across the skull (Fig. 4).

Implant manufacturing and file formats

We used in-house 3D printing with PLA on an additive manufacturing 3D printer (Bibo 2 Maker E, Shaoxing Bibo Automatic Equipment Co, Ltd and Formlabs) for rapid prototyping of all implants and for a physical 3D skull model. Implant dummies together with a printed skull model allow to control for the accuracy of the implant fit after production and to simulate surgical procedures. Prototypes are not necessary for the final implant production. Final implants are milled in-house using a five-axis

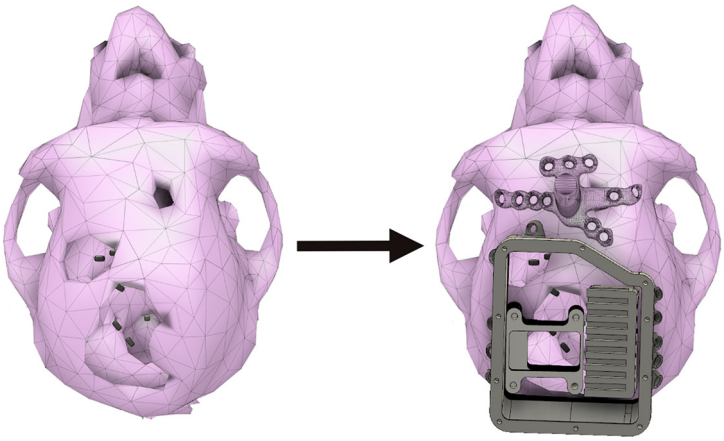

Figure 4. Example of custom-fitted implant for an animal with discontinuous skull surface. Left, The skull contains three holes from previous craniotomies and implants. Right, A headpost was designed and custom-fitted taking the anterior hole into account by designing the most posterior leg as a cover for the hole. An extended chamber with inlays for the use with wireless headstages was matched to the skull curvature around two large preexisting craniotomies. Black rectangles on the cortical surface mark the planned microelectrode array positions.

CNC milling machine or 3D printed by commercial services (EOS P770, P396, P110, Shapeways HQ).

For headposts presented here, we used titanium because of its biocompatibility (Plecko et al., 2012), lightweight sturdiness and good chance of osseointegration. It was either milled out of a block of titanium (in-house) or 3D-printed (EOS M280/M290, Sculpteo). In case of printing, the thread for the pin necessary for our head-fixation pole was cut afterward and not included in the print itself as it is too fine to be printed.

Chambers were milled (in-house) out of a block of PEEK to provide biocompatibility, MR-transparency and smooth surfaces. During surgery, chambers were screwed onto the skull by using ceramic screws (6–8 mm, Thomas Recording) in case of small chambers around a craniotomy or titanium screws in case of the large chamber. There is no need for applying acrylic dental cement to the bone and implant for mechanical stability with this approach, while cement or biocompatible glue might still be useful in small amounts for sealing the inner side of the chamber against the outside.

Chamber inlays not getting into contact with organic tissue, e.g., because a thin layer of cement covers bony surfaces inside the chamber, were 3D printed using selective laser sintering with lightweight plastics (PA2200, Shapeways) if produced externally; in-house, we used fused deposition modeling with polyactid acid (PLA) on the Bibo printer.

For all 3D printings we use the Stereolithography (.STL) data format, while for CNC milling the STandard for Exchange of Product model data (.STEP) format was used. In general, for switching between different CAD programs, the .STEP format is recommended as it is supported universally across different CAD programs. However, for importing to Rhinoceros, we recommend to use the Initial Graphics Exchange Specification (.IGES) format. This is because .STEP is handled as a block instance in Rhinoceros, which does not allow access to the full range of functions required to custom-fit an implant to the skull.

As 3D slicer uses the .STL format to export the extracted skull and brain models, the original extracted models need to be transformed into NURBS or .IGES surfaces to enable the full functionality of implant fitting tools. After creating a mesh that represents the originally extracted 3D skull model, we converted this mesh into a 3D NURBS surface.

An overview of the used software packages can be found in Extended Data.

Animals and surgery

Eleven male rhesus monkeys (*Macaca mulatta*) were implanted with headposts, standard or extended chambers in sterile surgeries under deep anesthesia and perisurgical and postsurgical analgesia. Data for this study was collected opportunistically, i.e., none of the animals was implanted for the purpose of the current study but instead to be part of neuroscientific research projects. Implant planning was done based on anatomic scans also conducted under anesthesia. Ten of the animals were chronically implanted with a transcutaneous titanium headpost. One animal was implanted with a standard chamber with preexisting headpost. One of the eleven animals was implanted with a chronic chamber for wireless recordings similar to the one described previously (Berger et al., 2020).

All animals were or are housed in social groups with one to two male conspecifics in facilities of the German Primate Center. The facilities provide cage sizes exceeding the requirements by German and European regulations, access to an enriched environment including wooden structures and various toys and enrichment devices (Calapai et al., 2017; Berger et al., 2018).

Each implant was implanted during a single sterile surgery under deep gas anesthesia and analgesia via an intravenous catheter. Additionally, the animals receiving a craniotomy were prophylactically treated with systemic antibiotics cobactan, duphamox, or synulox 1 d presurgery and 2–5 d postsurgery. Analgesia was refreshed on a 5- to 6-h cycle continuously for up to three postsurgical days for noncraniotomy types of surgery (e.g., headpost implantation) and four to five postsurgical days for surgeries with craniotomies (e.g., chamber implantation) using levomethadon or rimadyl, depending on need.

All procedures have been approved by the responsible regional government office [Niedersächsisches Landesamt für Verbraucherschutz und Lebensmittelsicherheit (LAVES)] under permit numbers 3392 42502-04-13/1100 and 33.19-42502-04-18/2823 and comply with German Law and the European Directive 2010/63/EU regulating use of animals in research.

Results

Versatility and efficiency of the design process

Our universal guide describes how to design a variety of implant types and how to deal with special preconditions of the surgical subject, like discontinuous skulls (e.g., skull with holes) and uneven skulls, with a small set of software tools. We so far custom-fitted twelve implants with this approach: 10 headposts (virtually bent); two of which were designed for preimplanted skulls, one extended chamber (virtually cut) for preimplanted skull condition and one standard chamber (hybrid) for a nonimplanted skull.

We exemplify the design processes with an extended chamber and its inlays and a headpost, both fitted to a discontinuous skull containing holes (Fig. 4).

The design process is versatile. Besides the custom-fitting of implants by virtual cutting, our guide additionally describes the procedure of virtual bending, which maintains the thickness of an implant when molding it to the skull curvature (Fig. 5*B*). All implant types presented here can be customized to both skull conditions (Fig. 5*A*). Within the same framework and with the same set of tools, all implant types can be prepared for production in various metal and nonmetal materials using milling or printing methods.

Our step-by-step guide is efficient and accessible. Additionally, our proposed way of using the mentioned

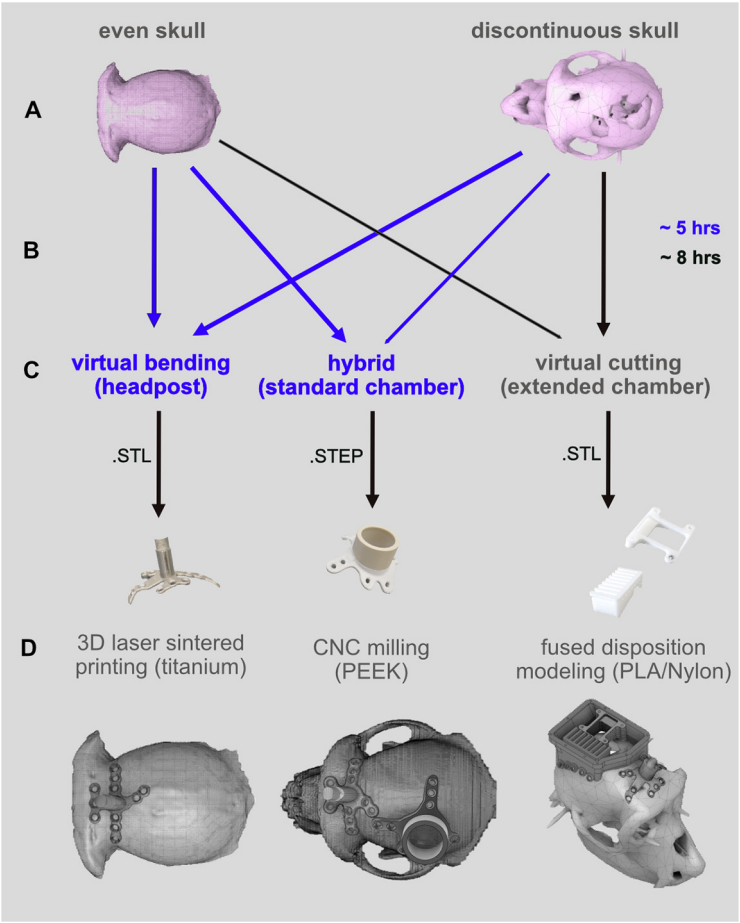

Figure 5. Versatility of our design process. ***A***, Our approach is suitable for intact and discontinuous skulls. ***B***, Arrows indicate the presented combination of skull condition and implant type. Lines indicate possible combination of skull condition and implant type, which were not presented in this article. The process and guide are adapted to users without any prior knowledge in CAD programming. Single-piece designs were achieved within ~5-h designing time (blue), more complex implant systems within ~8 h (black). ***C***, Three types of implant fitting methods are covered: virtual bending, virtual cutting, and the combination of both (hybrid), which can be saved in different file formats (e.g. Stereolithography (.STL) or STandard for Exchange of Product model data (.STEP)). ***D***, The resulting designs are producible in various (bio-compatible) implant materials (e.g. titanium, polyetheretherketon (PEEK), polylactide (PLA), Nylon).

software packages does not need prior expertise in CAD programming. For users who were naive to our guide and to CAD programs, reconstruction of a 3D skull model required net 5 h and the design of a standard chamber or headpost another 5 h (approximate durations). Approximately 8 h were needed to design the extended chamber (Fig. 5*B*) with its inlays for users who were not familiar with general CAD programming or the procedures described in this guide.

Implant functionality and longevity

With our guide we created designs that adhere to the following criteria: (1) manufacturing in the desired biocompatible material; (2) close fit of the implant to the skull without need for further bending or cutting modification during surgery; and (3) functionality of the implant for extended periods of time after implantation.

The surgery data were collected opportunistically, so that we do not have quantitative measurements of the closeness between implant and skull. We consider an implant to be a close-fit, if (1) it sits flush against the skull without demanding any physical modification during surgery to avoid wiggling, and if (2) the closeness between implant and skull is not bigger than ~1/10th of the implant leg thickness (2-mm total leg thickness), and if (3) no local cavities between bone and implant would encourage to fill-in bone growth material (Hydroxyapatite, Mathys, DePuySynthes). Figure 6 depicts three exemplary implants, which we classified as "closely fitting implants."

The implants mostly showed lasting functionality (Fig. 7). At the time of submission of this manuscript, eight out of 10 headposts, which were first-time implantations, are stable and functional up to three years postimplantation. Inflammation at the wound margins compromised animal H's headpost functionality after four months; since there was no scientific need use of the headpost was discontinued while use of a second implant on this animal was continued. Also, animal Z's re-implanted headpost required surgical intervention nine months postimplantation.

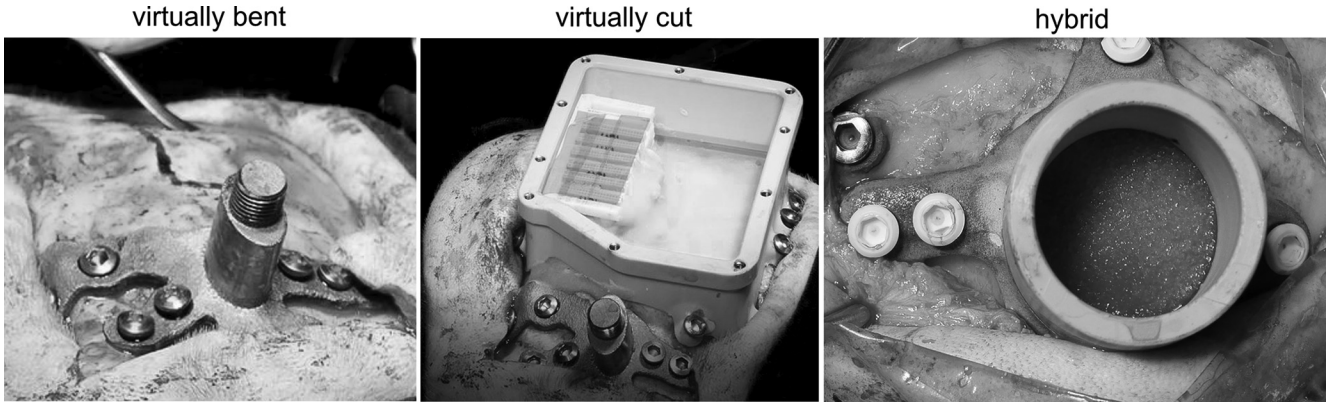

Figure 6. Examples of close-fitting implants. Left, Titanium headpost on a discontinuous skull with holes, which was designed by virtually bending. Middle, Extended chamber for array recordings with its inlay on the same discontinuous skull. Right, Standard chamber created by virtually bending the legs and virtually cutting the top part (hybrid).

The extended chamber for wireless recordings, which is covering two-thirds of animal H's discontinuous skull is stable up to date (1182 d postimplantation) requiring a small intervention on the chamber inside after 896 d postimplantation. The standard chamber in animal T is robust till date (385 d postimplantation).

Figure 8 shows an example of osseointegration of a titanium headpost produced with a precursor of this guide. As eight out of 10 headposts are still functional, we do not have such documentation yet for these headposts.

In summary, using our beginners-friendly guide 12 custom-fit implants of different complexities for both skull types, even skulls and skulls with discontinuities, were designed. Eight out of 12 (67%) implants were designed by users, who had no prior knowledge with CAD programming. All designed implants could be manufactured either using 3D printing or CNC milling, depending which biocompatible material was desired. All customized and produced implants were closely fitting without requiring any intervention (e.g., bending) during surgery. Ten out of 12 (83%) implants remain functional up to date not losing their functionality because of in precise fitting on the skull.

Discussion

We present a universal guide, including video tutorials (in Extended Data), to create implants of diverse types for skulls in various conditions, e.g., smooth skulls and discontinuous or uneven skull surfaces. The guide is well accessible to users who are not CAD experts already. Additionally, to the common method of virtual cutting, we introduce virtual bending and the combination of both. The resulting custom-fitted implant designs and file formats can be used for CNC milling or 3D printing. Using this approach, we successfully implanted eleven animals with headposts, one with a simple cylindrical and one with an extended multicompartment chamber in animals with even and discontinuous skull surfaces, and demonstrate lasting functionality.

Previous studies have shown that a close implant fit to the skull reduces the risk of subimplant tissue growth and bacterial infections thereby improving implant longevity (Betelak et al., 2001; Johnston et al., 2016; Chen et al., 2017). When starting out from nonmolded implants with predefined standard shapes that only approximate but do not fit the individual animal, the gap between bone and implant is often minimized by either using acrylic dental cement (McAndrew et al., 2012; Chen et al., 2017) or by physically bending implants to the skull curvature (Adams et al., 2007, 2011).

Acrylic dental cement is widely successfully used (Wegener et al., 2021). Nevertheless, there are still disadvantages. As acrylic undergoes an exothermic reaction, the heat enhances the risk of of bone necrosis (Treon et al., 1949; Ormianer et al., 2000; Dunne and Orr, 2002; Dotson et al., 2017). As the cement does not bind to the

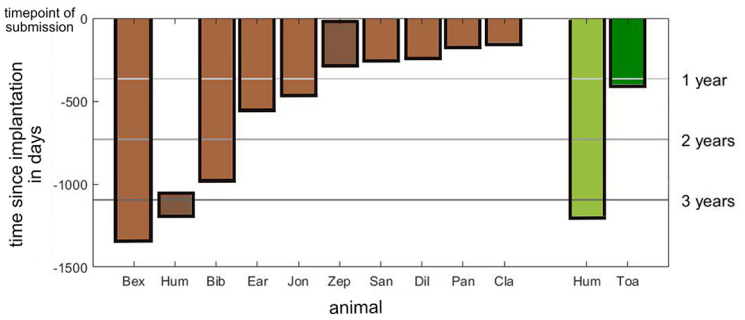

Figure 7. Summary of implant duration in days. Light brown bars indicate days since headpost implantation with still lasting functionality by the time of submission of this manuscript. Dark brown, Duration of two headposts, which lost their functionality. Light green, Extended chamber implanted on a discontinuous skull. Dark green, Days since implantation of the standard chamber-both still intact.

Figure 8. Example image of osseointegration of titanium headpost in bone of the skull.

underlying skull directly, tissue growth can create a gap between implant and bone over time, which may increase the risk of implant instability and infections (Betelak et al., 2001; Adams et al., 2007; Overton et al., 2017). Tightly fitting titanium implants, in contrast, can become integrated into the bone, preventing such unwanted tissue growth (McAndrew et al., 2012; Raphel et al., 2016). Also, thin implant strips on the bone, like the "legs" of our implant designs can be covered with skin. Stabilizing implants by form-fitting with cement requires anchoring screws in the bone. The overall larger volumes of cement which typically cannot be covered with skin, create larger skin openings with more extensive margins that need to be cleaned and protected against infections regularly. Screwing the implant directly to the bone, instead of using anchoring screws plus form-fitting with cement, also allows to adjust the pressure with which the implant presses against the bone when tightening the screws.

As an alternative, nonmolded implants, which are commercially available or produced in a standard shape without custom-fitting to the skull, could be used and be physically adjusted during surgery or before surgery when a 3D-printed skull replica is available as template. This method is limited by material constrains, though. Plastic materials mostly cannot be adjusted in shape by bending but only by cutting or filing off. Metal materials instead are difficult to cut or file off especially during surgery. Brittleness and reduced durability after hot-bending or forging prohibits larger changes in shape, for example for titanium implants (Adams et al., 2007; Ohayon and Tsao, 2012; Lanz et al., 2013; Overton et al., 2017). Physical cutting, filing or bending may lead to imperfect skull fitting, making the osseointegration more challenging as it can result in gaps between implant and bone. For large-scale implants precise fitting and the associated challenges are particularly relevant (Blonde et al., 2018).

More recent work suggests designing custom-fitted implants in 3D CAD programs ensuring a closer fit to the skull curvature compared with bending of commercially available standard implants (Mulliken et al., 2015; Johnston et al., 2016; Chen et al., 2017; Blonde et al., 2018). The proposed CAD-based 3D fitting procedures can successfully customize implant shapes, but commonly use the Boolean Difference method ("virtual cutting") to fit the skull curvature. Constant thickness of implants along the skull surface is difficult to achieve with cutting methods compared with bending. Virtual bending easily allows for thin implant structures to fit screws of constant length and with surface-normal orientation to both bone and implant for optimal direction of the forces, while still being covered by skin. By combining virtual cutting with virtual bending, as described in our guide, the design of a broad range of implants is possible, e.g., single piece headposts maintaining their leg thickness, extended, complex multicompartment implants, or standard chambers with legs, etc.

While previous methods require a certain proficiency in CAD programming, our aim was to provide a method that can be easily learned and used by nonproficient CAD users. Testing with users who were previously naive about CAD design showed that the guide with its tutorials allows designing of implants of decent complexity and custom-fit to individual animals within a few hours. The final virtual product can then be manufactured using both production pathways, CNC milling or 3D printing.

With our approach, we also wanted to target the challenge of custom-fitting implants for uneven animal skulls, especially skulls with discontinuities, e.g., holes. While such skull conditions probably are not encountered often, the possibility to re-implant otherwise healthy animals and thereby reduce the number of animals needed for a study, is especially relevant for large and long-living animal models, like nonhuman primates. These animals often underwent very time-consuming preparation for a study, e.g., behavioral training, additionally increasing their value. Approaches in human reconstructive surgery try to virtually reconstruct skulls with holes by producing a mirror image of the contralesional half of the skull (Ming-Yih et al., 2002; Singare et al., 2009). However, for this approach at least one unaffected hemisphere is necessary. We demonstrated successful application of our approach in an example for which skull discontinuities spread across both hemispheres. Our guide enabled us to design a headpost, an implant type matched to the skull by virtual bending while maintaining its thickness, and an extended chamber with its inlays for wireless recordings, which was fitted by virtual cutting, to fit the discontinuous skull. It allowed us to customize and plan the implants by including the skull discontinuities without removing other nontargeted uneven features of the skull as it is the case with common smoothing tools. The extended chamber is to date stable, well-integrated, and functional.

Further method refinement

Our guide makes use of different software packages of which only part of their functionality is used. Additional features might help optimizing the planning and implant design. For example, 3D slicer cannot only be used to extract a 3D skull and brain model but also to extract vascularity of the animal's brain (Extended Data). This can help to improve the surgery planning by avoiding major vasculature, which otherwise might complicate the access to the planned ROI during surgery. A contrasted MRI (e.g., using Gadovist) is necessary to make the blood vessels visible.

The presented and extracted 3D brain models in this guide show a less well-defined structure in the anterior brain regions. In our MRI scans, the distinction between brain and nonbrain tissue in this area is less distinct and clear as for the posterior part. The brain extraction can be improved by adding seeds for nonbrain tissue in the respective regions. As we did not target these anterior brain regions with our chamber implants, we did not invest time to optimize this aspect.

We attempted to use 3D printing techniques for extended chambers out of PEEK. We considered the resulting printed versions of the chamber not sufficiently smooth on the outside surfaces, even after several revisions. Also, the eyelets for screwing the implant to the bone could not be printed well enough. The same file could be printed in PLA during rapid prototyping without these problems, indicating that the yet not very common PEEK 3D printing technique itself might not be sufficient. However, this might become a valid option in the future. CNC milling did not cause any problems and the implants could be manufactured appropriately.

References

Adams DL, Economides JR, Jocson CM, Horton JC (2007) A biocompatible titanium headpost for stabilizing behaving monkeys. J Neurophysiol 98:993–1001.

Adams DL, Economides JR, Jocson CM, Parker JM, Horton JC (2011) A watertight acrylic-free titanium recording chamber for electrophysiology in behaving monkeys. J Neurophysiol 106:1581–1590.

Berger M, Calapai A, Stephan V, Niessing M, Burchardt L, Gail A, Treue S (2018) Standardized automated training of rhesus monkeys for neuroscience research in their housing environment. J Neurophysiol 119:796–807.

Berger M, Agha NS, Gail A (2020) Wireless recording from unrestrained monkeys reveals motor goal encoding beyond immediate reach in frontoparietal cortex. Elife 9:e51322.

Betelak KF, Margiotti EA, Wohlford ME, Suzuki DA (2001) The use of titanium implants and prosthodontic techniques in the preparation of non-human primates for long-term neuronal recording studies. J Neurosci Methods 112:9–20.

Blonde JD, Roussy M, Luna R, Mahmoudian B, Gulli RA, Barker KC, Lau JC, Martinez-Trujillo JC (2018) Customizable cap implants for neurophysiological experimentation. J Neurosci Methods 304:103–117.

Calapai A, Berger M, Niessing M, Heisig K, Brockhausen R, Treue S, Gail A (2017) A cage-based training, cognitive testing and enrichment system optimized for rhesus macaques in neuroscience research. Behav Res Methods 49:35–45.

Chen X, Possel JK, Wacongne C, van Ham AF, Klink PC, Roelfsema PR (2017) 3D printing and modelling of customized implants and surgical guides for non-human primates. J Neurosci Methods 286:38–55.

Dotson NM, Hoffman SJ, Goodell B, Gray CM (2017) A large-scale semi-chronic microdrive recording system for non-human primates. Neuron 96:769–782.

Dunne NJ, Orr JF (2002) Curing characterisitcs of acrylic bine cement. J Mater Sci Mater Med 13:17–22.

Evarts EV (1968a) A technique for recording the activity of subcortical neurons in moving animals. Electroencephalogr Clinl Neurophysiol 24:83–86.

Evarts EV (1968b) Methods for recording activity of individual neurons in moving animals. In: Methods in medical research, pp 241–250. Chicago: Year Book.

Ferrea E, Suriya-Arunroj L, Hoehl D, Thomas U, Gail A (2018) Implantable computer-controlled adaptive multielectrode positioning system. J Neurophysiol 119:1471–1484.

Galashan FO, Rempel HC, Meyer A, Gruber-Dujardin E, Kreiter AK, Wegener D (2011) A new type of recording chamber with an easy-to-exchange microdive array for chronic recordings in macaque monkeys. J Neurophysiol 105:3092–3105.

Gardiner TW, Toth LA (1999) Stereotactic surgery and long-term maintenance of cranial implants in research animals. Contemp Top Lab Anim Sci 38:56–63.

Johnston JM, Cohen YE, Shirley H, Tsunada J, Bennur S, Christison-Lagay K, Veeder CL (2016) Recent refinements to cranial implants for rhesus macaques (*Macaca mulatta*). Lab Anim (NY) 45:180–186.

Lanz F, Lanz X, Scherly A, Moret V, Gaillard A, Gruner P, Hoogewoud HM, Belhaj-Saif A, Loguet G, Rouiller EM (2013) Refined methodology for implantation of a head fixation device and chronic recording chambers in non-human primates. J Neurosci Methods 219:262–270.

McAndrew RM, Lingo VanGlider JL, Naufel SN, Helms Tillery SI (2012) Individualized recording chambers for non-human primate neurophysiology. J Neurosci Methods 207:86–90.

Ming-Yih L, Chong-Ching C, Chao-Chun L, Lun-Jou L, Yu-Ray C (2002) Custom implant design for patients with cranial defects. IEEE Eng Med Biol 21:38–44.

Mulliken GH, Bichot NP, Ghadooshahy A, Sharma J, Kornblith S, Philcock M, Desimone R (2015) Custom-fit radiolucent cranial implants for neurophysiological recording and stimulation. J Neurosci Methods 241:146–154.

Ohayon S, Tsao DY (2012) MR-guided stereotactic navigation. J Neurosci Methods 204:389–397.

Ormianer Z, Laufer BZ, Nissan J, Gross M (2000) An investigation of heat transfer to the implant-bone interface related to exothermic heat generation during setting of autopolymerizing acrylic resins applied directly to an implant abutment. Int J Oral Macillofac Implants 15:837–842.

Overton JA, Cooke DF, Goldring AB, Lucero SA, Weatherford C, Recanzone GH (2017) Improved methods for acrylic-free implants in non-human primates for neuroscience research. J Neurophysiol 118:3252– 3270.

Plecko M, Sievert C, Andermatt D, Frigg R, Kronen P, Klein K, Stübinger S, Nuss K, Bürki A, Ferguson S, Stoeckle U, von Rechenberg B (2012) Osseointegration and biocompatibility of different metal implants - a comparative experimental investigation in sheep. BMC Musculoskelet Disord 13:32.

Raphel J, Holodniy M, Goodman SB, Heilshorn SC (2016) Multifunctional coatings to simultaneously promote osseointegration and prevent infection of orthopaedic implants. Biomaterials 84:301–314.

Saleem K, Logothetis N (2012) A combined MRI and histology atlas of the rhesus monkey brain in stereotaxic coordinates. San Diego: Academic Press.

Sandhaeger F, von Nicolai C, Miller EK, Siegel M (2019) Monkey EEG links neuronal color and motion information across species and scales. Elife 8:e45645.

Schwarz DA, Lebedev MA, Hanson TL, Dimitrov DF, Lehew G, Meloy J, Rajangam S, Subramanian V, Ifft PJ, Li Z, Ramakrishnan A, Tate A, Zhuang KZ, Nicolelis MAL (2014) Chronic wireless recordings of large-scale brain activity in freely moving rhesus monkeys. Nat Methods 11:670–676.

Singare S, Lian Q, Wang WP, Wang J, Liu Y, Li D, Lu B (2009) Rapid prototyping assisted surgery planning and custom implant design. Rapid Prototyp J 15:19–23.

Treon JF, Sigmon H, Wright H, Kitzmiller KV (1949) The toxicity of methyl and ethyl acrylate. J Ind Hyg Toxicol 31:317–326.

Wegener D, Oh DQP, Lukaß H, Böer M, Kreiter AK (2021) Blood analysis of laboratory *Macaca mulatta* used for neuroscience research: investigation of long-term and cumulative effects of implants, fluid control, and laboratory procedures. eNeuro 8:ENEURO.0284-21.2021.

Chapter 3

Neural correlates of action effect anticipation during action planning in the frontoparietal reach network

3.1 Abstract

Every day, we execute voluntary actions to produce desired changes in our environment. These effects caused by our actions are assumed to be an integral part of action planning. But how and when the anticipation of action effects is involved during action planning needs yet to be identified.

Existing human psychophysics studies present contradicting results. Some studies claim bare anticipation of action effects is sufficient to activate the corresponding motor program supporting the ideomotor theory. Other studies conclude action effect anticipation can only be made use of after motor program selection.

In this study we address the role of action effect anticipation during planning by studying the underlying neural activity on single neuron resolution in rhesus macaques *(m.mulatta)*. We introduce a novel paradigm called the action effect anticipation task (AEA task), which links action effects immediately to one's own action. We recorded across the areas of the frontoparietal reach network using chronically implanted arrays.

Our results suggest that the anticipation of action effects is evident on a single neuron level in the dorsal premotor area (PMd) during action planning. Complementary results of population analysis using demixed PCA provide evidence of action effect anticipation's involvement during motor program selection, which is in line with the ideomotor theory, and during an internal simulation of the selected motor program prior to execution. We

place our findings in the theoretical framework of the internal model and propose a possible extension towards the planning phase.

3.2 Introduction

In daily life we perform actions to produce a desired change in our environment. These effects of our voluntarily produced actions have been studied extensively from the view of predictive coding (O'Neil and Schultz, 2018, Kok and Lange, 2015), mirror neurons (Killner et al., 2007), mismatch negativity (Baldeweg, 2007; Kimura, 2012; Stefanics et al., 2015) and prediction error (Matsumoto et al., 2007; Abe and Lee, 2011; Zarr and Brown, 2016). In short, these mechanisms imply we are constantly comparing the predicted action effect with the actual action effect measured by the sensory systems. These concepts can help explaining visuomotor adaptation (Wise et al., 1998; Mandelblat-Cerf, 2009; Stavisky et al., 2017). Propositions have been made on how action effects can be placed in a theoretical framework of the internal model (Francis and Wonham, 1976, Kawato and Wolpert,1998; Shadmehr and Krakauer, 2008; Stavisky et al., 2017). The internal model describes a neural system, which simulates the sensorimotor system and therefore enables it to predict the consequences of motor commands.

While we assume we have an understanding of action effects during action execution, the role of action effect anticipation during planning, so in other words during action preparation and prior to execution, remains unknown and highly controversial.

Since decades scientists have been collecting evidence for the role of action effect anticipation. On one hand, the ideo-motor theory was proposed by James (1890). It describes that the bare anticipation of action effects is sufficient to activate the corresponding motor program (Stock and Stock, 2004; Paelecke and Kunde, 2007). This theory is supported by several behavioral studies in humans using the dual-task Psychological Refractory Period (PRP) paradigm. Here, associations between keypresses and a subsequent visual or auditory cue are established as an action effect during a learning phase. Later, during the testing phase, participants have to multi-task by responding to two subsequent stimuli. The same keypresses are followed by either the compatible (expected) or incompatible (unexpected) action effect (Paelecke and Kunde, 2007; Janczyk and M., Kunde, 2010). Wirth and colleagues (2015) adopted this dual-task paradigm to a continuous task and trial-based task by introducing a mouse controlled avatar and concluded action effect anticipation precedes motor program selection.

Other studies criticize this interpretation of action effects are an integral part of actin selection and claim that action effect anticipation can only be used once the motor program is selected (Ziessler and Nattkemper, 2011; Ziessler et al., 2004). In these studies, an adapted flanker paradigm (Eriksen and Eriksen, 1974) was used. Participants first learned

associations between stimulus and effect letters establishing compatible (expected) action effect associations. During testing, the stimulus letters were presented flanked on both sides either resembling the compatible or incompatible letter.

It has been suggested to differentiate between stimulus-based (exogenous) and intention-based (endogenous) action effects (Pfister et al., 2010; 2011; Liu et al., 2019). Both paradigms mentioned earlier produce stimulus-based actions instead of actions, which are based on intrinsically motivated action effects and are therefore not necessarily ecologically relevant as they are not immediately linked to one's own action. Ziessler and colleagues (2012) additionally criticize that in real-life scenarios the presentation of an action effect before or during action execution is usually considered as a successfully completed action rather than as a source to trigger the action itself. Therefore, existing results could be partially artifacts of the experimental situation.

To our best knowledge, no evidence on single neuron resolution has been provided up to date for either of these theories. Previous studies with recorded single-unit activity in rhesus macaques *(macaca mulatta)* have demonstrated how action encoding can be separated in visual movement and motor movement in the premotor cortex (PMd, Shen and Alexander, 1997, Ochiai et al., 2002; Kuang et al., 2016) and parietal reach region (PRR, Kuang et al., 2016) during planning. However, these studies could not dissociated between the action effect direction (visual consequence direction), visual goal (goal location) and motor goal (endpoint of physical arm movement). For example, using a reversal prism together with a center-out reach task a dissociatin of motor and visual goal can be achieved, the visual consequence (visual arm movement direction) and visual goal coincide spatially (Kuang et al., 2016).

This study is the first study addressing the question of action effect anticipation during action planning in the frontoparietal reach network while dissociating visual goal from visual movement and motor movement on a single neuron resolution. We present the novel action effect anticipation task (AEA task), which links the action effects immediately to the action resembling a more ecologically valid scenario. In brief, AEA consists of a cursor (physical movement) and a responder (action effect) controlled by the cursor, which either follows the cursor direction or goes in the opposite direction.

In this context, we propose the following four hypotheses based on directional tuning properties of neurons (Georgopoulos, 1982;1986; Kalaska et al., 1983): The Null-hypothesis states we will not find any encoding, which can be explained by action effect direction (Fig.1). As a control, we expect, at least in the primary motor cortex, to find neurons tuned for the physical arm movement direction during movement (Hyp I). Our main hypotheses are that we will find neurons, which are tuned solely for the action effect direction (Hyp IIa) or neurons with mixed selectivity (tuned for the combination of physical movement with action effect direction) (Hyp IIb).

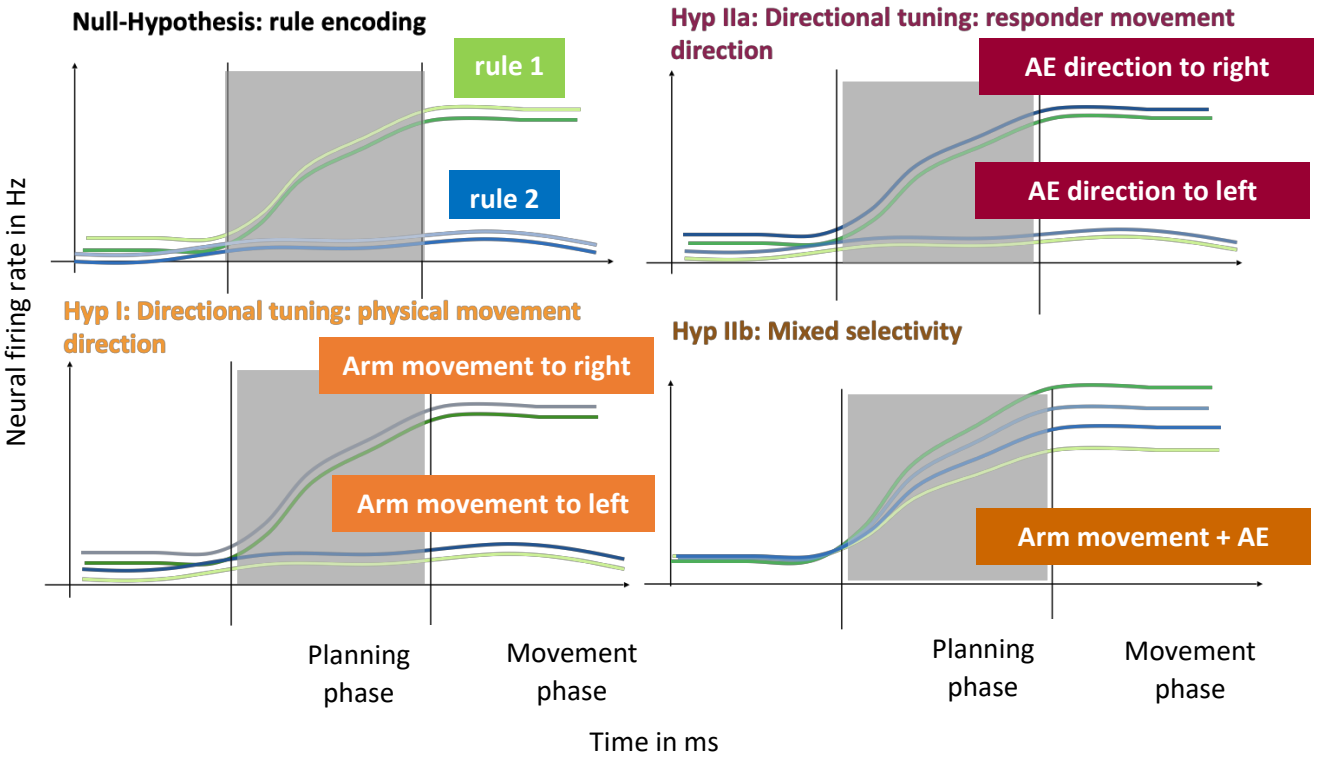

Figure 1: Hypothesis of AEA task: Null hypothesis stating on the neural level we find rule encoding. Hypothesis states that at least in M1 we find neurons, which are tuned for physical arm movement direction. Hypothesis IIa and b stipulate we find encoding for action effects during planning. Either we find neurons, which are solely tuned for action effect direction (Hyp IIa) or for combinations between physical arm movement direction and effect direction (Hyp IIb).

We report tuned neurons for only action effect direction as well as mixed selectivity in PMd and PRR, but not in M1. Our population analysis suggests action effects are involved already prior to action execution, which is in line with the ideomotor theory. Taken together we conclude action effects play a two-fold role as they are involved during motor program selection and during the internal simulation of the selected motor program prior to execution. We place our findings in the theoretical framework of the internal model and propose an extension towards action planning.

3.3 Results

We trained two adult rhesus macaques on the Action Effect Anticipation (AEA) task. The aim of the task is to move the responder (a rectangle) to the goal, which is the center of the screen. The responder is controlled by a cursor, which again is controlled by the monkey. The responders starting position can be either the right or left side of the screen. An additional stimulus in the center of the screen shows, whether the action effect, which is the movement direction of the responder relative to the cursor movement, follows the

cursor movement direction (non-inverse trial) or goes in the opposite direction of the cursor (inverse trial).

Action effect anticipation is represented in the frontoparietal reach network on single neuron level during action planning

To test our hypothesis of neural correlates for action effect anticipation during planning movement execution, we recorded simultaneously across the brain areas dorsal premotor cortex (PMd), primary motor cortex (M1) and parietal reach region (PRR), which together form the frontoparietal reach network. Figure 3 summarizes our results on a single neuron level. Based on our results, we can reject the null-hypothesis of pure rule encoding in the brain during action planning and prior to execution (movement onset is indicated with the vertical line, Fig. 3). As expected we find neurons, which have a preferred tuning for the physical arm movement direction in both animals, especially in M1 (Fig. 3A, first panel). Interestingly, in PMd we find two types of neurons: Neurons, which are tuned for the action effect direction (in line with Hyp IIa) and neurons with mixed selectivity, which are tuned for a combination of physical arm movement and action effect direction (in line with Hyp IIb). A general linear model (GLM) with stepwise regression was trained to calculate the percentage of tuned neurons for either action effect direction tuning (Fig. 3B, purple), physical movement direction (green) or interactions of action effect with movement direction (turquoise). In area PMd (monkey B), we find around 25% of neurons (12) present mixed selectivity for action effect and physical movement interactions and around 22% (10) tuned purely for action effect direction. Animal J's neural data shows around 26% (14) are tuned for interactions between action effect and physical movement direction and only 1% (2) are tuned for action effect direction only. In the mainly movement associated M1 we find with around 70% (36) neurons during planning, which are tuned for the upcoming physical movement and only 1% (3) for interaction between action effect and physical movement direction in animal B; 45% (22) are tuned for physical movement, 10%(7) for interactions between physical movement and action effect direction and 3% (4) for action effect movement direction in animal J. Across sessions (11 sessions for monkey B and 8 sessions for monkey J), we find that around 19 % of neurons are tuned for purely action effects and 21% for interactions in monkey B (Fig.3C). For monkey J we report around 8.5% of tuned neurons for action effects and 14.5% of neurons tuned for interactions ($p<0.05$, Wilcoxon Rank sum test).

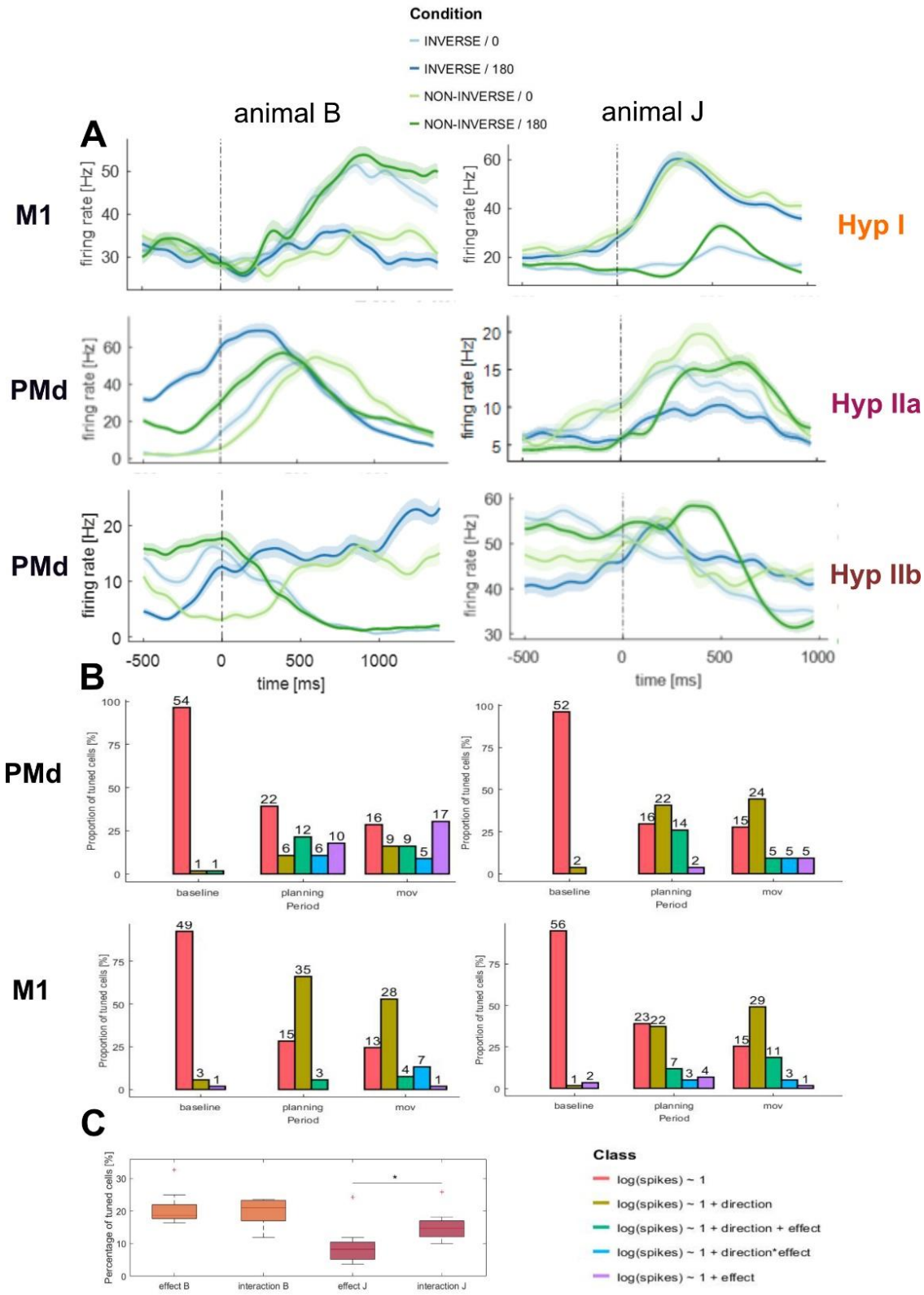
Condition
INVERSE / 0
INVERSE / 180
NON-INVERSE / 0
NON-INVERSE / 180
A
animal B
animal J
M1
PMd
PMd
Hyp I
Hyp IIa
Hyp IIb
firing rate [Hz]
time [ms]
B
PMd
M1
Proportion of tuned cells [%]
baseline
planning
mov
Period
C
Percentage of tuned cells [%]
effect B
interaction B
effect J
interaction J
Class
log(spikes) ~ 1
log(spikes) ~ 1 + direction
log(spikes) ~ 1 + direction + effect
log(spikes) ~ 1 + direction*effect
log(spikes) ~ 1 + effect

Figure 3: Single neuron results of recorded neural activity in PMd and M1. Panel A depicts example neural spike densities across all 4 conditions. The activity in M1 confirms our control hypothesis (Hyp I). Neurons in PMd present action effect encoding during action planning confirming both hypotheses (Hy IIa and Hyp IIb). Panel B describes the results of the general linear model to compute the proportions of tuned neurons in each brain area for both monkeys across 3 different task epochs (baseline, planning phase and movement phase).. Panel C depicts the average percentage of tuned neurons in both animals for area PMd across 11 and 8 sessions for monkey B and J respectively. Effect depicts the tuned neurons for action effect direction only, interaction the combination of action effect and physical arm movement direction and direction the physical arm movement direction.

Population analysis reveal action effect anticipation is involved during motor program selection in PMd and PRR

Next we analyzed how action effect anticipation is represented across the population of each brain area. First, we analyzed the neural trajectories of the population activity per recorded brain area from 1000ms before until 2500ms after the action effect stimulus was provided (Fig.4A, vertical line) assuming that before this cue not enough information is provided to perform the task correctly and therefore to plan the upcoming movement. We used principal component analysis (PCA) and plotted the second and third component (Fig.4A) since the first was mostly modulated by the trial structure. Around 200-300ms after cue onset the components separate in all four conditions in PMd while in M1 components only split for the physical movement direction (dark green and light blue vs dark blue and light green). As a single case, we can report PRR in animal J presents a selectivity for effect direction (light blue and green vs dark blue and green). The 3D trajectories (Fig. 4B) were plotted starting from action effect stimulus onset until the end of the planning phase (before movement onset). Results present all trajectories starting from the same point. However, for areas PMd in both animals and area PRR in animal J the trajectories split such that they can be distinctly identified across all four conditions. In M1 however, the 3D trajectories rather group together for the two physical movement directions, not action effect.

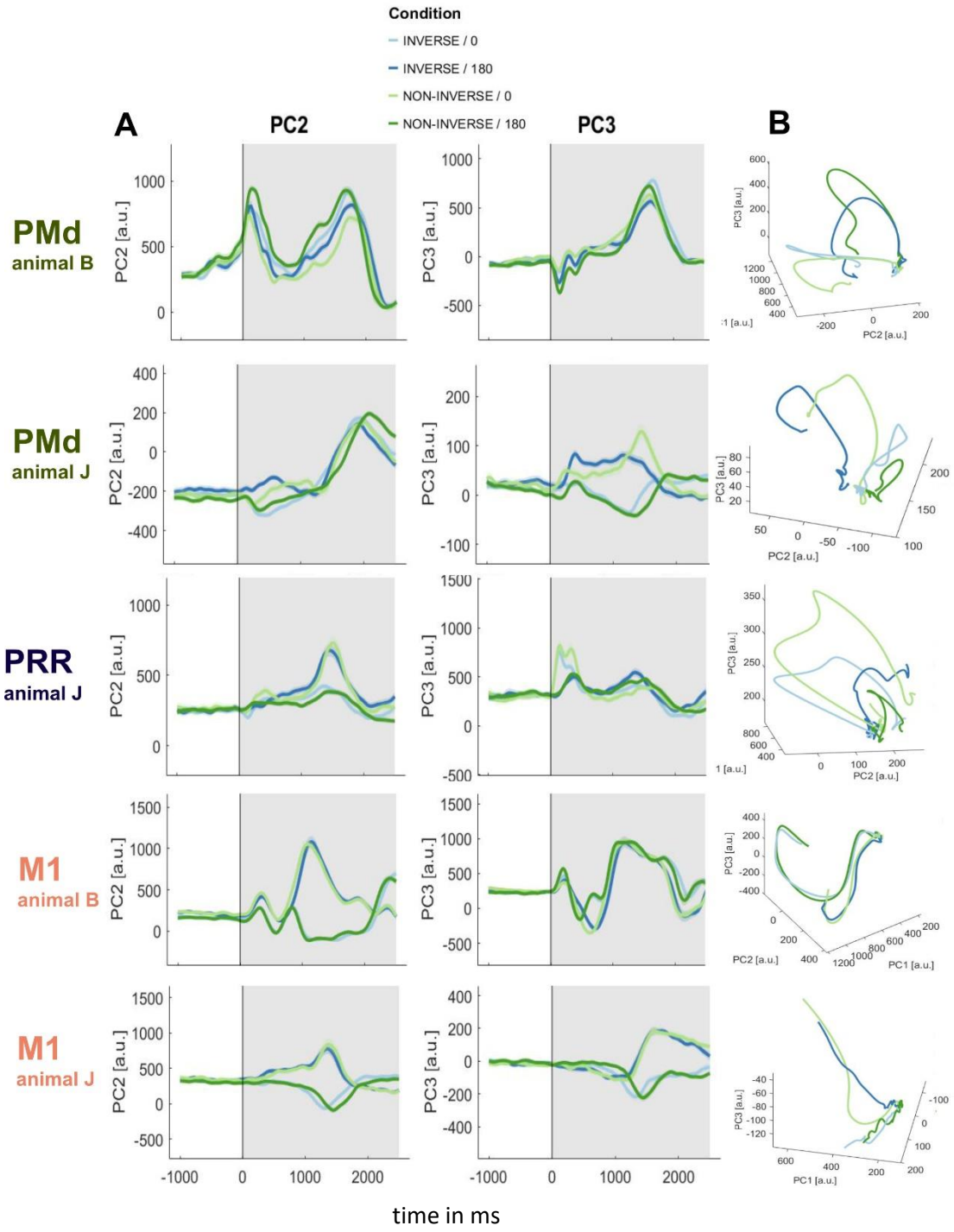

Figure 4: PCA results for both animals in area PMd, PRR and M1. Panel A depicts the second and third PC components after last cue onset until the end of the movement phase. Panel B depicts the 3D neural trajectories only for the planning phase. Areas PMd and PRR show a separation between action effect directions, M1 presents a separation of trajectories in physical arm movement direction.

Action effect components of population encoding explain variance during action planning in PMd and PRR, not M1

To further investigate whether the mixed selectivity evident from single neurons has an effect on our population analysis, we applied a demixed PCA (dPCA), which enables us to not only extract the underlying temporal dynamics but also assign which parameter of the task explains the effect. For better readability , we are showing only partial results in Fig.4. For the full result figures, please refer to supplementary S-Fig.1. Each panel consists of two rows. The upper row shows components with the highest variance explained based on the action effect and the lower panel shows components with the highest variance explained based on the physical movement direction. Additionally, the bar plot depicts each of the total 20 components and is color-coded by whether it explains the variance based on task irrelevant components (gray), action effect (turquoise), physical movement (yellow) or interactions between effect and physical movement (red). First we report our results in area PMd. We find that around 12% and 5 % of total variance in the data can be explained by the action effect in PMd during action planning in monkey B and monkey J respectively given this example session (Fig. 4A). Another 5% can be explained in monkey J by an interaction effect between action effect and physical movement direction. Around 10 % can be explained by the physical movement direction in animal B and 70% in animal J.

Most importantly, the time course of each component is similar for both monkeys. Before the last cue is provided, the animal does not know in which direction to move and therefore should not be able to plan the upcoming action. Right after the action effect stimulus (Fig.5, vertical line) the monkey has all information needed to plan and execute its upcoming action. Precisely after the stimulus onset both component types, action effect and physical action direction, start splitting and explaining the variance in the data, which is task dependent.

Next we report the results in area M1. We get 0.5% variance explained by action effects in monkey B and 2.8% in monkey J in area M1. As predicted, the majority of task relevant components are explained based on physical arm movement with 75% in animal B and 15.4% in animal J.

As a single case study we report in area PRR in animal J with 38% of variance can be explained by the action effect and 14% by the arm movement direction. However, the neural activity in PRR could not be demixed as clearly as in areas PMd and M1 (Fig. 5C).

Lastly, we compare these results across sessions (Fig. 5D). In animal B on average 9% is explained by action effects in PMd and only 1% in M1. 11% is explained by the physical arm movement in PMd and 31% in M1. Also in monkey J areas PMd and PRR are on average explaining 20% of the variance by action effects whereas in M1 it remains significantly below with only 4% ($p<0.001$, Wilcoxon rank sum test). The variance explained based on the physical movement direction is on average 45% in area PMd, 40% in M1 and 22% in PRR.

Areas PMd and PRR explain a significantly higher amount of variance based on action effects than area M1 ($p<0.001$, Wilcoxon rank sum test).

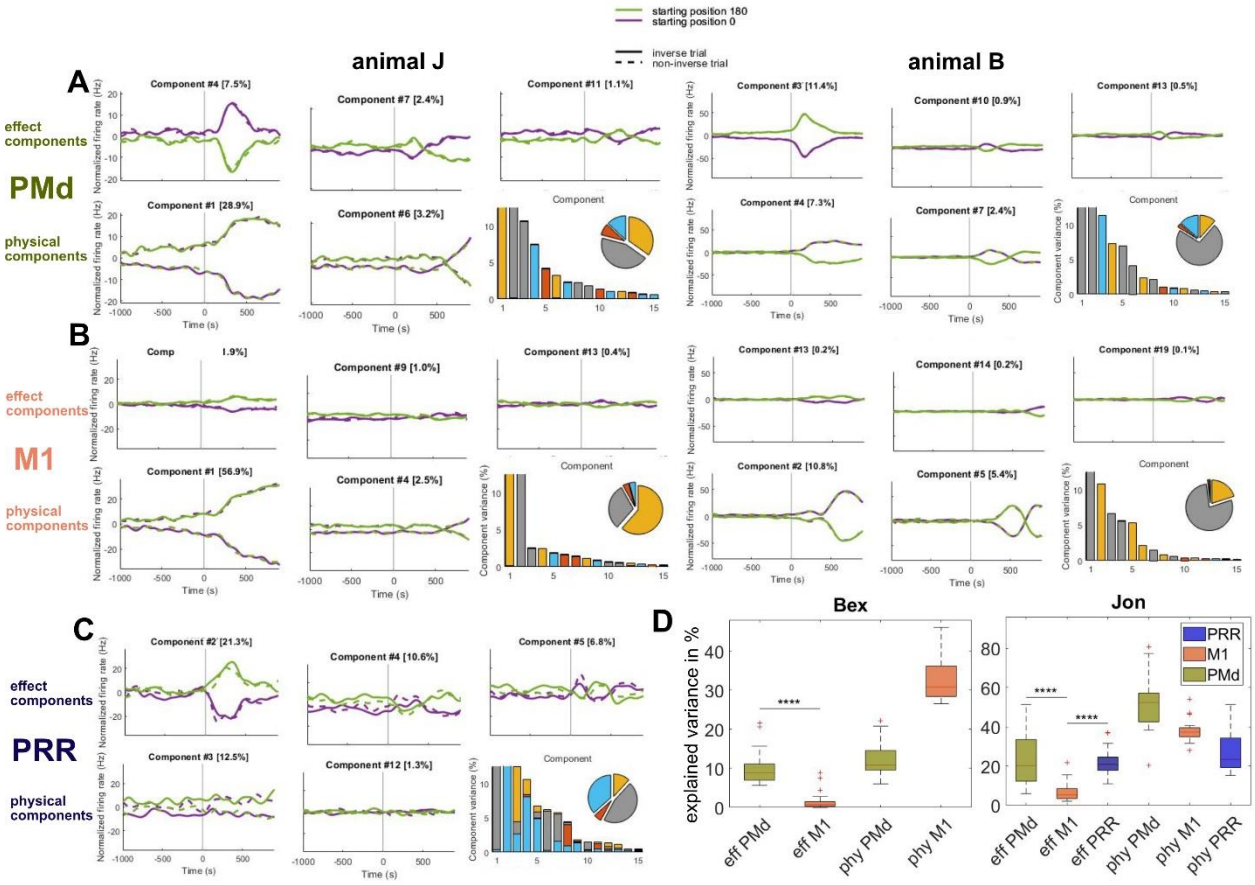

Figure 5: Simplified dPCA results of AEA task. Panel A to C depict the demixed PCA components, which explain the variance based on action effects (upper panel) and physical arm movement direction (lower panel) for the time window 1000ms before responder cue onset until 900ms after (planning phase). The bar and pie charts provide an overview of the explained variance by components. Panel D summarizes the percentage of explained variance based on effect or based on physical arm movement in areas PMd and M1 (left panel) for monkey B across 24 sessions, and areas PMd, M1 and PRR (right panel) for monkey J across 17 sessions.

If action effect anticipation is involved in internal simulation of the selected motor program, we hypothesize they are present only after response selection. If they are preceding response selection, they might be rather involved in selecting the motor program. Interestingly, the dPCA analysis shows that action effects can be demixed earlier than arm movement directions by on average 90ms in monkey B and 40ms in monkey J suggesting action effect anticipation is involved in motor program selection. However, in monkey B the onset difference is significantly larger than compared to monkey J (Fig 6, $p<0.01$, Wilcoxon rank sum test).

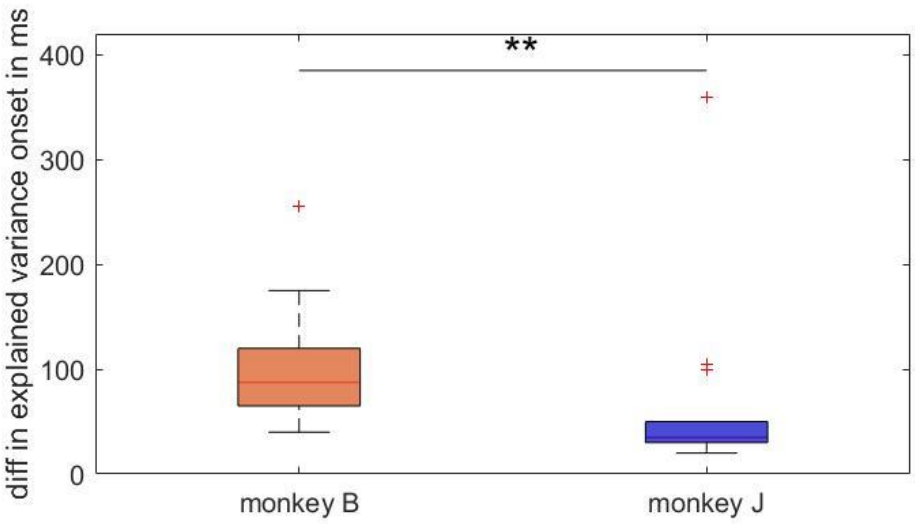

Figure 6: Averaged latency difference between demixing onset of physical movement and action effect. Difference above 0 implies the onset for action effect baked on the explained variance using dPCA precedes physical movement, difference below 0 means action effect follows physical movement. We calculated the difference across 16 sessions for animal B and 17 sessions for animal J.

3.4 Discussion

We designed a novel, ecologically more relevant paradigm called Action Effect Anticipation task (AEA) to investigate the role of action effect anticipation during action planning. We present on a single cell level that action effects are encoded during action planning in PMd and PRR but not in M1. We find representations of action effects encoding as mixed selectivity - combination of physical movement and effect movement direction. On the population level our results suggest that action effect anticipation precedes movement preparation suggesting they are involved in motor program selection as well, which is in line with the ideomotor theory.

No RT and MT differences across conditions

In existing paradigms, the mean of measuring the involvement stage of action effects is RT differences (Pfister et al., 2011; Pfister et al., 2014; Paelecke and Kunde, 2007; Ziessler et al.,2004). The underlying hypothesis is that action effect representation is evoked early during action planning. If then this activated action effect matches the later presented compatible action effect stimulus, response time (keypress time) is facilitated. If the activated action effect does not comply with the presented incompatible action effect, the response selection (correct key to press) is slowed down (Ziessler et al., 2012; Paelecke and Kunde, 2007).

Contrary to those paradigms, our AEA task does not contain the element of confirmation or disagreement meaning there is no perturbation of the anticipated action effect right before action execution. The monkeys prepare a response based on the cues provided and anticipate the action effects. These anticipated effects always match the expectation. Correspondingly, we do not find RT differences (S-Fig.1).

Single neuron encoding of action effect anticipation

Our results suggest action effect is encoded either as action effect direction only or as mixed selectivity on single neuron level confirming both of our hypotheses Hyp IIa and IIb (Fig.1). In animal B both types of neurons are present in PMd whereas in animal J the mixed selective neurons are dominant (Fig.3). This could hint towards a two-fold role of action effects during action planning. Action effects could be used for internal simulation of the selected motor program and for motor program selection by defining the goal based on the to-be-expected action effect.

Existing studies use varying timings to understand the role of action effect anticipation. Ziessler and colleagues (2012) tested the role of action effect anticipation with a modified perturbation task. In this task, participants first learned stimulus effect associations. Later, during the testing phase, first the stimulus cue is provided and after different stimulus onset asynchronies (SOAs) a Go-cue is presented together with either the compatible or incompatible action effects. Contrary to previous results the authors do not find an SOA related effect in RT difference suggesting action effect encoding might play a role in goal definition, so during motor program selection, as well as during internal simulation. Amongst the sparse literature of action effect anticipation with neural recordings, an ERP study in humans has suggested that action effect anticipation might play a role from perception to action (Nikolaev et al., 2008).

If the different representations of actions effects on the neural level are linked to different functions, we should be able to measure those. For this, we introduced an additional control condition, in which the monkeys had to integrate action effects more dynamically on a trial-by-trial basis (see *Methods*). While animal B, which shows strong action effect direction encoding on single neuron level (Fig.3), could generalize without difficulties presenting the same behavioral patterns in both conditions (main task condition and control condition), animal J, which shows a dominant mixed selectivity and is few neurons with pure action effect direction encoding, could not generalize towards the trial wise condition. This is in line with our hypothesis that animal J might be using action effects mainly for internal simulation of the selected motor program instead of motor program selection by defining the goal based on the to-be-expected action effect. Animal B might be using action effect anticipation for defining the goal as well for internal simulation (Fig.8).

Population encoding of action effect anticipation

As our brain consists of billions of neurons, we wanted to explore the population dynamics. To disentangle mixed selectivity of neurons in both animals, we applied demixed PCA. We provide two clear results. First, around 20% of variance of data can be explained by the action effect in PMd and PRR in both animals during action planning (Fig 5). Separation of the different components appears after the action effect stimulus (last stimulus) is presented and all necessary information is provided. Second, this separation starts earlier for those modulated by action effects than for physical movement in both animals showing that action effect encoding precedes physical arm movement encoding (Fig.6). Taken together, our findings favor the hypothesis that action effect anticipation is already utilized to define the action goal and to select the motor program, which is in line with the ideomotor theory.

Possible implications on our understanding of reference frames

Reference frames refers to a spatial framework, relative to which a movement or target location can be described. For instance gaze-centered reference frames involves spatial coordinates relative to the eyes and have been shown to be present in area PRR (Batista et al.,1999; Buneo et al., 2002; Chang and Synder, 2010). It has been shown that this spatial selectivity is independent of immediate visual input at the target location (Gail and Andersen, 2006; Hwang and Andersen, 2012).

Physical goal encoding can relate to two aspects of an arm movement: either to the endpoint of the arm movement relative to gaze (gaze-centered reference frame) or to the physical movement direction relative to the starting positin of the hand (hand-centered reference frame). Ochiai et al., 2005 have shown that neurons in the ventral premotor cortex encoded movements in a hand-centered reference frame while these neurons were spatially selective for the visual rather than physical movement.

Kuang and colleagues (2016) dissociated the physical endpoint of the arm movement (hand-centered reference frame) from the visual goal (eye-centered reference frame) by using a center-out reach task together with a reversal prism. However, in their experiment they could not dissociate between the visual goal and the visual consequence (visual arm movement) as both switched coherently from task to task (left right on the screen). In our study we overcame this limitation by using an out-centered instead of center-out paradigm therefore keeping the visual goal steady in the center of the scree thereof not coinciding with the movement direction of the visual consequence (responder movement).

Our findings show a spectrum of neural activity patterns for spatial encoding and support the speculation by Kuang and colleagues (2016) that this spectrum of spatial encoding might be specific to task context and might serve as a mediator between different frames of references, which are relevant to cope with the current spatial behavioral demands.

Extending the internal model towards action planning phase

The role of action effects during action execution has been studied extensively in the context of predictive coding (O'Neil and Schultz, 2018, Kok and Lange, 2015) and prediction error (Matsumoto et al., 2007; Abe and Lee, 2011; Zarr and Brown, 2016). It has been formulated in a theoretical framework of the internal model (Shadmehr and Krakauer, 2008; orange panel, Fig.8). It proposes that our neural system predicts the sensory outcome of movements using an efference copy of the motor command used to generate this movement (Wolpert & Kawato, 1998).

While this concept has been established for the action execution phase (orange panel, Fig.8), the role of action effects during action planning (purple panel, Fig.8) still remains unknown. It has been proposed that the premotor cortex does not represent purely the intended motion but rather the goal, which is strongly involved in decision-making processes (Cisek, 2005; Klaes et al., 2011). Based on results from behavioral studies in humans it was suggested to differentiate between desired and anticipated action effects (Ziessler et al., 2011). Desired effects represent the goal while anticipated action effects are rather representing the expected effects after motor program selection prior to motor execution. Provided our results, we propose a potential extension of the internal model towards the action planning phase in line with literature (Blakemore et al., 2002; Ziessler et al., 2011). We theorize that action effects play a two-fold role during planning. First, the anticipation of action provides a basis for selecting the motor goal and therefore are directly involved in motor program selection. Second, the selected motor program is internally monitored before action execution based on the possible action effect.

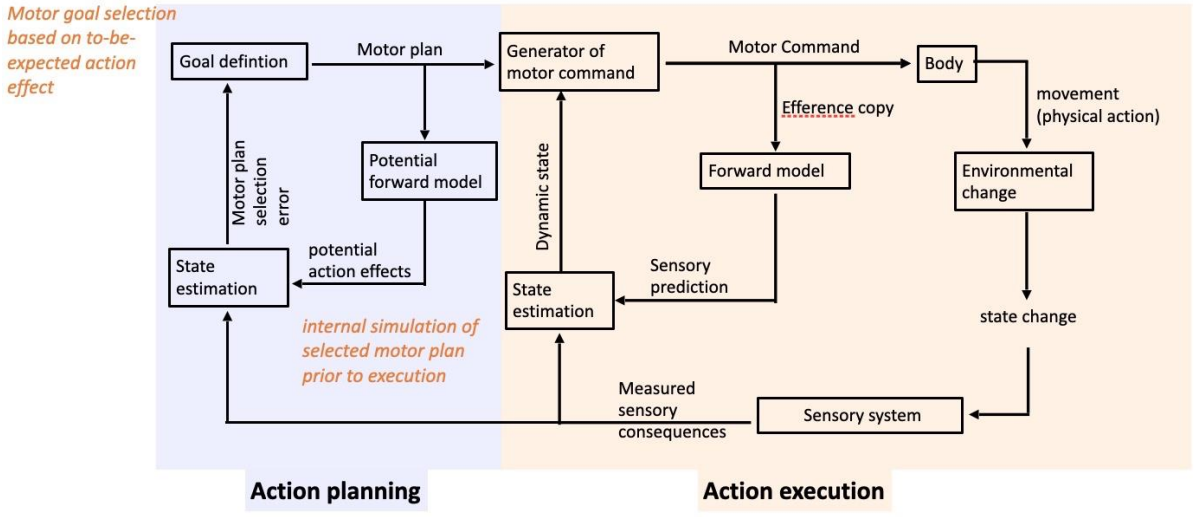

Figure 8: Internal model of adaptive feedback control and a proposed extensions towards the action planning phase. The orange panel summarizes based on Shadmehr and Krakauer (2008) the current understanding of action effects and their role during action execution. The purple panel describes apotential extension of the internal model towards the action planning phase. in line with Kuang et al., 2016, our results suggest that action effects play a twofold role during action planning. Action effects are involved in response selection by the goal selection based on to-be-expected sensory action effects. Additionally, it might be involved during an internal monitoring process of the selected motor program prior to execution.

However, which brain area would be the source of the forward model needs yet to be identified. Desmurget and colleagues (1999) have proposed that the posterior parietal cortex computes a dynamic motor error to correct ongoing movements. Takei and colleagues (2021) have recently found evidence that PMd is involved in generating goal-directed motor corrections, hence it might be involved in generating the forward model. The explicit source still needs to be identified and could be a potential question for future studies.

Action effect anticipation or spatial attention?

As our action effect cue is presented on one of the two peripheral sides of the screen (*Methods*), a potential explanation for the neural correlate could be purely spatial attention to the responder stimulus (Pellegrino, G. D., & Wise, 1993; Lebedev and Wise, 2001). Studies have presented evidence that while the majority of premotor neurons represent motor preparation, around 30% represent spatial attention (Boussaoud and Kermadi 1997; Boussaoud and Wise 1993a,b)

We attempted to control for this by introducing the covering areas *(see Methods)*, which range up to the center of the screen (uncovered center of screen 90mm width, 11.8° visual angle) keeping spatial attention towards the center of screen throughout the trials. Nevertheless, it is possible that spatial attention is directed towards the stimulus appearance position behind the covering area. To test this and under the assumption that the location of spatial attention is represented in gaze direction (Moore et al., 2003), we recorded the main condition without enforcing eye fixation across 4 sessions (S-Fig.4). We find differences in gaze for different trial conditions. However, these differences cannot explain effects of spatial attention.

Encoding differences between endogenous or exogenous action effects?

Our AEA paradigm evokes endogenous action effects. However, it would be interesting to compare whether the neural correlates on a single neuron level are different between endogenous and exogenous action effects as it has been suggested (Pfister et al., 2011; Ziessler et al., 2012). To provide some first evidence, we recorded the task in a block wise manner in which the monkeys can ignore the responder stimulus during planning as it appears from the same side and only consider it during movement to move the responder to the goal. Our results do not indicate a systematic difference in neural encoding between the block wise and semi-block wise condition (S-Fig.5). However, further studies are necessary to investigate and compare endogenous and exogenous action effects more systematically.

3.5 Methods

Experimental setting

Task design

As we wanted our task to be ecologically closer to real life scenarios, our task design is an version of the daily situation “reverse park a car in a parking slot”. In the left panel of Fig.9, x marks the visual goal, which is a representation of a parking lot. The aim of this task is to reverse park the car (responder) or a car with a trailer attached to it in the given parking slot (goal). In the task, the cursor is controlled by the monkey and the responder is controlled by the cursor. In non-inverse conditions (green square) the responder follows the direction of the cursor; in inverse conditions (blue square) the responder moves in the opposite direction of the cursor.

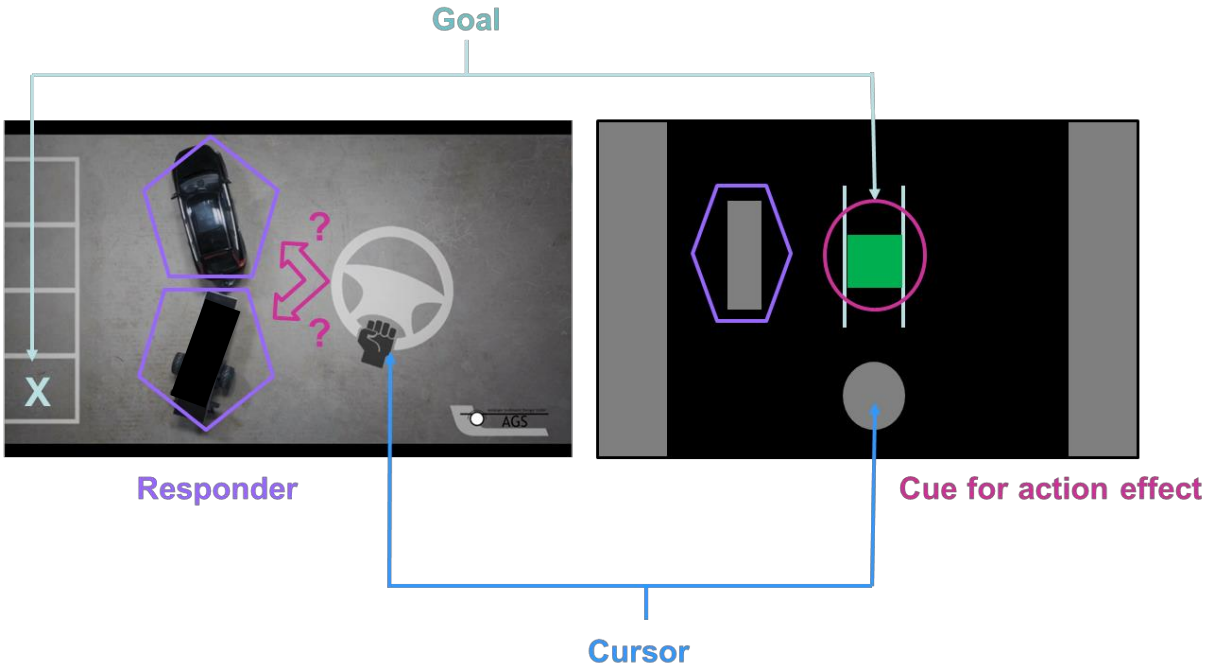

Figure 9: Task concert overview. Left panel depicts the real life example of reverse parking the car into a parking lot with or without a trailer attached to it. Right panel shows our AEA task paradigm resembling the real life example.

This task design allows us to dissociate the relevant parameters action effect direction (responder movement direction), action goal (visual goal), and physical action direction (arm movement direction) when we compare two conditions against each other (Fig. 10).

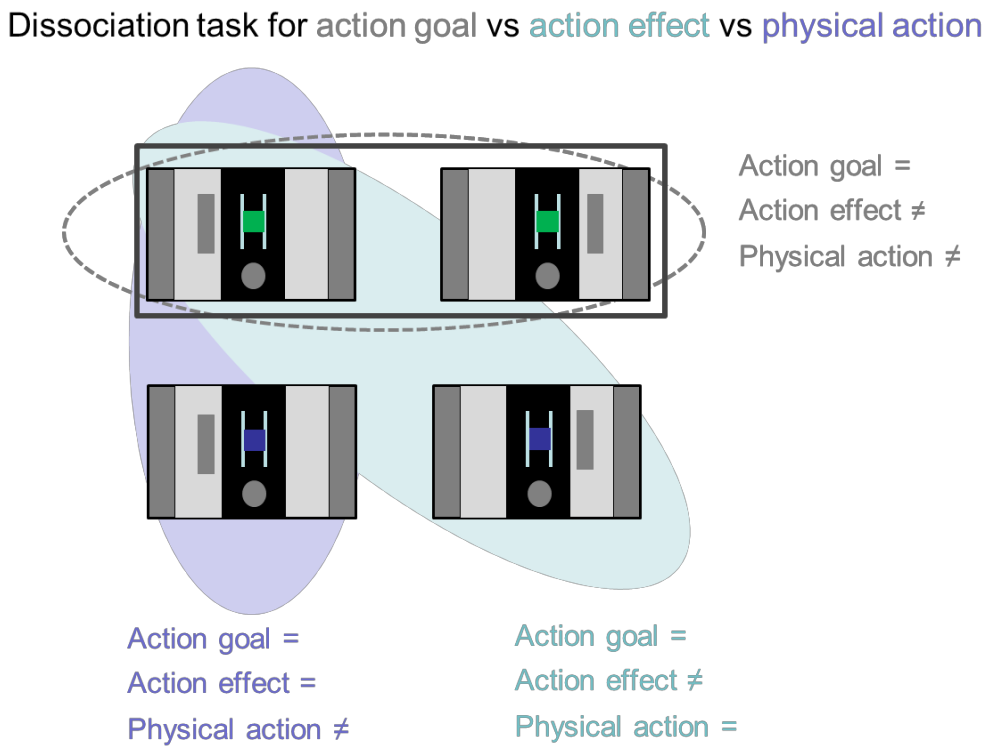

Figure 10: Overview of the 4 task conditions. Purple ellipse: When comparing these two conditions, when the starting position of the responder stimulus is identical but the action effects are difference, the parameters action goal are identical in both (=), the action effect is identical (=) as in both cases the movement direction of the responder will go from left towards right and the physical action are different (≠) as in the upper case the cursor needs to be moved towards the right and in the lower case the cursor needs to be moved towards the left. Green ellipse: Comparison of these conditions will maintain the action goal and the physical action (cursor needs to be moved to the right in both cases) but the action effects are different (≠), as the responder will move to the right in the upper, left case and to the left in the lower, right case.Grey ellipse: action effect and physical action are different when comparing both conditions, only action goal remains the same.

Artificial Finger (ArFi)

The Action Effect Anticipation task is a swiping task requiring continuous contact with the touchscreen. As the monkey's hands are often not clean enough to guarantee precise contact session by session we developed a sliding artificial finger (ArFi, Fig.11). The finger consists of a metal rod with a soft patch protection, which is used for furniture protection against scratches. A spring behind the rod allows continuous adjustment of the finger pressure (rod) to the touch screen. The animal controls the ArFi by holding the black grip with his full hand and sliding the ArFi to the left or to the right. The continuous x- and y-coordinates are sent from the touchscreen to the main PC controlling the experiment (C++, OpenGL). The eye position was detected by a video-based eye tracker with a sampling rate of 1 kHz (EyeLink 1000 Plus, SR Research, Ottawa, Canada).

Figure 11: Artificial finger (ArFi). The black handle is manipulated by the monkeys allowing them to slide the artificial finger (white stab) along the touchscreen to perform a swiping task.

Task timeline

In the following, we explain the detailed timeline of the task. The task is initiated by placing the cursor displayed with a yellow circle (diameter = 20 mm) in the gray fixation square (30 mm; 4.3° visual angle) on the bottom of the screen (Fig.12). This cursor is controlled by the ArFi.

This is immediately followed by displaying a red eye fixation square (10mm, 1.4° visual angle, fixation tolerance 3.6° visual angle) in the center of the screen that needs to be fixated throughout the entire trial. This red square is placed on top of a gray square (effect cue, 30mm, 4.3° visual angle) in the center of the screen. After acquiring both fixations (hand and eye), the animal needs to maintain the fixations for 600 to 900 ms (uniform distribution). Then the effect cue changes its color for 300 ms. It turns either green indicating a non-inverse trial type, which implies the responder will move in the same direction as the cursor; or blue indicating an inverse trial type implying the responder will move in the opposite direction of the cursor's movement direction. Once the effect cue turns back gray, the gray covering areas on both sides (130 x 180mm) are removed revealing the responders starting position (dimensions: 30 x 80mm, 100mm above the cursor) under one of them for the duration of 300 ms. The covering area re-appears to cover the responder cue leaving an uncovered area open in the center of the screen (90mm width, 12.8° visual angle). The monkey has to withhold movement execution for a delay period of 600 to 1100 ms. This Go-cue is indicated by the disappearance of the effect cue (gray square in the center of the screen). The trial is successfully completed when the cursor is moved such that the responder is placed in the space between the two vertical lines in the center of the screen (goal, distance between both vertical lines 35mm, 5° visual angle). An overshooting of the responder across the goal results in trial abortion. Throughout the trials

the gain between distance of cursor movement and distance of responder movement was varied between 1.0 (responder cue and cursor move equidistantly) and 0.6 (responder cue moves by only 60% of the distance relative to the cursor movement) to enhance the direct link and sense of control between cursor and responder cue.
The main condition was recorded in a semi block wise condition. In this condition the action effect type stays the same within a block but the starting position of the responder cue is selected randomly such that in case of a failed trial the condition is put back to the pot of potential directions until it is resolved. The block size was 20 hits. We additionally recorded this task in the trial wise condition, in which the action effect types as well the responder cue starting position are randomized across each trial. At last, we recorded block wise sessions with block size of 50 hits, in which neither the responder's starting position nor the action effect type changed.

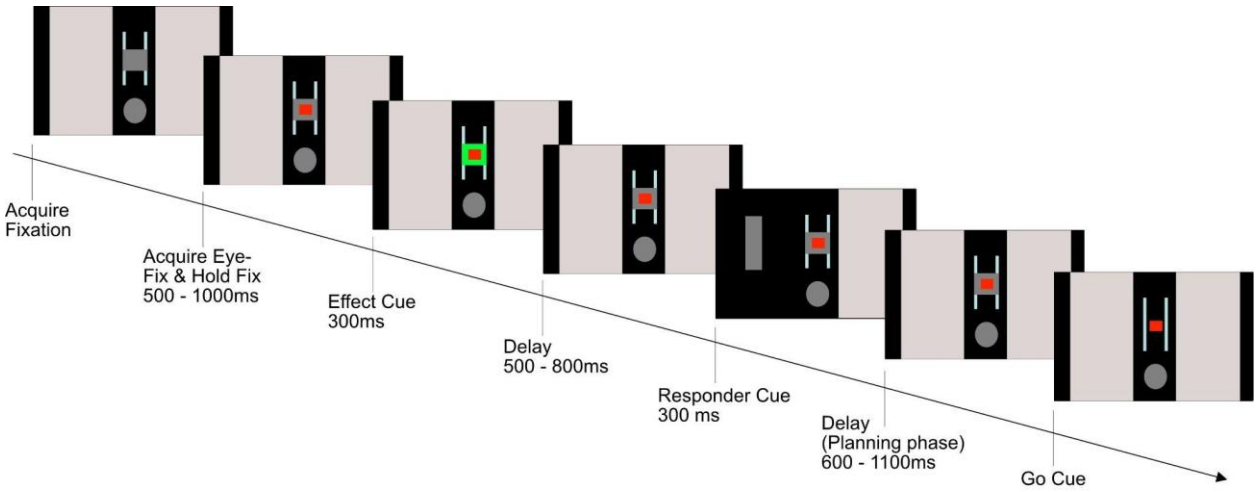

Figure 12: Implemented timeline of the AEA task.

Animals and Surgery

We trained two adult male rhesus macaques (monkey B 16 kg, monkey J 8.9 kg) on the AEA task who had no prior experience in performing experiments before entering this study. Both animals were trained on sitting in the primate chair using positive reinforcement training. Once they got accustomed to the setup and learned the AEA task, they were implanted with custom designed and fitted implants (Ahmed et al., 2022). Both animals were implanted on the left hemisphere (contralateral to their hand, which they use to perform the task) with 8 floating microwire arrays, 32 electrodes each (250 micro electrode separation, impedance 0.1 to 0.4 MOhm, Microprobes for LifeScience, Gaithersburg, Maryland, USA). We implanted 2 arrays in PMd, M1, S1 and PRR for each monkey resulting in 256 channels in total. The array connectors were placed in a custom-designed (Ahmed et

al., 2022) array connector surrounded by a custom fitted chamber, which is suited also for wireless neural recordings (Berger et al., 2020).
All animals are housed in social groups with one to two male conspecifics in facilities of the German Primate Center. The facilities provide cage sizes exceeding the requirements by German and European regulations, access to an enriched environment including wooden structures and various toys and enrichment devices (Calapai et al., 2017; Berger et al., 2018).
Each custom-fitted implant was implanted during a single sterile surgery under deep gas anesthesia and analgesia via an intravenous catheter. Additionally, the animals receiving a craniotomy were prophylactically treated with systemic antibiotics cobactan, duphamox, or synulox 1 d presurgery and 2–5 d post-surgery. Analgesia was refreshed on a 8- to 9-h cycle continuously for up to three post-surgical days for non-craniotomy types of surgery (e.g., headpost implantation) and four to five postsurgical days for surgeries with craniotomies (e.g. chamber implantation) using levomethadone or rimadyl, depending on need.
All procedures have been approved by the responsible regional government office [Niedersächsisches Landesamt für Verbraucherschutz und Lebensmittelsicherheit (LAVES)] under permit numbers 3392 42502-04-13/1100 and 33.19-42502-04-18/2823 and comply with German Law and the European Directive 2010/63/EU regulating use of animals in research.

Behavioral data analysis

For behavioral analysis we used events recorded from the main task controlling PC and identified the successful trials. We then used the timestamps of the 'Go cue' and calculated when the touchscreen registered an ArFi movement. We set this calculated point as the movement onset point. For further analysis we calculated the reaction times (RT) and movement times (MT). RT was calculated by the difference between go cue onset and cursor movement onset; MT was calculated by the difference between cursor movement onset and the time point of acquiring the target successfully, which is defined as the time point of responder moving onto the goal.

Neural data analysis

Data acquisition

We recorded with eight 32-channel digital CerePlex M Blackrock headstages (Blackrock Microsystems LLC, Salt Lake City, USA) to record from two arrays per brain area (PMd, M1, S1, PRR) per session simultaneously with a sampling rate of 30kHz per channel. The recorded and digitized signal was sent to the Cerebus Neural Processor Blackrock Microsystems LLC, Salt Lake City, USA). We recorded the raw signal as well as a high-pass filtered signal (250Hz Butterworth filter 4th order), which was thresholded at -4.5 x RMS.

Single unit analysis

For single unit analysis we sorted 11 sessions of monkey B and 8 from monkey J manually using the Plexon Offline Spikesorter (Plexon, Inc, Dallas, Texas, USA). We calculated the spike density function from the spikes of each unit, which exceed the average firing rate of 2 Hz, by convoluting the spike trains (spike event times) with a Gaussian kernel (σ = 50 ms). Spike counts and spike density functions (sampled at 200 Hz) were temporally aligned to the start and end point of each trial, whereby the start point reflected the previously calculated movement onset and the end point was defined by the reward or error signal for each trial.

To quantify how many neurons were tuned for physical movement direction or effect direction (responder movement direction), we used a generalized linear model with a stepwise regression (stewiseglm(); Matlab 2018b) with poisson distribution to model spike counts. We used effect direction - the starting position of the responder cue - and physical movement direction, which is a combination of starting position of the responder cue with condition type (inverse or non-inverse) as the categorical predictors. Details about GLM with stepwise regression can be found in McCullagh, P. (1983). In summary, after running the model (with p-value <0.01 predictor added; with p-value >0.05 predictor removed), we can get up to 5 resulting models noted as followed (Wilkinson-Rogers notation):

(model 1.1) spike count ~ 1
includes neurons, which are not tuned to any of the predictors or their combinations

(model 1.2) spike count ~ 1 + direction
contains neurons, which are tuned for movement direction (physical arm movement);

(model 1.3) spike count ~ 1 + effect
entails neurons, which are tuned for effect direction

(model 1.4) spike count ~ 1 + direction + effect
Includes neurons, which are tuned for the combination of movement with effect direction

(model 1.5) spike count ~ 1 + direction * effect
contains neurons, which are tuned for interaction between movement and effect directio.

We applied this model for the epochs ‘baseline’, which is 500 ms of holding the fixation point; ‘planning phase’, 900ms after responder cue (last cue) onset and ‘movement phase’, from movement onset until 1500ms after onset.
We applied the Lilliefors test to test the data with the null-hypothesis of normal distribution. When the null-hypothesis was rejected, we used the non-parametric Wilcoxon rank sum test for statistical significance test.

Population analysis

For population analysis using PCA and dPCA we included all sessions, sorted or unsorted, based on Trautmann et al.,2019, who systematically tested and found that spike sorting did not change the results on population level significantly. Additionally, we compared 2 sessions of monkey B and monkey J by calculating the dPCAs of spike sorted and unsorted neurons within the same session (S-Fig.5) concluding the results of Trautmann and colleagues (2019) can be confirmed in our dataset.

Principle Component Analysis (PCA)

To analyze population dynamics, we projected our high-dimensional data onto a low-dimensional space using principal component analysis (PCA). In brief, for each condition we calculated the trial average response of individual neurons in a matrix $\boldsymbol{R_c}$ of size $\boldsymbol{t} \times \boldsymbol{n}$, with $\boldsymbol{t}$ the samples over time starting from planning until movement end and $\boldsymbol{n}$ the number of neurons. We then concatenated the individual condition-averaged matrices to on matrix $\boldsymbol{R}$ with shape $\boldsymbol{tc} \times \boldsymbol{n}$, where $\boldsymbol{t}$ is the number of time points, $\boldsymbol{c}$ the number of conditions, and $\boldsymbol{n}$ the number of neurons. In order to avoid single neurons with high firing rate to dominate the computation, we z-scored the matrix by subtracting the row-average and dividing by the row standard deviation.

Applying PCA to matrix $\boldsymbol{R}$ produces a lower dimensional representation $\boldsymbol{W}$ by:

$$\boldsymbol{W} = \boldsymbol{RC}$$

where $\boldsymbol{C}$ is a transformation matrix of size $\boldsymbol{n} \times \boldsymbol{q}$, with $\boldsymbol{n}$ the number of units and $\boldsymbol{q}$ the number of components. Each row of $\boldsymbol{W}$ is a linear combination of the rows in $\boldsymbol{R}$. The transformation matrix $\boldsymbol{C}$ is found by minimizing the reconstruction error between the projection $\boldsymbol{W}$ and the actual data:

$$L = \|\boldsymbol{R} - \boldsymbol{RCC}^{\mathrm{T}}\|^2$$

The components in $\boldsymbol{C}$ are constrained to be orthogonal to each other and are ordered by how much variance of the data they capture. Here, we looked at the first 3 components as they were capturing most of the variance (over 90%).

In order to project the trial-by-trial data onto the low-dimensional space, we multiplied the trial matrix $\boldsymbol{R_t}$ with the transformation matrix $\boldsymbol{C}$. Single trial data was then averaged across conditions and plotted with 95%-confidence interval.

Demixed PCA

To disentangle mixed selectivity, we used demixed principal component analysis (dPCA) introduced by Kobak et al. (2016). Similarly, to standard PCA, dPCA reduces the dimensionality of the input data. However, it additionally takes task parameters into account: each of the resulting components is related to only one task dimension making it easier to interpret. This is achieved by reconstructing the condition averages $\boldsymbol{R_c}$ instead of actual data and additionally introducing an encoder axis to reconstruct the data. Therefore, the reconstruction error can be formulated as:

$$L = \|\boldsymbol{R_c} - \boldsymbol{RCE}\|^2$$

With $\boldsymbol{E}$ being the encoder matrix. Each row in $\boldsymbol{E}$ reflects one demixed principal component (dPC) again sorted by the amount of variance explained in the data. In contrast to standard PCA, these components are not constrained to be orthogonal to each other since they are computed individually for each task parameter.

As a result, one can compute how much of the variance in the data can be explained by components reflecting changes in action effects, the physical movement, or a combined effect of both. For each session we fitted the dPCA individually. Then we extracted the amount of variance explained by each task parameter and averaged these values across sessions.

References

Abe, H., & Lee, D. (2011). Distributed coding of actual and hypothetical outcomes in the orbital and dorsolateral prefrontal cortex. *Neuron*, *70*(4), 731-741. doi:10.1016/j.neuron.2011.03.026

Aflalo, T.N, Graziano, S.A. (2007). Relationship between Unconstrained Arm Movements and Single-Neuron Firing in the Macaque Motor Cortex. *Journal of Neuroscience*, 27(11), 2760-2780. doi: 10.1523/JNEUROSCI.3147-06.2007.

Baldeweg, T. (2007). ERP repetition effects and mismatch negativity generation: A predictive coding perspective. *Journal of Psychophysiology*, *21*(3-4), 204. doi: 10.1027/0269-8803.21.34.204.

Blakemore, S. J., Wolpert, D. M., & Frith, C. D. (2002). Abnormalities in the awareness of action. Trends in cognitive sciences, 6(6), 237-242. doi: 10.1016/S1364-6613(02)01907-1.

Boussaoud, D., & Kermadi, I. (1997). The primate striatum: neuronal activity in relation to spatial attention versus motor preparation. *European Journal of Neuroscience*, *9*(10), 2152-2168. doi: 10.1111/j.1460-9568.1997.tb01382.x.

Boussaoud, D., Wise, S.P. Primate frontal cortex: effects of stimulus and movement. *Exp Brain Res* 95, 28–40 (1993). doi: 10.1007/BF00229651.

Boussaoud, D., Wise, S.P. Primate frontal cortex: neuronal activity following attentional versus intentional cues. *Exp Brain Res* 95, 15–27 (1993). doi: 10.1007/BF00229650.

Chase, S. M., Kass, R. E., & Schwartz, A. B. (2012). Behavioral and neural correlates of visuomotor adaptation observed through a brain-computer interface in primary motor cortex. *Journal of neurophysiology*, *108*(2), 624-644. doi: 10.1152/jn.00371.2011.

Cisek, P. Neural representations of motor plans, desired trajectories, and controlled objects. *Cogn Process* 6, 15–24 (2005). doi: 10.1007/s10339-004-0046-7.

Desmurget, M., Epstein, C. M., Turner, R. S., Prablanc, C., Alexander, G. E., & Grafton, S. T. (1999). Role of the posterior parietal cortex in updating reaching movements to a visual target. Nature neuroscience, 2(6), 563-567. doi: 10.1038/9219.

Eriksen, B.A., Eriksen, C.W. Effects of noise letters upon the identification of a target letter in a nonsearch task. *Perception & Psychophysics* 16, 143–149 (1974). doi: 10.3758/BF03203267.

Francis, B. A., & Wonham, W. M. (1976). The internal model principle of control theory. *Automatica*, *12*(5), 457-465. doi: 10.1016/0005-1098(76)90006-6.

Hocherman, S., & Wise, S. P. (1991). Effects of hand movement path on motor cortical activity in awake, behaving rhesus monkeys. Experimental brain research, 83(2), 285-302. doi: 10.1016/j.cub.2021.01.049.

Kilner, J. M., Friston, K. J., & Frith, C. D. (2007). Predictive coding: an account of the mirror neuron system. *Cognitive processing*, *8*(3), 159-166. doi: 10.1007/s10339-007-0170-2.

Gail, A., & Andersen, R. A. (2006). Neural dynamics in monkey parietal reach region reflect context-specific sensorimotor transformations. *Journal of Neuroscience*, *26*(37), 9376-9384. doi: 10.1523/JNEUROSCI.1570-06.2006.

Georgopoulos, A. P., Kalaska, J. F., Caminiti, R., & Massey, J. T. (1982). On the relations between the direction of two-dimensional arm movements and cell discharge in primate motor cortex. *Journal of Neuroscience*, *2*(11), 1527-1537. doi: 10.1523/JNEUROSCI.02-11-01527.1982.

Georgopoulos, A. P., Schwartz, A. B., & Kettner, R. E. (1986). Neuronal population coding of movement direction. *Science*, *233*(4771), 1416-1419. doi:10.1126/science.3749885.

Golub, M. D., Byron, M. Y., & Chase, S. M. (2015). Internal models for interpreting neural population activity during sensorimotor control. *Elife*, *4*, e10015.doi: 10.7554/eLife.10015.

James, W. (1890). The principles of psychology (2 vols.). New York: Holt

Janczyk, M., Kunde, W. Does dorsal processing require central capacity? More evidence from the PRP paradigm. *Exp Brain Res* 203, 89–100 (2010). doi: 10.1007/s00221-010-2211-9.

Kalaska, J.F., Caminiti, R. & Georgopoulos, A.P. Cortical mechanisms related to the direction of two-dimensional arm movements: relations in parietal area 5 and comparison with motor cortex. *Exp Brain Res* 51, 247–260 (1983). doi: 10.1007/BF00237200.

Wolpert, D. M., & Kawato, M. (1998). Multiple paired forward and inverse models for motor control. *Neural networks*, *11*(7-8), 1317-1329.doi: 10.1016/S0893-6080(98)00066-5.

Kilner, J. M., Friston, K. J., & Frith, C. D. (2007). The mirror-neuron system: a Bayesian perspective. *Neuroreport*, *18*(6), 619-623. doi: 10.1097/WNR.0b013e3281139ed0.

Kimura, M. (2012). Visual mismatch negativity and unintentional temporal-context-based prediction in vision. *International Journal of Psychophysiology*, *83*(2), 144-155. doi: 10.1016/j.ijpsycho.2011.11.010.

Kobak, D., Brendel, W., Constantinidis, C., Feierstein, C. E., Kepecs, A., Mainen, Z. F., & Machens, C. K. (2016). Demixed principal component analysis of neural population data. *Elife*, *5*, e10989. doi: 10.7554/eLife.10989.

Kok, P., & Lange, F. P. D. (2015). Predictive coding in sensory cortex. In *An introduction to model-based cognitive neuroscience* (pp. 221-244). Springer, New York, NY.

Kurata, K., Wise, S.P. Premotor and supplementary motor cortex in rhesus monkeys: neuronal activity during externally- and internally-instructed motor tasks. *Exp Brain Res* 72, 237–248 (1988). doi: 10.1007/BF00250247.

Pfister, R., Pfeuffer, C. U., & Kunde, W. (2014). Perceiving by proxy: Effect-based action control with unperceivable effects. *Cognition*, *132*(3), 251-261. doi: 10.1016/j.cognition.2014.04.012.

Kuang, S., Morel, P., & Gail, A. (2016). Planning movements in visual and physical space in monkey posterior parietal cortex. *Cerebral cortex*, *26*(2), 731-747. doi: 10.1093/cercor/bhu312.

Lebedev, M. A., & Wise, S. P. (2001). Tuning for the orientation of spatial attention in dorsal premotor cortex. *European Journal of Neuroscience*, *13*(5), 1002-1008. doi: 10.1046/j.0953-816x.2001.01457.x.

Liu, K., Hu, W., & Chen, Y. (2019). Encoding of Stimulus-driven and Intention-driven Actions in Monkey's Primary Motor Cortex. In *Proceedings of the 2019 6th International Conference on Biomedical and Bioinformatics Engineering* (pp. 99-106). doi: 10.1145/3375923.3375945.

Mandelblat-Cerf, Y., Paz, R., & Vaadia, E. (2009). Trial-to-trial variability of single cells in motor cortices is dynamically modified during visuomotor adaptation. *Journal of Neuroscience*, *29*(48), 15053-15062. doi: 10.1523/JNEUROSCI.3011-09.2009.

Matsumoto, M., Matsumoto, K., Abe, H. *et al.* Medial prefrontal cell activity signaling prediction errors of action values. *Nat Neurosci* 10, 647–656 (2007). doi: 10.1038/nn1890.

McCullagh, P. (1983). Generalized Linear Models (2nd ed.). Routledge. doi: 10.1201/9780203753736.

Moore, T., Armstrong, K. M., & Fallah, M. (2003). Visuomotor origins of covert spatial attention. Neuron, 40(4), 671-683. doi: 10.1016/S0896-6273(03)00716-5.

Nikolaev, A. R., Ziessler, M., Dimova, K., & van Leeuwen, C. (2008). Anticipated action consequences as a nexus between action and perception: evidence from event-related potentials. *Biological Psychology*, *78*(1), 53-65.doi: 10.1016/j.biopsycho.2007.12.010.

O'Neill, M., & Schultz, W. (2018). Predictive coding of the statistical parameters of uncertain rewards by orbitofrontal neurons. *Behavioural brain research*, *355*, 90-94. doi: 10.1016/j.bbr.2018.04.041.

Ochiai, T., Mushiake, H., & Tanji, J. (2002). Effects of image motion in the dorsal premotor cortex during planning of an arm movement. *Journal of neurophysiology*, *88*(4), 2167-2171. doi: 10.1152/jn.2002.88.4.2167.

Paelecke, M., & Kunde, W. (2007). Action-effect codes in and before the central bottleneck: evidence from the psychological refractory period paradigm. *Journal of Experimental Psychology: Human Perception and Performance*, *33*(3), 627. doi: 10.1037/0096-1523.33.3.627.

Pellegrino, G. D., & Wise, S. P. (1993). Effects of attention on visuomotor activity in the premotor and prefrontal cortex of a primate. *Somatosensory & motor research*, *10*(3), 245-262. doi: 10.3109/08990229309028835.

Pfister, R., Kiesel, A. & Hoffmann, J. Learning at any rate: action–effect learning for stimulus-based actions. *Psychological Research* 75, 61–65 (2011). doi: 10.1007/s00426-010-0288-1.

Shadmehr, R., Krakauer, J.W. A computational neuroanatomy for motor control. *Exp Brain Res* 185, 359–381 (2008). doi: 10.1007/s00221-008-1280-5.

Shen, L., & Alexander, G. E. (1997). Preferential representation of instructed target location versus limb trajectory in dorsal premotor area. *Journal of neurophysiology*, *77*(3), 1195-1212. doi: 10.1152/jn.1997.77.3.1195.

Stavisky, S. D., Kao, J. C., Ryu, S. I., & Shenoy, K. V. (2017). Trial-by-trial motor cortical correlates of a rapidly adapting visuomotor internal model. *Journal of Neuroscience*, *37*(7), 1721-1732. doi: 10.1523/JNEUROSCI.1091-16.2016.

Stefanics, G., Astikainen, P., & Czigler, I. (2015). Visual mismatch negativity (vMMN): a prediction error signal in the visual modality. *Frontiers in human neuroscience*, *8*, 1074. doi: 10.3389/fnhum.2014.0107.

Stock, A., Stock, C. A short history of ideo-motor action. *Psychological Research* 68, 176–188 (2004). doi: 10.1007/s00426-003-0154-5.

Wirth, R., Pfister, R., Janczyk, M., & Kunde, W. (2015). Through the portal: Effect anticipation in the central bottleneck. *Acta Psychologica*, *160*, 141-151. doi: 10.1016/j.actpsy.2015.07.007.

Wise, S., Moody, S., Blomstrom, K. *et al.* Changes in motor cortical activity during visuomotor adaptation. *Exp Brain Res* 121, 285–299 (1998). doi: 10.1007/s002210050462.

Zarr, N., & Brown, J. W. (2016). Hierarchical error representation in medial prefrontal cortex. *NeuroImage*, *124*, 238-247. doi: 10.1016/j.neuroimage.2015.08.063.

Zhang, M., Barash, S. Neuronal switching of sensorimotor transformations for antisaccades. *Nature* 408, 971–975 (2000). doi: 10.1038/35050097.

Ziessler, M., Nattkemper, D., & Vogt, S. (2012). The activation of effect codes in response preparation: new evidence from an indirect priming paradigm. *Frontiers in psychology*, *3*, 585. doi: 10.3389/fpsyg.2012.00585.

Ziessler, M., & Nattkemper, D. (2011). The temporal dynamics of effect anticipation in course of action planning. *Quarterly Journal of Experimental Psychology*, *64*(7), 1305-1326. doi: 10.1080/17470218.2011.553067.

Ziessler, M., Nattkemper, D. & Frensch, P.A. (2004). The role of anticipation and intention in the learning of effects of self-performed actions. *Psychological Research* 68, 163–175. doi: 10.1007/s00426-003-0153-6.

Supplementary

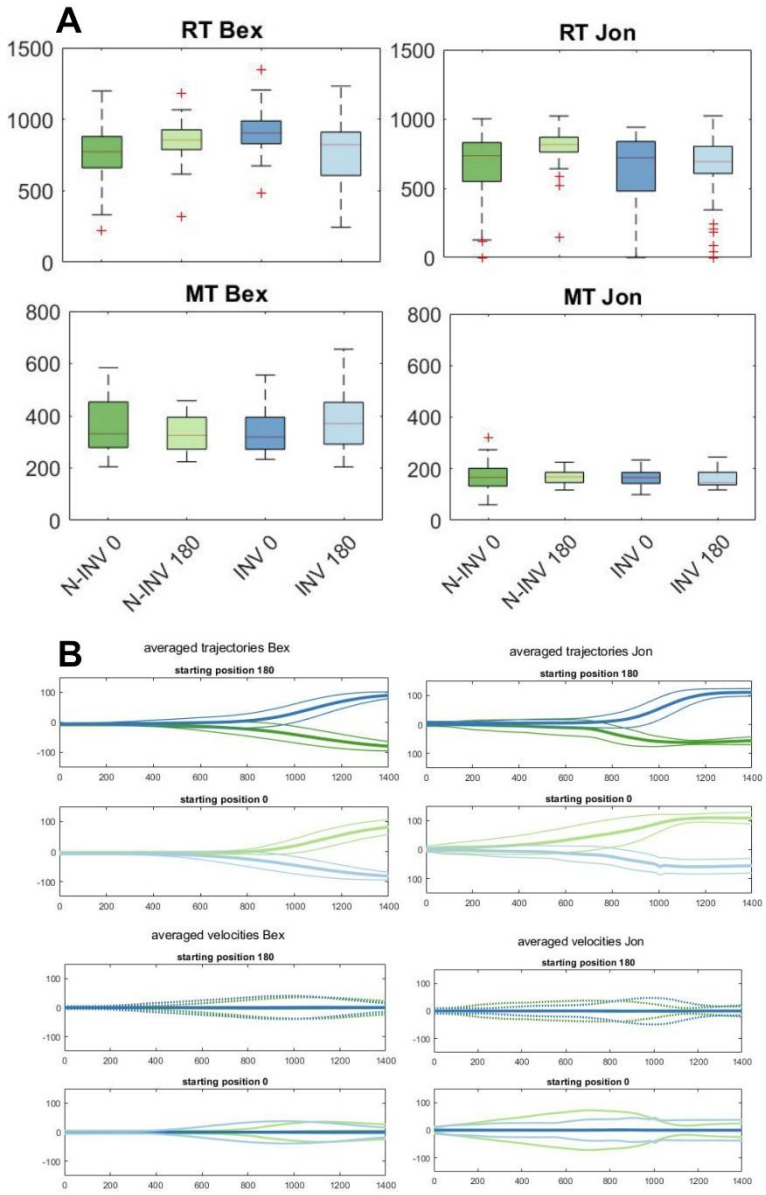

S-Figure 1: Behavioral data of both monkeys performing AEA. Panel A describes the reaction times (RT) and movement times (MT) of both monkeys across all 4 tested conditions. Panel B presents the averaged movement trajectories across all 4 conditions. Monkey B shows a constant movement profile whereas monkey J has a rather abrupt and fast movement.

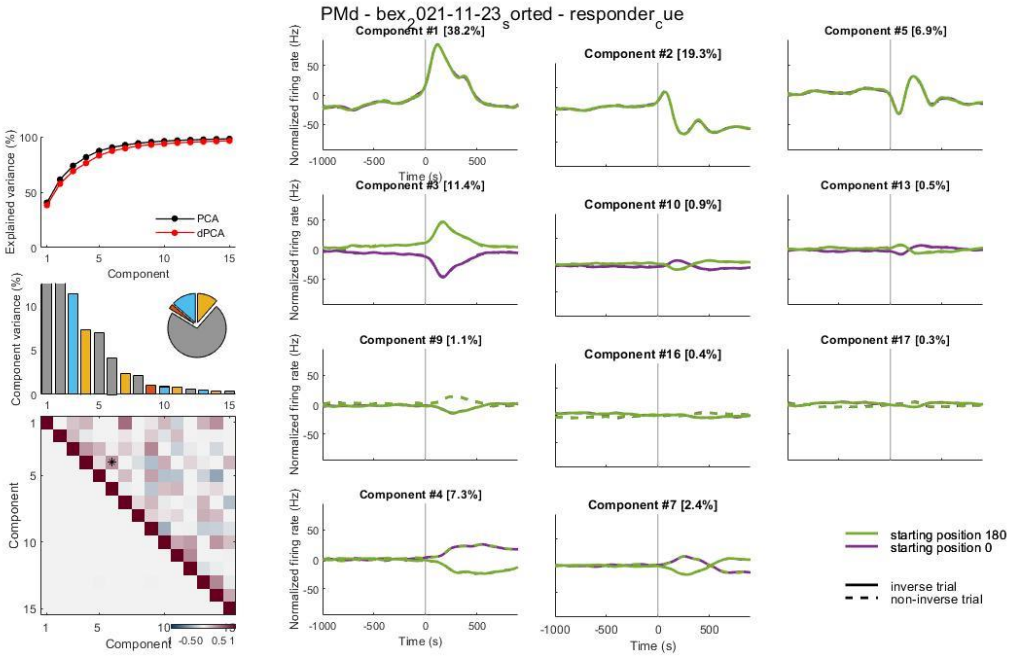
PMd - bex_2021-11-23_sorted - responder_cue
Component #1 [38.2%]
Component #2 [19.3%]
Component #5 [6.9%]
Component #3 [11.4%]
Component #10 [0.9%]
Component #13 [0.5%]
Component #9 [1.1%]
Component #16 [0.4%]
Component #17 [0.3%]
Component #4 [7.3%]
Component #7 [2.4%]
Normalized firing rate (Hz)
Time (s)
Explained variance (%)
Component
PCA
dPCA
Component variance (%)
starting position 180
starting position 0
inverse trial
non-inverse trial

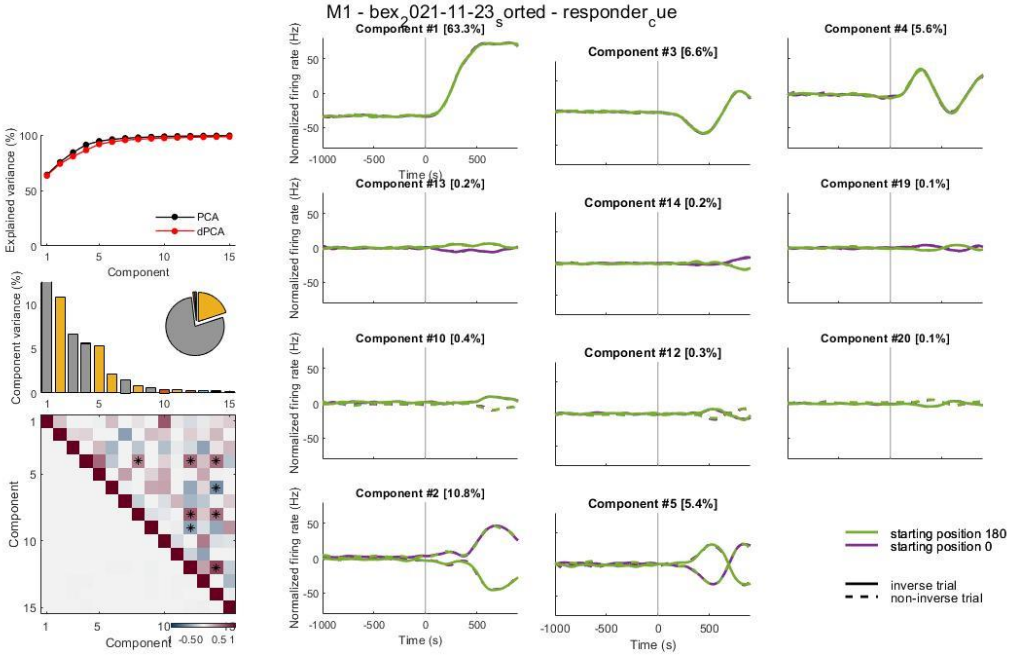
M1 - bex_2021-11-23_sorted - responder_cue
Component #1 [63.3%]
Component #3 [6.6%]
Component #4 [5.6%]
Component #13 [0.2%]
Component #14 [0.2%]
Component #19 [0.1%]
Component #10 [0.4%]
Component #12 [0.3%]
Component #20 [0.1%]
Component #2 [10.8%]
Component #5 [5.4%]
Normalized firing rate (Hz)
Time (s)
Explained variance (%)
Component
PCA
dPCA
Component variance (%)
starting position 180
starting position 0
inverse trial
non-inverse trial

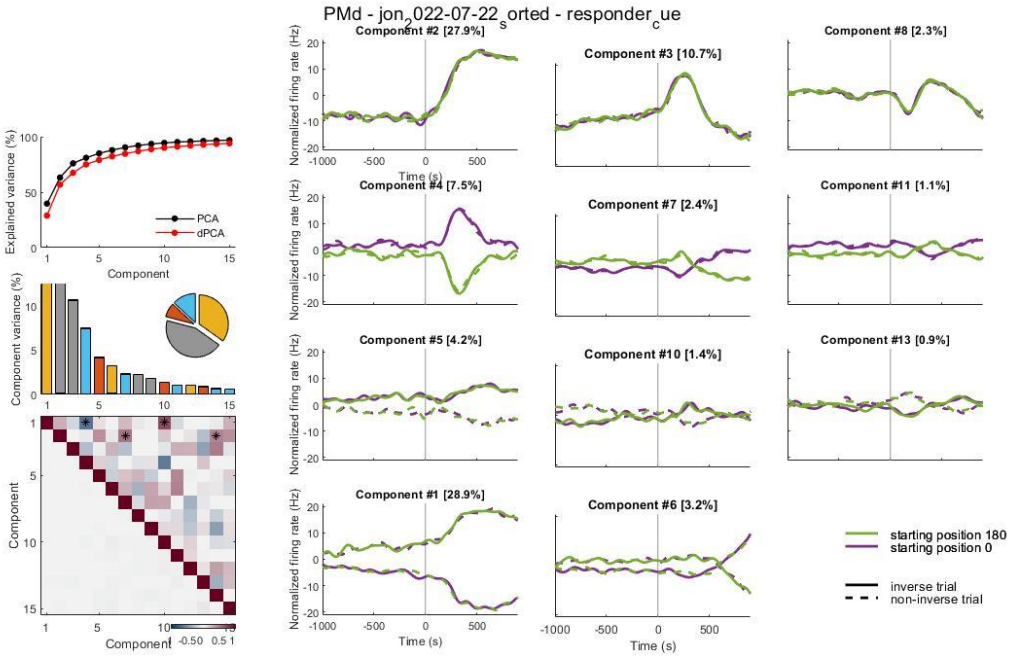
PMd - jon_2022-07-22_sorted - responder_cue
Component #2 [27.9%]
Component #3 [10.7%]
Component #8 [2.3%]
Component #4 [7.5%]
Component #7 [2.4%]
Component #11 [1.1%]
Component #5 [4.2%]
Component #10 [1.4%]
Component #13 [0.9%]
Component #1 [28.9%]
Component #6 [3.2%]
Explained variance (%)
PCA
dPCA
Component
Component variance (%)
Normalized firing rate (Hz)
Time (s)
starting position 180
starting position 0
inverse trial
non-inverse trial

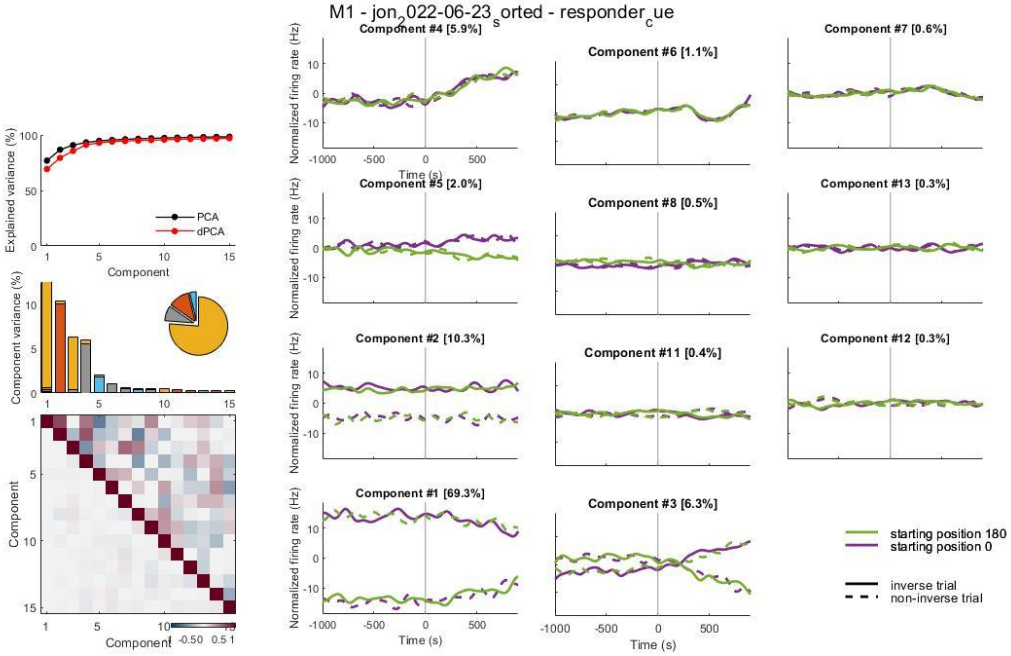
M1 - jon_2022-06-23_sorted - responder_cue
Component #4 [5.9%]
Component #6 [1.1%]
Component #7 [0.6%]
Component #5 [2.0%]
Component #8 [0.5%]
Component #13 [0.3%]
Component #2 [10.3%]
Component #11 [0.4%]
Component #12 [0.3%]
Component #1 [69.3%]
Component #3 [6.3%]
Explained variance (%)
PCA
dPCA
Component
Component variance (%)
Normalized firing rate (Hz)
Time (s)
starting position 180
starting position 0
inverse trial
non-inverse trial

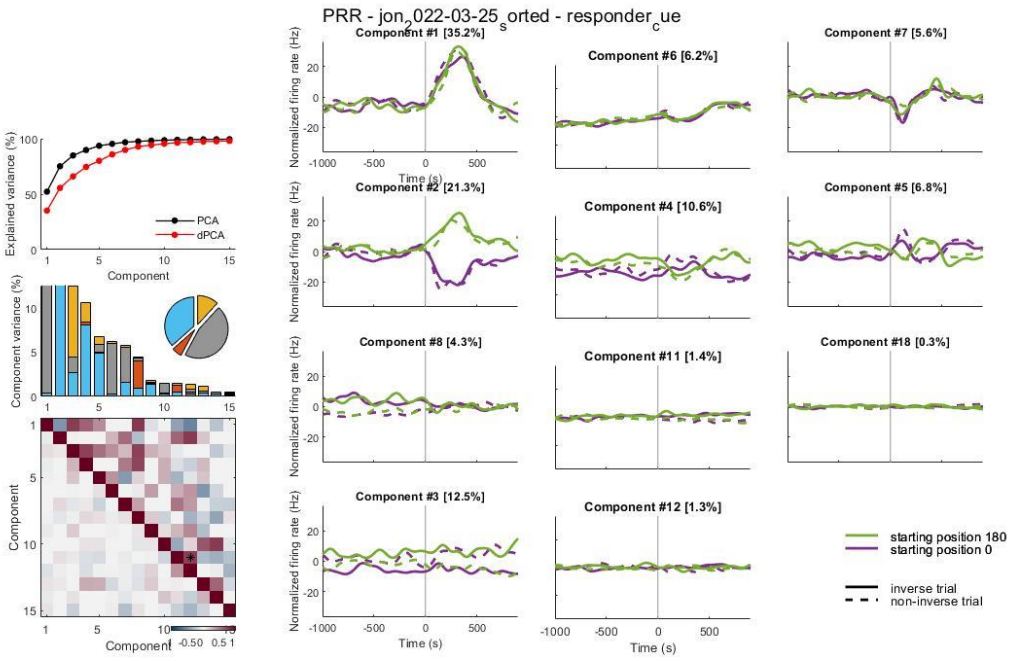

S- Figure 2: Full figures of dPCA for the sessions from Fig.5.

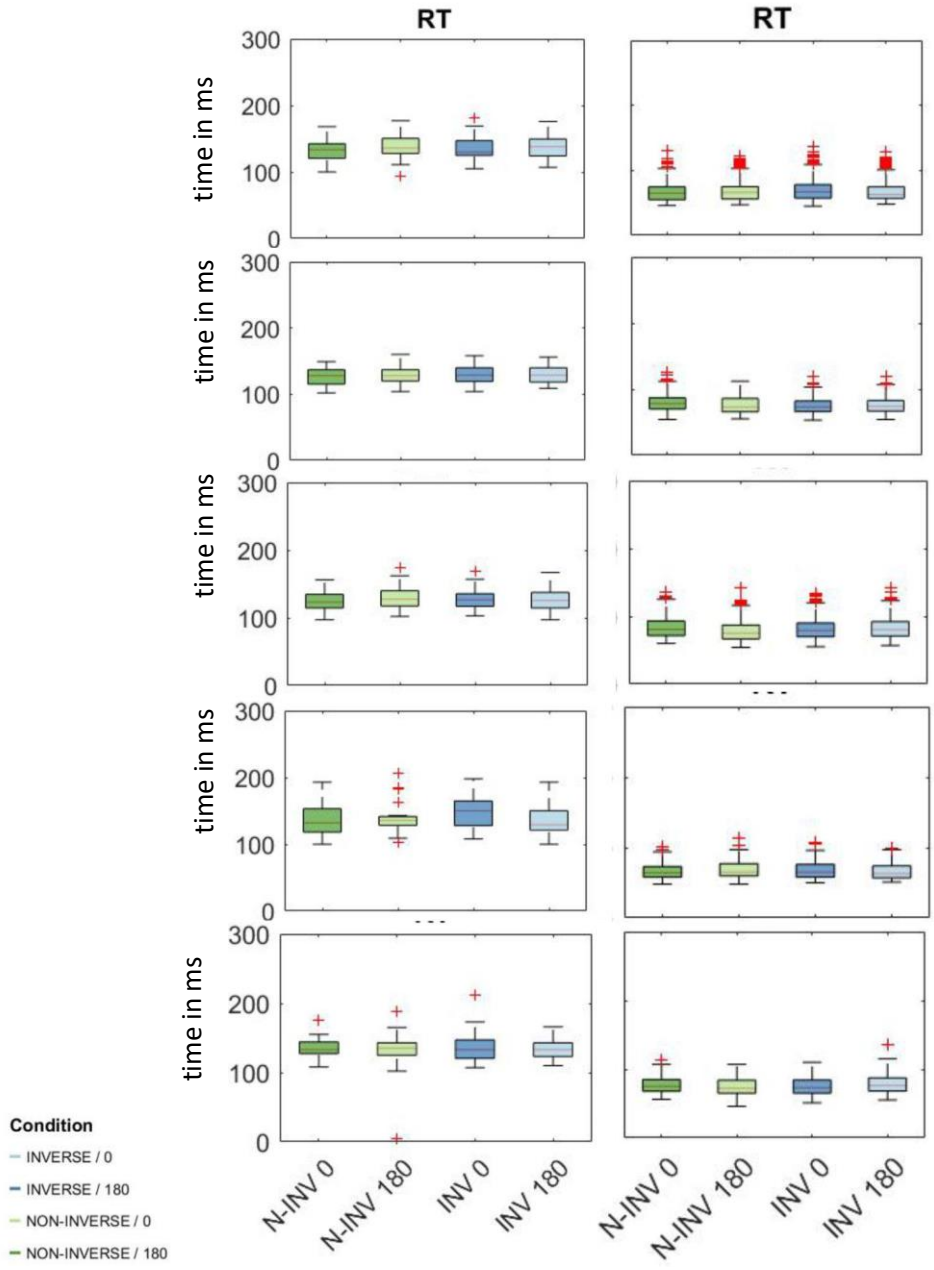

S - Figure 3: RT across all 4 conditions with a waiting period before go cue (left panel) and for a speeded reaction condition without waiting period (right panel).Each box represents the data of one subject, in total 10.

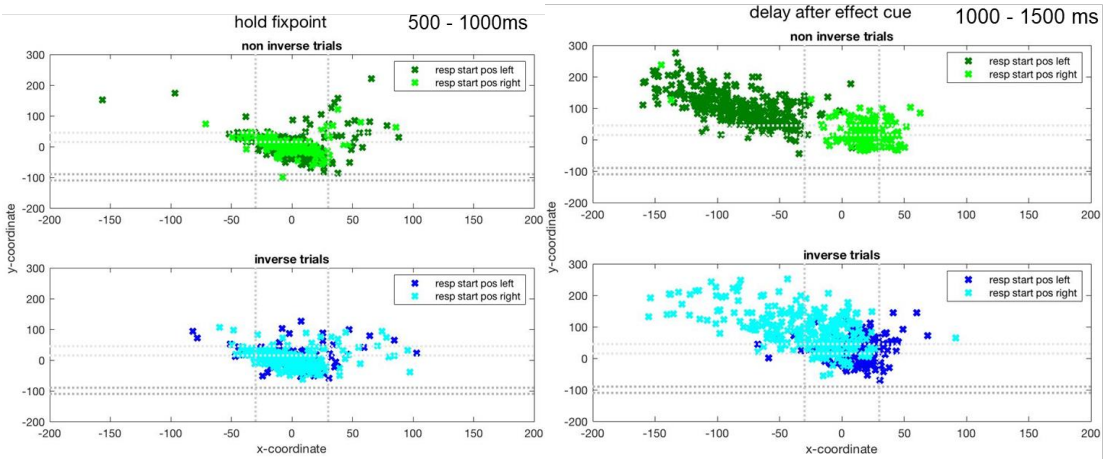

S - Figure 4: Averaged eye trajectories during baseline epoch (hold fixation period, left panel) and during planning phase (right panel) calculated across 2849 trails across 4 sessions for monkey B.

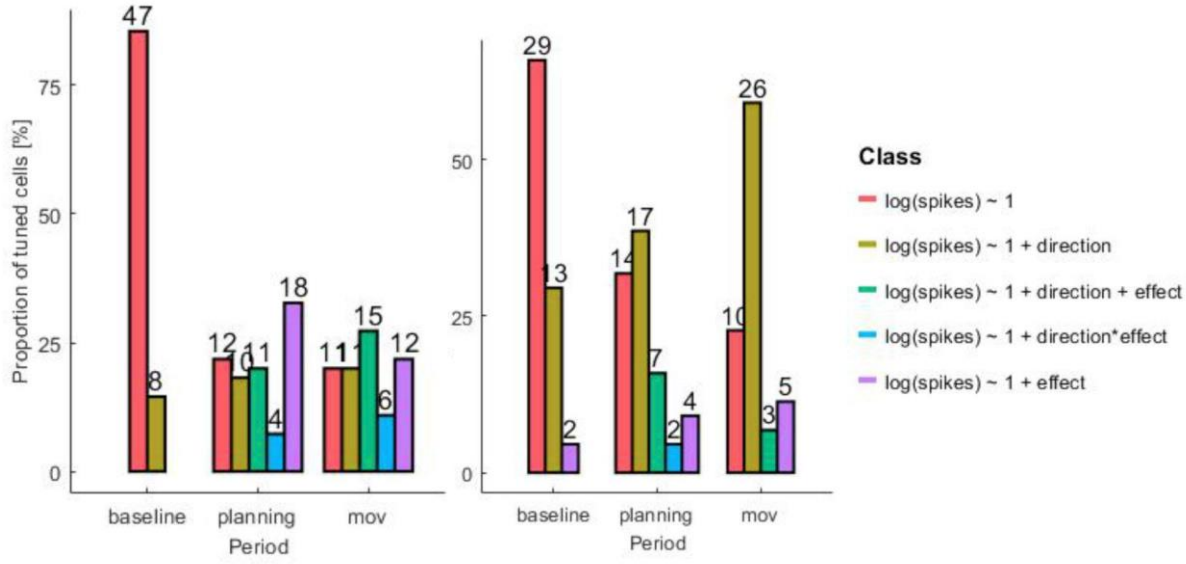

S- Figure 5: Percentage of tuned neurons for an example block wise session in monkey B (left) and monkey J (right).

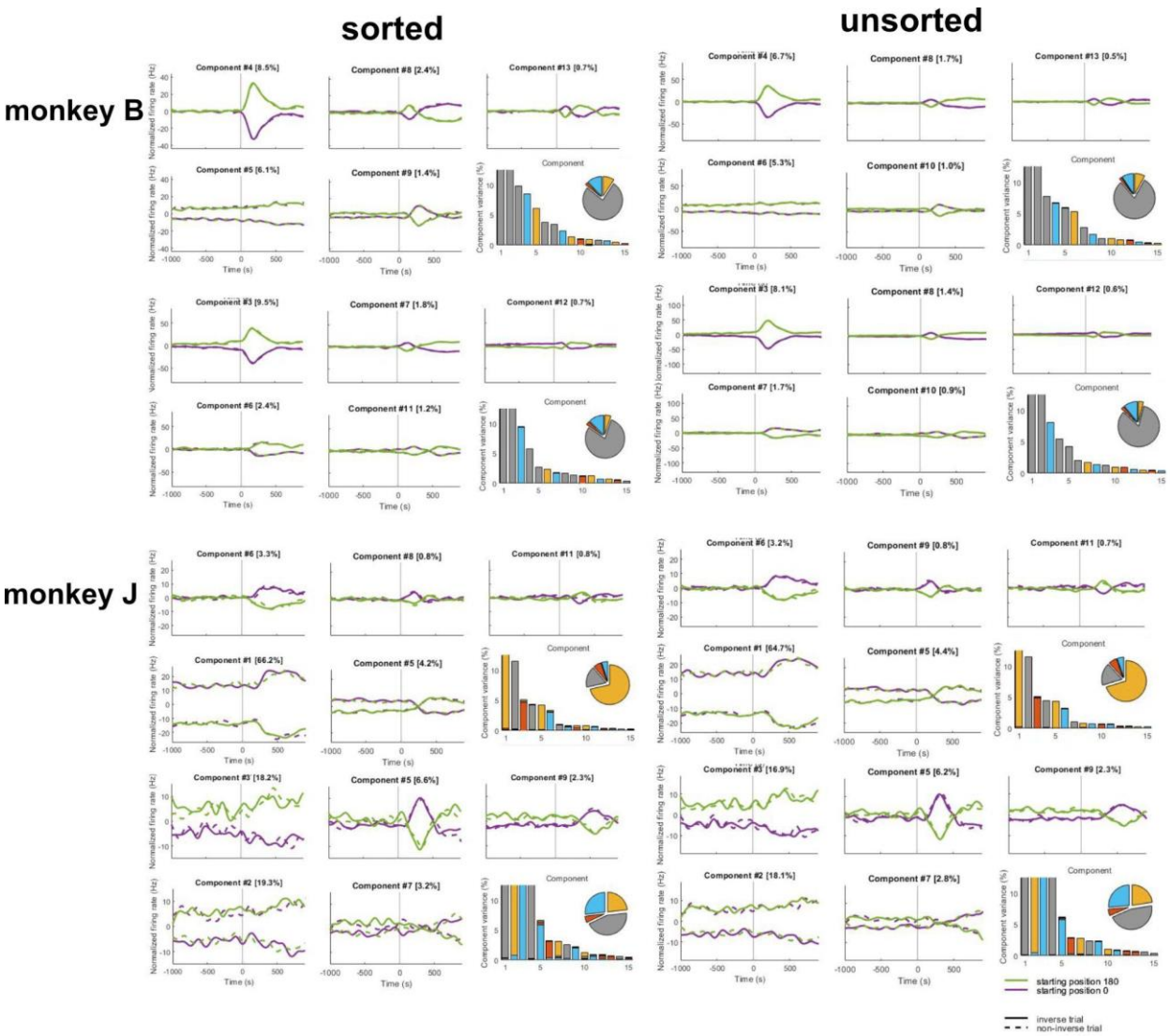

S- Figure 6: dPCA results in area PMd for two sessions in monkey B and monkey J. dPCA was calculated for unsorted sessions (left panels) and on sorted neurons within the same session (right panels).

Chapter 4

B PRIME - an interactive haptic device for controlled, free behaviors in rhesus macaques

4.1 Abstract

Rhesus macaques (m. mulatta) are widely used in systems neuroscience. When studying macaques in a free, yet controlled setting, macaque-proof devices are a limiting factor. Existing feeders mostly run in standalone mode allowing simple interactions for enrichment or patch searching tasks. They often cannot communicate with peripheral devices such as video or neural acquisition systems. When investigating neural correlates of sensorimotor and decision making processes in systems neuroscience, simple interactions like lever pressing are not sufficient.

We developed the B-PRIME - the Barrel edition of Primate Interaction, Movement and Enrichment device. This prototype consists of two independently rotating barrels. The inner barrel is motorized and fully computer-controlled to allow various manipulations of the device dependent on the monkeys interaction. The outer barrel is freely rotatable. Various off-the-shelf sensors are implemented to measure the rotation direction of both barrels. The inner barrel contains four reward pockets, which are connected to each of the four 3D printed treat dispensers. The monkey rotates the outer barrel until he can reach one of the four reward pockets. Once the monkey leaves the pocket, which is detected by IR sensors, the inner barrel is automatically rotated back to its centralized starting position.

The B-PRIME can run together with external task controllers (e.g. C++ based) allowing communication with motion tracking and neural recording systems or in a standalone mode.

For future purposes, a subset of the full range of the prototype's features can be implemented for potential use as an enrichment tool in housing facilities or zoos as well as a food source in field studies.

Metadata Overview

Main design files: https://github.com/ZuAh/BPRIME

Target group: Scientists in Systems Neuroscience

Skills required: -

desktop 3d printing - easy; surface mount PCB - easy; device assembling - prior experience recommended

Replication: No builds known to the authors so far

See section "Build Details" for more detail.

Keywords

Smart feeder, systems neuroscience, rhesus macaques, haptic device, interactive

4.2 Introduction

To observe controlled, yet free behavior in rhesus macaques (m. mulatta) ethologists developed feeders, which allow haptic interactions. These existing feeders require rather simple interactions e.g. pulling a drawer, which is suited for addressing questions related to group situations like social comparisons (Keupp et al., 2019) or co-feeding (Pastor-Nieto, 2001).

Similar ideas have been implemented in systems neuroscience to study risk adversity and affinity (Eisenreich et al., 2019) or the neural correlates of navigation (Mao et al., 2021, Maisson et al., 2022). While these interactive feeders using a simple lever to access reward are well suited to relocate the monkey in a large experimental setup, they are rather limited in their range of interaction.

When it comes to understanding the neural processes of more complex haptic interactions, existing studies use chair-seated animals. The generalizability of their findings towards more

free behaviors remains unknown. To study these behaviors in less constrained environments researchers have developed complex touchscreen based kiosk systems with which the animals can interact in e.g. home cages (Calapai et al., 2017; Berger et al., 2018). However, these systems are limited to simple touches.

There is no device to our knowledge, which allows more complex interactions beyond touching and grasping, e.g. rotating, and which would still enable us to study the complex mechanisms of action planning and decision-making. Therefore, we developed the prototype of the Barrel edition of the Primate Interaction, Movement and Enrichment device (B-PRIME). The B- PRIME consists of two individually rotating barrels. The inner barrel is motorized and controlled by the software allowing rotations to the left and right; the outer barrel is freely rotatable by the monkey. We implemented off-the-shelf sensors for detecting rotation direction and position of both barrels. We custom-designed and 3D printed reward pockets, which contain infrared sensors to detect whether or not a finger is inside. Five LEDs indicate different stages of the task trial. The B PRIME is programmed such that it can either run in standalone mode or with external devices e.g. C++ based task controller PC, which enables communication with motion tracking or neural recording systems.

In the following we will provide an overview of our developed hardware, software and the electrical components, which were implemented. Then we will discuss and present ideas how this prototype can be improved making it suitable for other use cases e.g. as an enrichment tool in zoos or facilities.

4.3 Overall Implementation and Design

Hardware development

The B-PRIME consists of two major components, the hardware and the software part. For the prototype we ordered two barrels (polycarbonate cylinder, diameter 244mm, www.kuslicht.de; polypropylene cylinder, diameter 225mm, www.Rosinsky-kunststoffe.de) and a axial deep groove ball bearing ('lazy susan') with diameter of 225mm (e.g. Amazon) , which is key to the two independently rotating barrels. All other mechanical components were custom designed or custom modified and can be 3D printed in PLA (files available on GitHub). Figure 1A shows the different layers of the B PRIME. We have in total 4 reward pockets, 2 on each side of the inner barrel. The outer transparent barrel contains a row of holes to provide grip for rotation. The inner barrel is connected to a 36V stepper motor and therefore controlled entirely by the software. The outer barrel can be rotated freely by the monkey in both directions. Both barrels are attached to the rings of the lazy susan; the inner ring is connected to the inner barrel and the outer ring to the outer barrel allowing both of them to be rotated independently along the same axis. The inside of the inner barrel contains two reward pocket holders (Fig 2A) on each side, which were custom designed in Fusion 360 (Autodesk, San Rafael, California, USA). Each reward pocket contains a hole on the right side such that if ball-shaped treats are released, they bounce back from the

opposite side wall and stop in the reward pocket. The base of each reward pocket is tilted by 20 degrees such that the back part is deeper than the front part to ensure the treat remains in the reward pocket and does not roll out by itself. Each of the side holes in the reward pocket is connected with a 4cm flexible pipe (Fig. 2A) to one of the 4 custom fitted treat dispensers (Fig 2B, C), which are motorized. These treat dispensers are placed on top of the B-PRIME (Fig. 2C).

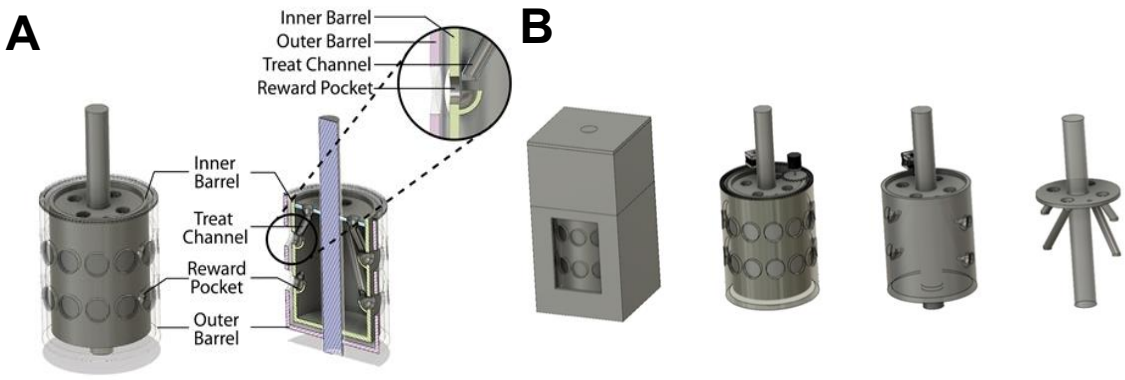

Figure 1: CAD designs of B PRIME. Panel A shows the two rotating barrels of the B-PRIME: the outer barrel is transparent and the inner barrel is solid and motor controlled. . Panel B demonstrates the different layers of the B PRIME starting from the outer encasing with a window of access for the monkey. Second image shows the B-Prime without the outer encasing. Third image shows the inner barrel with in total 4 food pockets. Last image is the B-PRIME stripped down to its inner treat dispensing pipes. Each pipe is dedicated to one food pocket. On the other side each pipe is connected to one whole on the top which again is connected to one food dispenser each.

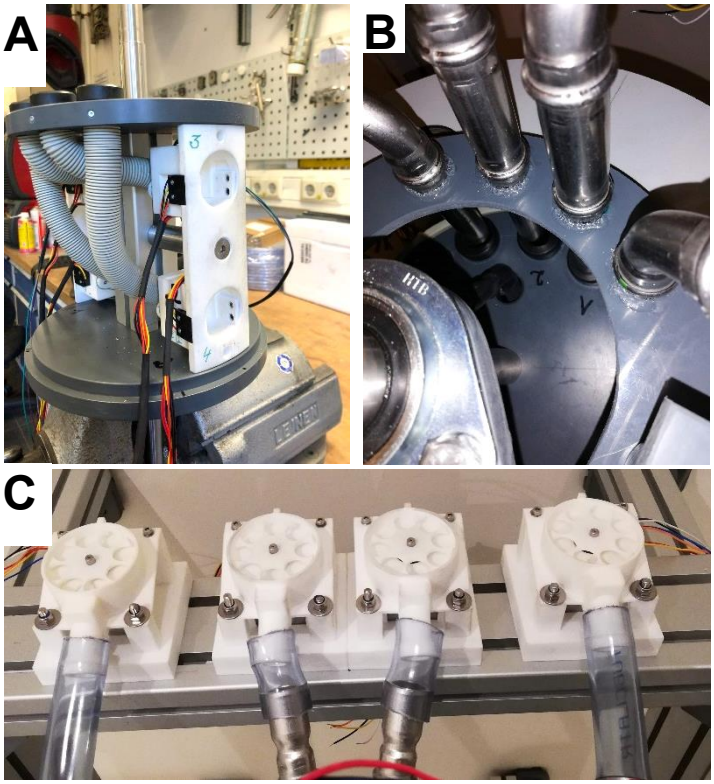

Figure 2: Detailed view of the treat reward system. Panel A displays the custom-designed reward pocket holders with two reward pockets each. We mounted 2 pairs of IR sensors per reward pocket for finger detection. Panel B shows the zoomed in view of the reward pipes coming from the 3D printed treat dispensers (Pane C) going to the B PRIME inner barrel.

At last, we cover the front part of the B-PRIME by mounting a front plate with a cut out of 30 by 80 cm to allow the monkey to interact with the B-PRIME within a given window of access. These windows can be adjusted by two plates (grey plates, Fig.3), which are mounted on the back of the front plate and are adjustable to reduce or enlarge the window size if necessary. Additionally, we attached 5 LEDs in the center of the B-PRIME, which can be computer controlled individually (Fig.3).

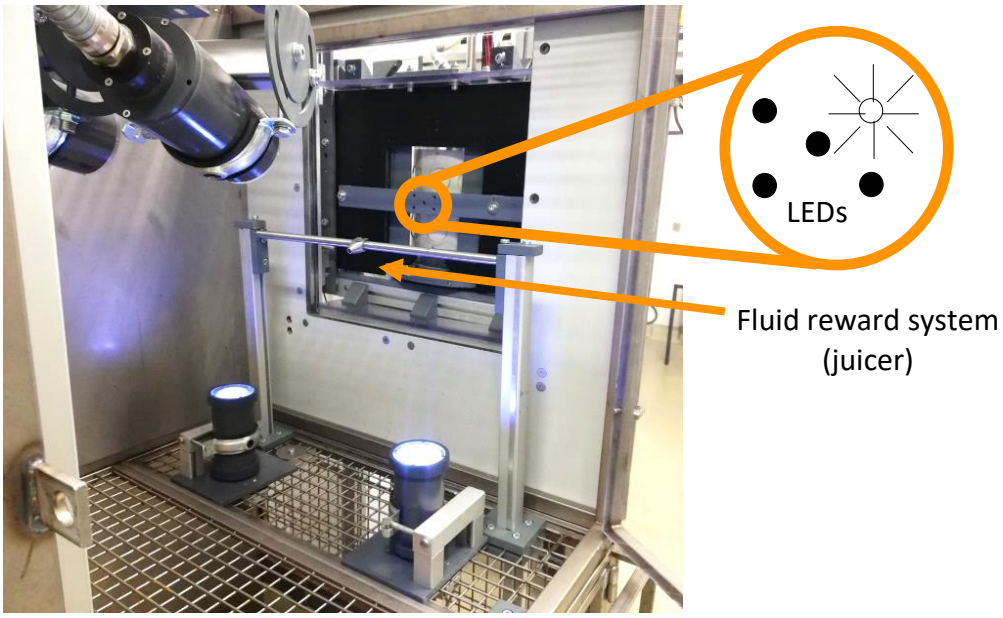

Figure 3:B-PRIME mounted in an experimental setup for free rhesus behavior. 5 LEDs were mounted on top of the front plate, which can be addressed individually. The B-PRIME can communicate with external devices e.g. a juicer which dispenses fluid reward when the trial was completed successfully.

Electrical components

Each of the reward pocket holders contains 2 infrared sensors with a transmitter and receiver on each side (Fig 2A), which allows it to detect if the monkeys finger is inside. The inner barrel is connected to a 36V stepper motor and to a encoder sensor (IS240 by GES Group), which is set to 0 at the beginning of each session to define the starting position. The encoder continuously sends the position information of the barrel. This enables us to reset the inner barrel to a defined starting position after each completed trial, if needed. The outer barrel is connected to an identical sensor and sends the position. Lastly, each of the food dispensers are connected to a 5V stepper motor, which can be activated independently depending on which reward pocket needs to be filled.

Software development

We developed an Arduino based software (firmware), which can control the B-PRIME either in a standalone mode or communicate with external devices (e.g. C++ based task controller PC). The firmware is developed to continuously read in the logic low interrupt from the IR break beams in all 4 reward pockets. As soon as a finger is detected, the motor of the inner

barrel is immediately put into stop-mode and only reactivated after 700ms, once the IR beam is established again as a safety measurement. Additionally, the firmware allows defining stages, in which the outer barrel should not be enabled for rotation. If it is rotated during that stage, an error command is sent, which triggers an alarm tone, stops the ongoing stage and restarts the entire trial. In stages, in which the outer barrel is enabled for rotation, the software continuously monitors the positions of both barrels. Depending on the position of the outer barrel and the adjusted step size, the inner barrel moves with no noticeable delay together or in the opposite direction of the outer barrel. If the inner barrel reaches the fixed position, in which the reward pockets are facing the animals, the inner barrel stops rotating further to protect an over twirling of the wires. Once the animal reaches for the correct reward pocket, the motor is put to stop and enabled only after 700 ms after reach end. The inner barrel is rotated back into the original reset position 0. If the wrong pocket was reached, the user can define to either let the B-PRIME go to error mode and reset itself once no finger is detected or to do nothing. Both are easily configurable in the firmware. The 5 LED rigs can be lid up individually in the color of choice indicating task relevant states (go cue, error cue, reward pocket cue). The firmware also contains a randomization function allowing to randomize either the selected reward pocket or the rotation translation of inner and outer barrel or the amount of treats. Additionally, the B-PRIME contains the function to send a signal to an external fluid reward system (Fig 3) to reward the monkey.

When not running in the standalone mode (mode 1) and the B-PRIME is controlled by an external task controller (mode 2), a bidirectional handshake is established by sending a char bit. Afterwards, all functions of the B-PRIME (e.g. randomization, LED selection) except the continuous sensor readouts of finger-detection and barrel positions are taken over by the task controller and the firmware becomes a translator only. The hybrid mode (mode 3) puts the responsibility of all main relevant tasks such as randomization or reward pocket selection on the task controller. During the rotation stage however, the B-PRIME firmware controls real time detection of barrel rotation in the right direction, finger detection and successful or failed trial by itself to avoid delays by stream overload depending on how many other peripheral devices are communicating with the task controller simultaneously. Our GitHub repository contains two versions of the firmware. One is the full version with all implemented functions of the B-PRIME in communication with an external task controller PC. The second is limited to the core functions of the B-PRIME in standalone mode to provide a better overview to a new user.

4.4 Quality control

Safety

Operators of the B PRIME should be aware of four hazards

- electric shock
- finger pinch

- wire over-stretching

Finger pinches
If the finger is put back into the reward pocket while the barrel is resetting itself or if the finger is close to the edge of the window of access, fingers can be pinched if not careful. However, we tested the device on humans and the pinch is a brief pinch. When the finger remains inside, the motor is configured such that the barrel can be kept in its current position with one finger without any force reducing the risk of injuries.

Electric shock
As some of the electronics need an external power source, it can cause electric shocks when assembling or testing the newly developed circuit if not careful. The stepper motor is run using 36V. All cables should be inspected for damage and replaced, if damaged.

Wire over-stretching
The current prototype is constructed such that rotation of the inner barrel up to 90 degrees in each direction is tolerated by the wiring inside. However, rotations beyond this can overstretch and damage the wires. When implementing the code, it is therefore highly recommended to first implement the security features of the fixed maximum rotation position (do not rotate further than this defined position). It is recommended to be close to the motor's power supply to turn it off manually, if the safety measures during first time implementations fail. Additionally, we used thicker wires than necessary (5mm) to increase the resistance of the wires. All wires taken together provide enough force to hold the motor in place even if the safety measures fail. However, you want to avoid this happening repetitively.

4.5 General testing

We tested the device with three rhesus macaques (m. mulatta) in a chair seated setup, in which the monkey could interact only with one arm and in a less restrained environment in which the monkey could interact with the device in any way he intended. In all cases, the animals learned to interact with the B PRIME within a week and started learning more complex tasks for systems neuroscience studies, one of which is currently in preparation for submission. The B-PRIME resisted any interactions with the monkeys and successfully rewarded them with fluid reward upon finishing the trial. We did not run into any problems regarding device failure or interaction problems between monkey and B-PRIME (Fig. 4).

Figure 4:A rhesus macaque interacting with the B-PRIME in a conventional chair-seated setup (left) and in a setup for less constrained behaviors (right).

4.6 Use case(s)

One use case for the BPRIME, for which the prototype was primarily developed for, is systems neuroscience related research questions going towards more free behaviors allowing less constrained interactions with the environment. In this context the B-PRIME was used for two studies, one making use of all four reward pockets and one making use of the inverted and non-inverted rotation direction of the inner barrel compared to the outer barrel. The second is a full study recorded with two rhesus macaques with wireless neural recordings and is currently in progress for manuscript submission.

After the experience with this prototype, we have conceptualized several ideas on how to make the device smaller, lighter, more flexible and therefore suited also as an enrichment device either in animal facilities or zoos or even as a tool for field studies.

Reuse potential and adaptability

The current version can be assembled and used for systems neuroscience related questions with potential research focus on decision-making, action planning or visual neuroscience.

The prototype B-PRIME however can be made lighter and more flexible. The in detail implementation can be discussed with the corresponding author. In the following, we will provide only an overview of some core changes we propose for future implementations.

First, we suggest not using the current treat dispensers, which are limited as they rely on round and uniform treats. Instead, at the inner barrel always resets to a defined starting position, mounting treat dispensers at the entrance of each reward pocket directly would be recommended instead of using an indirect and complex pipe system as currently in place. For this batteries of reward can be used to dispense treats modifying coin dispenser with a spring. This is a similar concept to the super market dispensers, e.g. when you take the most front chocolate bar and the remaining ones are pushed from the back to the front. The end of the dispenser could be covered with a 3D printed lid, which is only opened by a small 5V

stepper motor, whenever that specific reward pocket is chosen for the next trial. 3D models of coin dispensers are openly available and can be adapted to your specific design (e.g. https://www.thingiverse.com/thing:4719465).

With this modification the entire B-PRIME can be reduced in size allowing the use of smaller lazy susans and more importantly smaller sized barrels. Here we propose to print 2 half shells of the barrels instead of using a complete cylinder and connect them with M3 screws together on the lazy susan. This way the design is more flexible in terms of changing the color or surface of the outer barrel, even combining a smooth and a rough surface (half-half) depending on the question you are interested in. Additionally, it allows the device to open quickly allowing easier access to the wiring inside of the B PRIME. This enables us to use one IR sensor instead of two per reward pocket therefore reducing the number of total IR wires to half.

At last, the lighter and smaller barrel will not require a strong motor with 36V but should be sufficiently working with a smaller stepper motor. Using batteries or solar panels, this device could be used without any wired external power supply.

For future users or collaborators, who are interested in such an implementation, support will be provided by the corresponding author.

4.7 Build Details

Availability of materials and methods

As described earlier the prototype of this B-PRIME consists of commercially available cylinders (see hardware development). The future implementation however could be potentially done independently by using 3D printing. Lazy susans are commercially available in different sizes (e.g. Amazon). All electronic components are standard components and can be readily ordered from Amazon, Sparkfun, DigiKey, Conrad or Reichelt (the latter 2 are German companies). The current and future dispensers and the reward pocket holders can be 3D printed and also customized if needed using Autodesk Fusion 360. All 3D files are available on our GitHub repository.

Ease of build

The parts used for the current prototype B-PRIME can be assembled using common hand tools as hex keys, screwdrivers and pliers. The current implementation of the reward tubes on the inside of the inner barrel requires precise alignments for the round treats to fall all the way through. The new proposed reward dispensers however should be easier mountable.

Operating software and peripherals

The firmware was programmed based on Arduino version 1.8.15. Currently we are using a Teensy 3.5, however the system was also tested on Teensy 3.6 and 3.2, although the latter might not provide sufficient numbers of pins for all sensors of the current prototype. However, for future implementations with fewer sensors the smaller Teensy 3.2 might be sufficient.

Dependencies

The current firmware makes use of the Arduino libraries 'Rotary Encoder' to read out the positions of both barrels and 'Adafruit Neopixel' for LED communication.

Hardware documentation and files location:

Archive for hardware documentation and build files

Name: GitHub

Persistent identifier: https://github.com/ZuAh/BPRIME

Publisher: Zurna Ahmed

Date published: will be updated after manuscript acceptance

Software code repository together with the hardware within the same repository

4.8 Discussion

Conclusions

This study presents a novel interactive device, which is robust against rhesus macaques and allows complex interactions beyond reaches for systems neuroscience studies. As in other use cases in the field of neuroscience (Mao et al., 2021; Eisenreich et al., 2019), interactions with simple feeders are well suited to understand the neural correlates of more free behaviors, which require controlled relocation of the monkey in large experimental setups, e.g. navigation (Mao et al., 2021; Maisson et al., 2022). However, they allow only one interaction type by using a lever when it comes to the interaction with the feeder itself. For systems neuroscience this can be a limitation therefore we developed the prototype of the B-PRIME, which allows us to study complex mechanisms of action planning and decision making in free behaving rhesus macaques. We conclude the B PRIME enables us to investigate new aspects of systems neuroscience in freely moving non-human primates.

Future Work

Next steps in this work will be to first provide the neural study, which was conducted with the B-PRIME to show the full potential of the B-PRIME in systems neuroscience. As a next step implementation of our proposed improvements would be needed to increase the reuse potential of the B-PRIME.

References

Berger M, Calapai A, Stephan V, Niessing M, Burchardt L, Gail A & Treue S (2018) Standardized automated training of rhesus monkeys for neuroscience research in their housing environment. J Neurophy (119-3) 796-807. doi:10.1152/jn.00614.2017.

Calapai A, Berger M, Niessing M, Heisig K, Brockhausen R, Treue S and Gail A (2017) A cage-based training, cognitive testing and enrichment system optimized for rhesus macaques in neuroscience research. *Behav Res* Methods *49(1):35-45*. doi: 10.3758/s13428-016-0707-3.

Cisek P, Crammond DJ, Cisek p (2003) Neural Activity in Primary Motor and Dorsal Premotor Cortex In Reaching Tasks With the Contralateral Versus Ipsilateral Arm. J Neurophysiol 89(2):922-942. doi: 10.1152/jn.00607.2002.

Eisenreich, B.R., Hayden, B.Y. & Zimmermann, J. Macaques are risk-averse in a freely moving foraging task. *Sci Rep* 9, 15091 (2019). doi: 10.1038/s41598-019-51442-z.

Kuang, S., Morel, P. & Gail, A. (2016). Planning movements in visual and physical space in monkey posterior parietal cortex. Cerebral cortex, 26(2), 731-747. doi: 10.1093/cercor/bhu312.

Gail A, Andersen RA (2006) Neural Dynamics in Monkey Parietal Reach Region Reflect Context-Specific Sensorimotor Transformations. J Neuroscience 26(37): 9376-9384. doi: 10.1523/JNEUROSCI.1570-06.2006.

Keupp S, Titchener R, Bugnyar T, Mussweiler T, Fischer J (2019) Competition is crucial for social comparison processes in long-tailed macaques. Royal Society 15(3). doi: 10.1098/rsbl.2018.0784.

Maisson DJN, Voloh B, Cervera RL, Conover I, Zambre M, Zimmermann J, Hayden BY (2022) Widespread coding of navigational variables in prefrontal cortex. biorxiv. doi: 10.1101/2022.10.13.512139.

Mao D, Avila E, Caziot C, Laurens J, Dickman JD, Angelaki DE (2021) Spatial modulation of hippocampal activity in freely moving macaques. Neuron 109(21): 3521-3534. doi: 10.1016/j.neuron.2021.09.032.

Pastor-Nieto R (2001) Grooming, kinship, and co-feeding in captive spider monkeys (*Ateles geoffroyi*). ZooBiology 20(4): 293-303. doi: 10.1002/zoo.1029.

Chapter 5

The Exploration Room (ExR) – a novel environment for large scale, neurophysiological testing of ecologically relevant behavior for systems neuroscience

5.1 Abstract

Systems neuroscience is recently moving towards large-scale experimental setups to study the neural underpinnings of free behaviors in rhesus macaques. How long-standing neuroscience concepts from conventional setups translate to free behaviors and how established analysis methods can help to study decision-making, action planning and execution in unconstrained conditions remains unknown.

On this wake, we developed a novel, highly modular experimental setup for neurophysiological recordings in freely moving rhesus macaques called the Exploration Room (ExR).

We demonstrate monkeys engage in trial-based behaviors in large-scale setups, which enable direct translation of established experimental paradigms from conventional chair-seated setups in neuroscience within more naturalistic conditions. By exploiting the ExR's modularity, we designed a continuous foraging experiment (Playground Experiment, PE), which consists of food and fluid sources (patches) strategically arranged to allow the animals to freely express

complex, yet repeating behaviors. We illustrate a novel combination of markerless full-body 3D-keypoint tracking and 2D-pose estimation to identify between and at-patch behaviors using only a few cameras.
Finally, we provide proof-of-concept neural data with first analysis approaches to study arm- and full-body reach representation in the frontoparietal network. To analyze between-patch transitions, we applied single-trial analysis on 3D-reconstructed trajectories to identify the point of commitment and the associated neural activity. To study at-patch interactions, we compare goal-directed reaches during different patch-specific postures and their neural correlates.
We conclude that our large-scale freely moving setup ExR can substantially extend the possibilities in systems neuroscience as it allows studying neural correlates of complex, ecologically relevant full-body behaviors, so far not available.

5.2 Introduction

Over the years, substantial research efforts have been dedicated to understand the neural correlates of goal-directed actions and decision-making with a particular focus on the role of the frontoparietal reach network, which encompasses premotor and primary motor cortex and the parietal reach region. This line of research has brought sound insight on the role of this network in spatial direction encoding (Georgopoulus et al., 1986), spatial reference frames during reach movements (Buneo et al.,2002; Pesaran et al.,2006; Batista et al.,2007; Kuang et al.,2016), bimanual coordination (Donchin et al., 1998; Cisek et al., 2003; Moochagian et al.2021), eye-hand coordination (Hwang et al.,2014; Mooshagian and Snyder,2018), decision-making (Klaes et al., 2011; Thura and Cisek.,2014; Surija-Arunoj and Gail, 2019) and social interactions (Ferrari-Toniolo et al. 2019; Lacal et al., 2022).

While these studies have significantly contributed to our understanding of the neural basis of goal-directed behavior, their scope is limited, primarily focusing on hand and arm movements within a constrained context. Ethological observations of non-human primates in natural settings reveal a rich repertoire of diverse full-body behaviors extending beyond seated and single-arm movements. These behaviors include walking and foraging (Agetsuma, 1995; G. O'Brien and Kinnaird , 1997), tool use (Malaivijitnond et al., 2006), grooming and other social interactions (Maestripieri, 2005; McCowan et al., 2008; Zhang et al, 2021).

The complexity and variety of these natural behaviors suggest that traditional approaches in systems neuroscience may fall short in providing a comprehensive framework for understanding intentional behavior. Bridging the gap between systems neuroscience and ethology, recent studies have explored novel methodologies, such as virtual reality experiments

with non-human primates (Noel et al., 2022), offering a more naturalistic experience within controlled laboratory settings.

Most importantly, recent advancements in wireless neural recording techniques and markerless motion-tracking have further spurred interest in experimental setups with freely moving primates, overcoming the limitations of chair constraint (Foster et al., 2014; Shahidi et al., 2021; Berger et al., 2020). Recent studies demonstrate the feasibility of studying large-scale, unconstrained behaviors, expanding beyond short-range movements like walking (Bala et al., 2020; Voloh et al., 2021). However, challenges remain in how to experimentally induce a variety of full-body behaviors and how to extract relevant information from continuous behavioral streams for neural analysis.

This study addresses these challenges and provides further evidence supporting the suitability of large-scale experimental setups for freely moving rhesus macaques to study decision-making and arm reaches in systems neuroscience research. The Exploration Room (ExR), a modular and versatile experimental environment, is introduced, displaying its ability to induce complex and repeating full-body behaviors. This study also employs a combination of 2D pose and 3D keypoint tracking methods to parse continuous behavioral streams, enabling the investigation of decision-making, action planning, and execution. The findings demonstrate the potential of continuous behavior analysis in large-scale setups, offering new possibilities for understanding neural correlates in decision-making processes beyond the constraints of traditional neurophysiological approaches.

5.3 Results

Modular ExR for complex, full-body behaviors

We developed a modular large-scale environment called the Exploration Room (ExR) for a variety of experimentally induced free behaviors in rhesus macaques (Fig.1A). The dimensions of the ExR are 4.3 x 2.6 x 2.5m^3 (L x W x H). Floor and walls consist of single high pressure laminate (HPL) panels, which can be exchanged individually against interactive devices or other pane types, e.g. mesh grids, transparent panel (Fig.1 A, B). As examples, we used a prototype feeder B-PRIME (Ahmed et al., *Chapter 4*), which can be mounted on the wall, or dyadic feeders, a simplified version of the B-PRIME, which can be mounted on the floor. To provide interactive floor mounted devices with the required wiring (e.g. power supply, connections to the PC), which needs to be protected from monkey-interactions and fluids, we elevated the ExR's floor by 28cm allowing sufficient spacing beneath to pass wires and designed multi-media floor tanks. As an example for fluid-providing kiosk-based cognitive testing devices, we used

XBIs (Calapai et al.,2017; Berger et al., 2018), which are computer based touchscreen systems that can provide any type of fluid reward to the monkey in response to a required interaction. To further enhance the modularity of the ExR, we designed a balcony panel, which can be mounted along the wall at any given intersection between two superimposed wall-panels. This can be used either as an interaction platform (e.g. foraging between patches, which are placed on top of this elevated floor) or as a sitting or standing platform so the monkey can interact with any device mounted along the second panel row like the B-PRIME, Fig.1A). Additionally, a motorized transparent divider was installed, which separates the ExR into two symmetrical halves. The ExR is suited for social experiments for two or more animals within the same physical space or in a dyadic setting physically separated. Optionally, a transparent box (waiting room) can be mounted, from which a monkey can observe other conspecifics without having direct access to the main ExR environment.

Recorded video footage provides evidence that the monkeys display a variety of ecologically relevant behaviors inside the ExR such as sitting, walking, standing on two legs, walking on two legs, pulling a branch-like string and foraging with an object (Fig. 1C), These behaviors can also be observed across different monkey species when behaving in a more natural environment, in which they can explore freely confirming the ExR allows rhesus macaques to express ecologically relevant behaviors. The underlying neural activity was recorded in the primary motor cortex using a 32-channel TBSI wireless headstage. Results demonstrate different full-body movements have different underlying neural firing patterns in the primary motor cortex (Fig. 1C). For example, full-body movements involving all four limbs like walking present a higher increase in firing rate across a vast majority of channels while behaviors involving one limb only during sitting or standing on 4 legs present a decreased firing rates compared to the first.

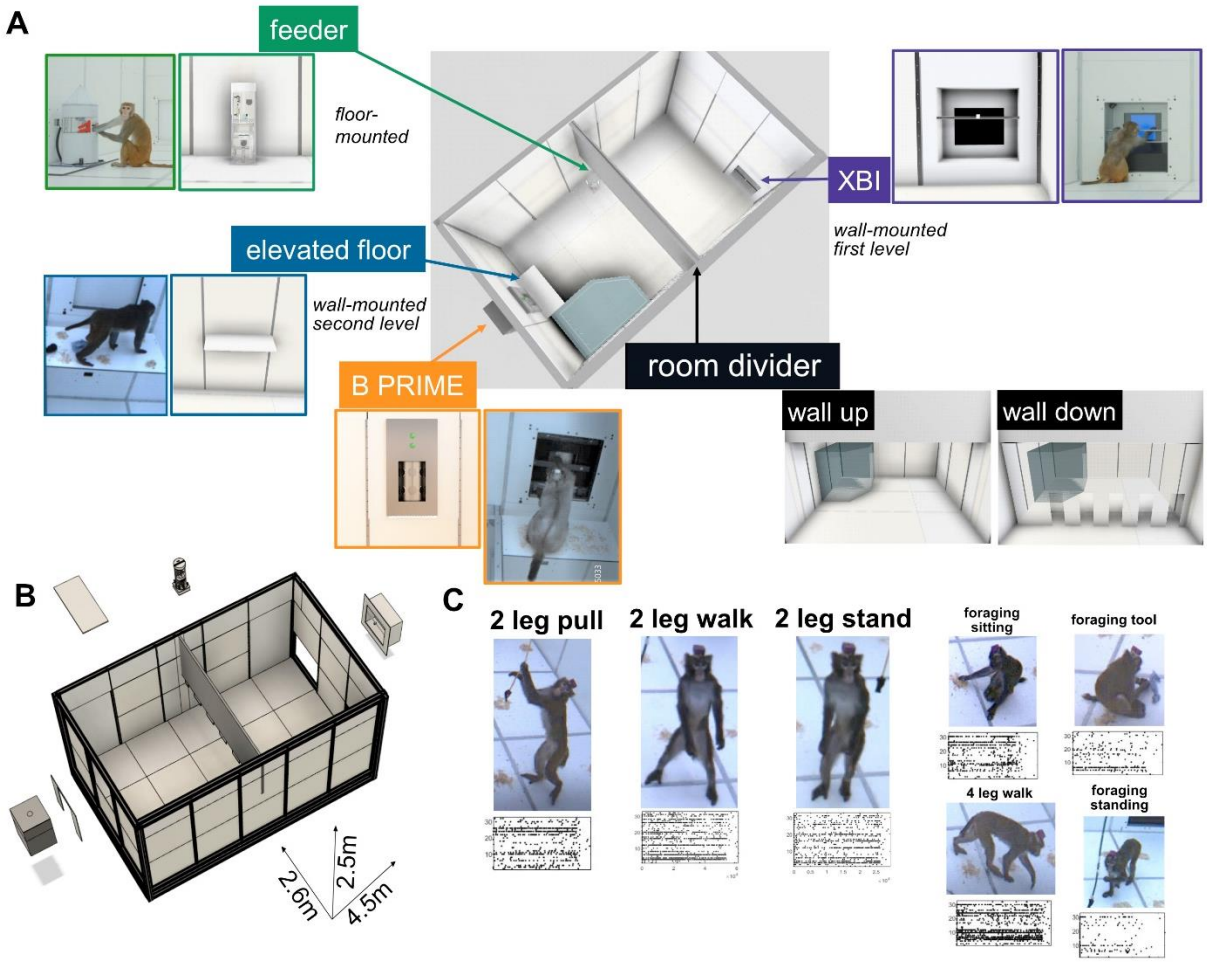

Figure 1: The ExR consists of individual panels, which can be exchanged against interactive feeders (A and B). These devices can be wall-mounted along the wall and the floor panels. A motorized transparent divider separates the ExR in two symmetrical halves. The ExR is 4.5m x 2.6m x 2.5m (L x W x H) big. Ecologically more relevant full-body behaviors can be observed in the ExR (C), which are also observed in more natural enclosures. Example brain activity for each behavior from primary motor cortex (M1) is presented.

Rhesus macaques successfully engage in trial-based repeating behaviors

Many established methods of analysis in systems neuroscience require data sampling through repetition of pre-defined testing conditions (trial testing). To be able to reproduce findings from constrained contexts in free, continuous behavioral conditions, large scale freely moving setups should be able to guarantee the feasibility of trial-based repeating studies as well. Here we demonstrate that the ExR's modularity can be used not only to make rhesus macaques express a variety of full-body behaviors but also for trial-based repeating behaviors within a specific task design. We tested two animals (monkey K and monkey H) while performing a full body walk-and-reach task (adapted from Berger et al., 2020) towards two possible far targets, within a pre-defined time window (Fig. 2A). The walking trajectories from across several sessions for

each monkey (Fig. 2B) show mostly goal-oriented walking patterns towards both targets across the long distance of the room (4.5m length).

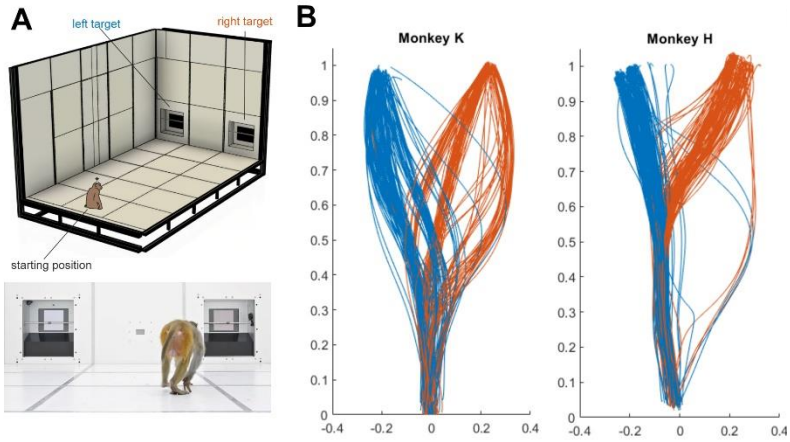

Figure 2: A: The animal was required to sit on a starting position to activate a trial by means of a capacitive sensor. When the trial started, the monkey was allowed to reach one of the two XBI kiosk systems, serving as targets and located on the opposite side of the room, within a predefined time window (8s for Monkey K, 12s for monkey H). B. Walking trajectories from monkey K (233 out of 778 trajectories from 7 sessions) and monkey H (244 out of 808 from 16 sessions.

Playground Experiment induces complex, yet repeating behaviors

Next, we present how the modularity of the ExR can be made use of to elicit a variety of complex behaviors, which are experimentally induced and therefore reproducible. For this purpose, we conceived the Playground Experiment (PE, Fig.3A). In the PE, monkeys are allowed to freely forage from 36 potential food and juice sources (patches) available in the ExR. We mounted 2 XBIs, 2 flexible hanging branches with different stretch resistance, and placed 2 kongs (hollow toys with food inside) and 30 wood piles with hidden food across the room (Fig.3B). Three animals were tested in sessions of 10 to 15 minutes of duration (10 sessions for animal L, 6 for animal K and H each).

We trained an image-based FairMOT model to predict the poses of the animal during the PE *(details see Methods).* The model was trained on the poses 'walking', 'standing on 4 legs', 'standing on 2 legs' and 'sitting' (Fig. 3B). Additionally, we created a SceneGraph on predicting interactions. SceneGraph was trained on the categories 'interacting with patch', 'interacting with branch', 'interacting with kong' and 'interacting with screen'. Results provide evidence that all three animals show an inter-individual difference in terms of how much time is spent in one of the four defined poses across sessions. Monkey L spends 10% walking, 12% sitting while interacting with a kong or XBI, 28% sitting while not interacting, 2% standing on 2 legs and 8% standing on 4 legs (Fig. 3C). Monkey K spent 12% walking, 7% sitting while interacting with a

kong or XBI, 49% sitting and not interacting, 1% standing on 2 legs and 2% standing on 4 legs. At last, monkey H spent 4% walking, 30% sitting while interacting with a kong or XBI, 18% sitting and not interacting, 3% standing on 2 legs and 8% standing on 4 legs (Fig 3C).

Poses representation during interactions

Next, we wanted to investigate, if the different full-body poses are motivated by the station interaction therefore experimentally induced or chosen by the monkeys independently of the experiment. For this, we correlated the full-body behavioral classifications of FairMOT with the interaction type classification by SceneGraph (Fig. 3D). When comparing the individual poses with the type of interaction (e.g., which pose did the monkey display while interacting with a branch), the poses are consistent and reproducible across sessions and animals. This replicability emerges without any need of human interference. (Fig. 3D).

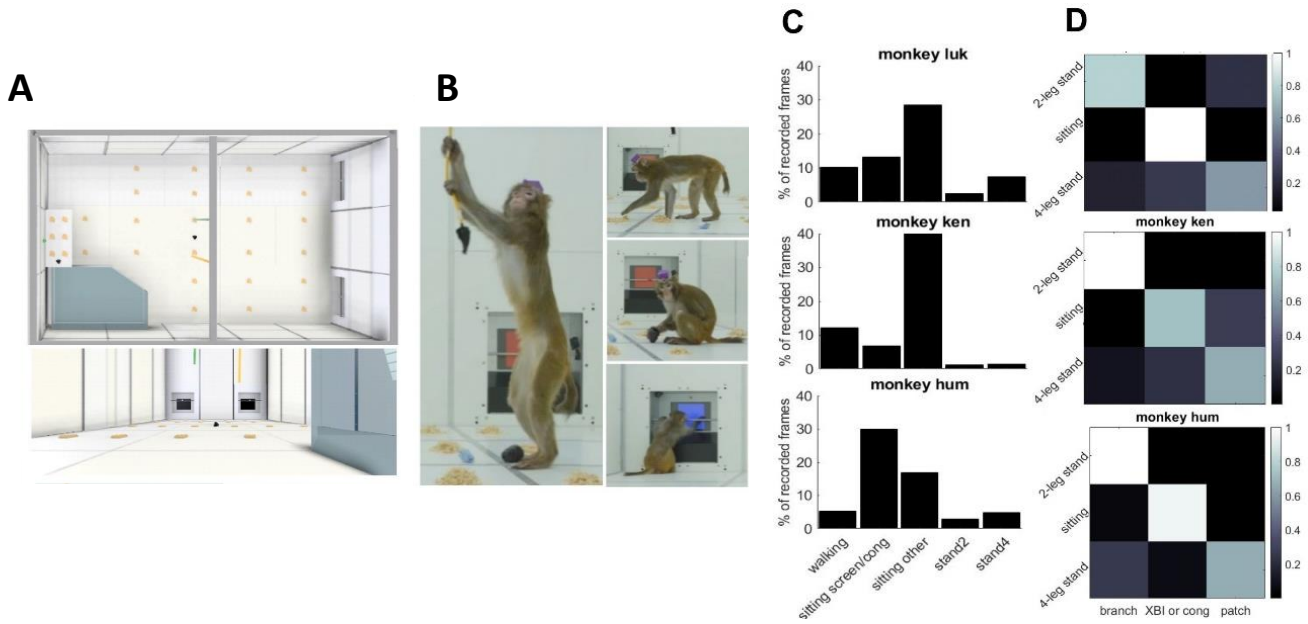

Figure 3: A. CAD renderings of the Playground Experiment (PE) with its in total 36 patches. B. Example images from monkey L while interacting with a branch, wood pile, kong and XBI; all elements from the PE. C. Individual behaviors during PE from each of the three monkeys (10 sessions for monkey L, 6 sessions for monkey K and H). D. Comparison between interaction types (output from interaction detection) and poses (out from pose detection) for each monkey across all present repetitive, stereotypical behaviors.

Single trial analysis of between-patch transitioning behavior

So far, we demonstrated the ExR's suitability for trial-based tasks and for experimentally induced full-body poses, which can be reproduced across animals. The latter can be tracked resulting in a continuous behavioral stream, which then can be parsed for different poses and interactions.

To follow, we show how established analysis methods can be applied on the parsed data from a continuous behavioral stream and used for correlations with neural data. In the following we will provide one example each: one for transition behavior (between-patch behaviors) and one for at-patch behavior.

First, we demonstrate how single trial analysis using the Cone method (Ulbrich and Gail,2021) can be applied on 3D reconstructed transition behaviors between two patches. To extract transition behaviors, we take all frames from FairMOT output, which predict 'walking' as a pose (Fig.4A). We then extract the 3D reconstructed skeleton model for the defined epochs and calculate the 3D walking trajectories by averaging the 3D coordinates of the shoulder, neck and start tail markers. Next, we apply the Cone method on each of the 3D walking trajectories individually to determine the point, and the corresponding time, of commitment (POC and TOC) towards the next patch. We analyzed three sessions of monkey L while recording either in area PMd, M1 or PRR. In the PMd session we identified 5 walking trajectories matching our set criteria, in M1 and PRR 6. The colored dots along each trajectory represents the identified POC (Fig.4A).

Fig. 4B shows example video frames 170ms before and after TOC. We find two types of walking trajectories around the POC: Either the monkey reached the final patch by continuing his ongoing trajectory direction (Fig. 4B lower panels) or by taking a turn (Fig. 4B upper panels).

We next calculated the difference in the average firing rate across each brain region from 600ms before until TOC or from TOC until 600ms after TOC (Fig. 4C). Differences, which are below 0 imply the averaged firing rate decreases after-TOC compared to before-TOC. All continuous trajectories without orientation-change show a decreased neural activity after TOC compared to before TOC (Fig.4C, triangles). Difference above 0 implies the average firing rate increases after-TOC compared to before-TOC. 7 out of 9 trajectories of the class "turn" present this underlying neural activity (Fig.4C, squares). We calculated the mean firing rates before- and after-TOC for trajectories with re-orientation (turns a.k.a. kink) and for trajectories without (no turns a.k.a. no kink). Results demonstrate the increase and decrease in average firing rate across all brain areas of the frontoparietal reach network are significant respectively ($p<0.01$ for trajectories with turns; $p<0.001$ for trajectories without turns, Wilcoxon Rank sum test, Fig.4D).

In Fig. 4E we demonstrate the averaged velocities pre- and post-TOC, again, separated for trajectories with and without re-orientation. The results demonstrate velocities are increased

and decreased significantly before- and after-TOC respectively ($p<0.0001$, Wilcoxon Rank sum test) corresponding to the velocity changes of the monkeys' walking trajectories.

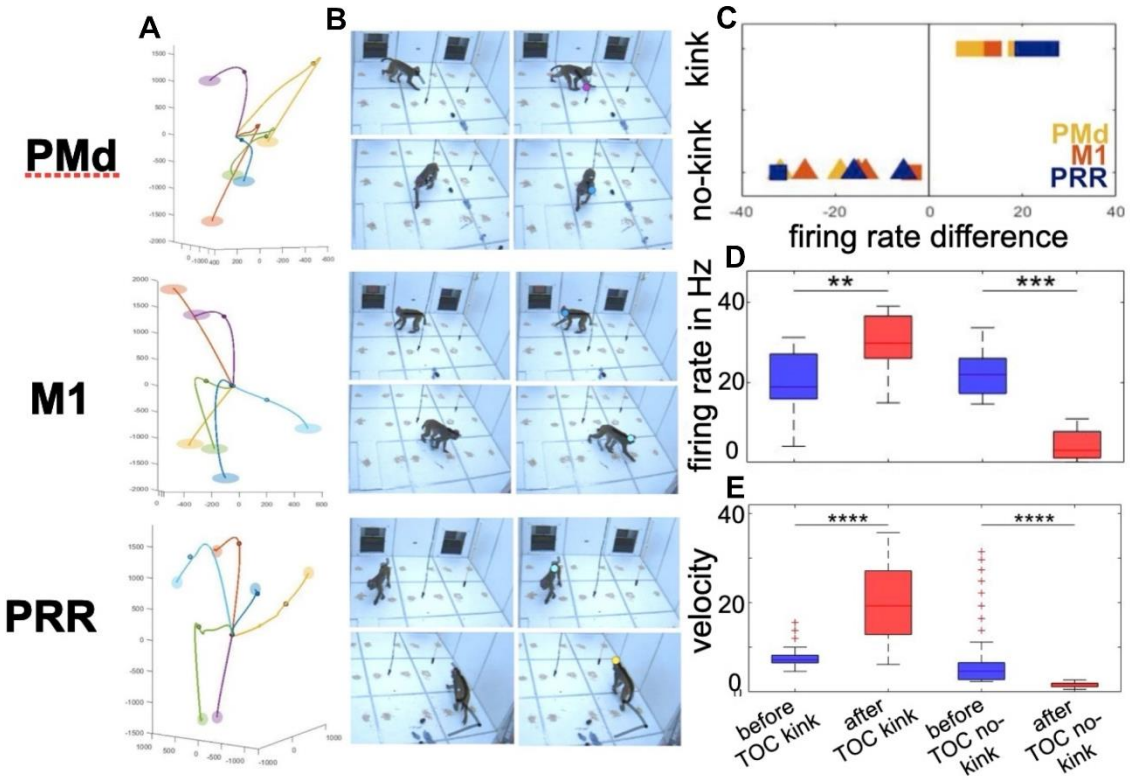

*Figure 4: A. Extracted 3D walking trajectories with the time of commitment (TOC, circular marker) respectively for three sessions. B. Frames from two example trajectories per session depicting 170ms before and after TOC. C. Difference of averaged firing rate before and after TOC (x-axis). Triangles indicate smooth trajectories without kinks, squares trajectories with kinks. D. Difference in averaged firing rate for trajectories with and without kinks (**p<0.01 and p>0.001 respectively, Wilcoxon Rank sum test). E. Averaged velocities of before and after TOCs for trajectories with and without kinks (**** p<0.0001, Wilcoxon Rank sum test).*

Reach encoding comparison as an example of at-patch behavior

As an example of at-patch behavior analysis, we took all frames from FairMOT output, in which animal L is either standing on 2 legs or 4 legs (Fig. 5A). Based on this epoch information, we extracted the 2D positions from our key-point tracking and calculated the Euclidean distance between both wrists and the head to identify reaches towards a patch with the ipsi-(right) or contralateral (left) arm (see *Methods*). Based on this classification, we calculated the averaged firing rate for each recorded unit across all arm reaches. Fig.5 (lower panel) depicts an overall increased firing rate for contralateral arm reaches (shifted distributions) compared to ipsilateral

reaches during a 4-stand leg. When we make the same comparison during a 2-stand leg, the difference in firing rate disappears in PMd and M1.

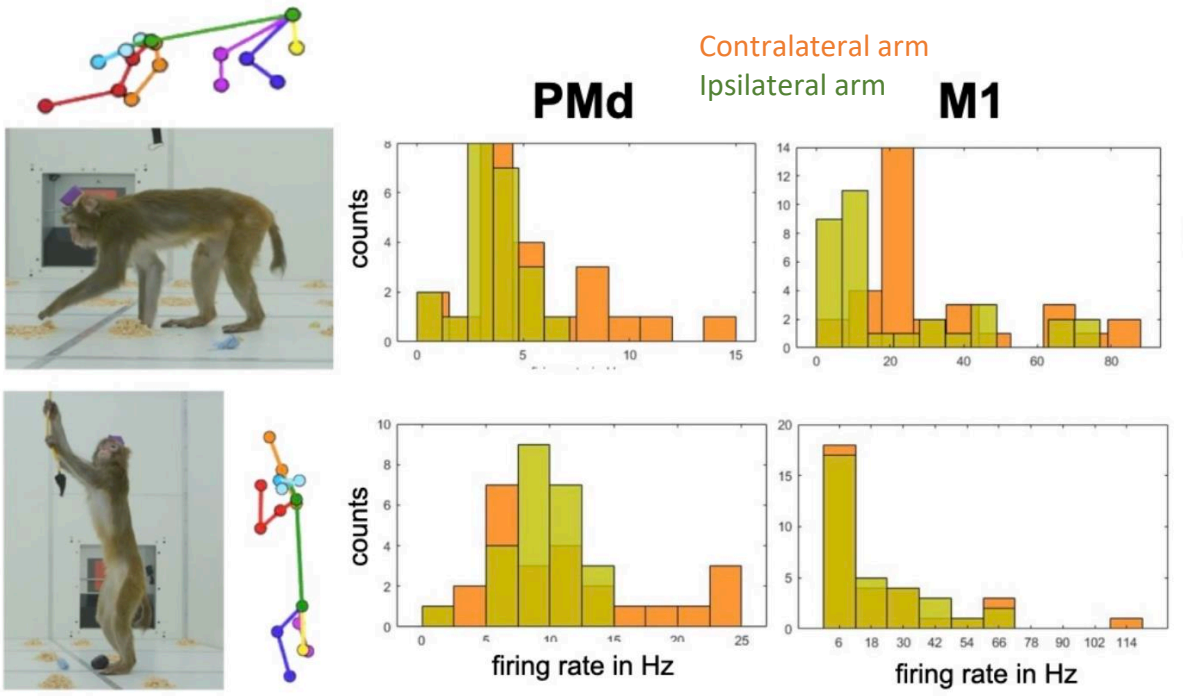

Figure 5: Left panel: Example frame with corresponding 3D reconstructed skeleton model of monkey L exploring a wood pile during a 4-leg-stand and interacting with a branch during a 2-leg stand. Right panel:. Averaged firing rate for each recorded unit across all instances, in which monkey L performed a reach towards a patch with his ipsi- (right) or contralateral (left) arm in areas PMd and M1.

5.4 Discussion

In this study, we present the Exploration Room as a novel modular experimental setup for studying freely moving rhesus macaques. We demonstrate how the modularity of the ExR can be leveraged to make the animals elicit a variety of complex, full-body behaviors, which are experimentally induced and therefore reproducible within and across sessions and without human interference (Fig.1). We provide first example neural recordings of such behaviors, like the 2-leg pull. Additionally, we demonstrate that by using our Playground Experiment we can collect these complex, yet repeating behaviors, which are reproducible across sessions and across monkeys (Fig.2C) and observable within 8 to 15 min of testing.

No study, up to date, has provided suggestions on how ecological relevant at-patch behaviors – as in contrast to transition-actions (e.g. jumping, walking, Voloh et al., 2022), can be experimentally induced for studying, as opposed to waiting for relevant behaviors to appear by themselves (Silvernagel et al., 2021; Voloh et al., 2021).

To complete the picture of the ExR's suitability for systems neuroscience with the focus on decision-making, action planning and execution, we demonstrate the monkeys can still engage in highly goal-oriented (Fig.3 B, C) trial-based repetitive behaviors despite the ExR's large size and the reduced behavioral constraints. This is a particularly important finding to show that a progressive transition from chair-seated to large scale, freely moving setups is possible. Being able to translate classical, touch screen-based trial-based tasks in unconstrained, more ecologically relevant testing conditions, can be of crucial importance to establish continuity and comparability between lab-based and field-based studies.

As the state-of-the-art analysis approaches in systems neuroscience heavily relies on trial-averaged responses for calculating the preferred tuning direction (Kalaska et al., 1983; Georgopoulos, 1982, 1986; Schwarz et al., 1988), and as analysis approaches for continuous non trial-based behaviors in rhesus macaques remain sparse, applications of existing large-scale setups are limited to walking mainly (Mao et al., 2021; Maisson et al., 2022). When a broader range of behaviors is introduced (Voloh et al., 2021; Voloh et al., 2022), the feasibility of such complex full-body behaviors for systems neuroscience with the particular focus on action planning and execution remains an unresolved question. It has been established how to track these types of behaviors using markerless deep learning approaches by mastering high demand engineering challenges (Bala et al., 2020). As these solutions come with heavy data load (3.5GB / s with 64 cameras) and intensive computing, we wanted to address the question of how far we can reduce this load without losing valuable information by combining different open access tracking approaches. In this study, we successfully present how by using a novel combination of 2D tracked pose estimation and 2D and 3D tracked key-points we are able to extract relevant behavioral patterns using 4 to 5 cameras only. This supports the idea that the number of cameras and tracking methods used should be defined depending on the specific experimental requirements – i.e., how fine-grained the to-be-analyzed behavior needs to be. If we take this perspective, the study of the neural basis of ecological, free behaviors in novel setups can become a concrete option for many more neurophysiological laboratories.

To demonstrate that the ExR has a huge potential for systems neuroscience studies, we present two explicit examples of how continuous behavior can be analyzed using existing analysis methods applied in an unconventional way, which to our best knowledge has not been suggested to date. Using our combination of tracking methods, we parse the continuous data for studying to-our-purpose relevant behaviors. We showed first exemplary use cases of how

existing single trial analysis can be applied to the extracted walking trajectories and made use of to compare the underlying neural activity. As a second example we showed how we can extract frames with ipsi- or contralateral reaches in different body postures and compare their neural underpinnings within one session. These two examples provide first evidence of the feasibility of the new experimental environment to the study of the involvement of the frontoparietal network in action planning and execution in more ecological contexts, where a complexity of new factors such as postures, location, company and motivation come into play.

While these results provide initial evidence of the ExR's potential to explore decision-making, action planning, and execution in a free, unrestrained environment for rhesus macaques, it's important to note that this study does not attempt to offer comprehensive scientific answers to the questions raised. Future studies, with increased channel counts, will be ncecessary to dive deeper into the neural correlates associated with the proposed research questions. However, the present work still provides a highly relevant result by demonstrating, for the first time, the feasibility and potential of studying the neural correlates of decision making during transition-behavior instead of action transition itself and action planning and execution during stationary behaviors.

Single trajectory analysis reveal potential decision and movement-time trade-off mechanisms in explorative foraging

We recorded continuous behaviors in the ExR during the PE and extracted between-patch and at-patch behaviors. We identified walking trajectories as between-patch behaviors and applied the Cone Method (Ulbrich and Gail., 2021) on each individual trajectory to detect the point of commitment (POC). From existing literature, we know that the speed of the arm or walking movement can be a predictor of decision variables. Johnson and Ebner (2008) have provided evidence by recording a 2D arm pursuit task that neurons in PMd and M1 are modulated by speed information. In a freer experimental setup, in which the monkeys were walking on a treadmill, recorded brain activity in PMd was reported as being modulated by the step velocity (Foster et al., 2014). In M1 velocity encoding has been leveraged for decoding brain activity to control a robotic wheelchair using BMI (Rajangam, 2016). Our results are in line with the existing literature proposing the neural activity before and after as well the walking velocity before and after the detected point of commitment allow interpretations about the confidence and commitment of the monkey towards the next patch.

It has been additionally demonstrated that during deciding, when unconfident, monkeys tend to slow down their movement (Dotan et al., 2018). It is also known that rhesus macaques present a decision and movement time trade-off. The longer the decision time is, the shorter the movement time therefore the faster the speed and vice versa (Thura and Cisek, 2014).

Based on this we interpret that our results might provide evidence of how based on single trajectories we can extract the point of commitment towards the next patch. The increase or decrease of velocity after POC can be interpreted as an indication towards the decision and movement time trade-off and could potentially suggest the monkey's commitment to the next patch.

Comparison of reach encoding relative to body posture

It has been previously demonstrated that neurons in the primary motor cortex are tuned for arm reach direction (Georgopoulus et al., 1982; Kalaska et al., 1983; Schwarz et al., 1988). When testing the tuning properties of motor cortex neurons in a semi-naturalistic and uninstructed setting, Aflalo and Graziano, 2007, found that the neuronal variance explained by the direction tuning properties is around 8% whereas when taken a subset of free reaches, which resemble the movements of a center-out reach task, the explained variance increases to 42%. We compared ipsi- and contralateral arm reaches during two different poses (2-leg-stand and 4-leg-stand). Our results show increased firing rates for contralateral reaches in a 4-leg-stand across all three brain areas of the frontoparietal reach network. During a 2-leg-stand this difference disappears in PMd and M1.

Behaviorally reaches during a 2-leg and 4-leg stand vary. During a 4-leg-stand the other, the not reaching arm, is remaining still while in the 2-leg-stand the non-reaching arm is moving holding the branch down. From studies performed in conventional chair-seated setups evidence has been provided that neurons in M1 maintain their representation during bimanual arm movements (Cross et al., 2020) compared to a unimanual reach. For PRR neurons it has been suggested that while LFPs reflect patterns of bimanual movements, the single unit activity encodes only the contralateral arm activity during planning (Mooshagian et al, 2021). Cisek and colleagues (2002) compared ipsi- with contralateral arm reaches, coming to the conclusion that M1 neurons are active during ipsi- and contralateral arm reaches, however the activity is distinctive between both. Ames and Churchland (2019) found evidence of motor cortex neurons being activated independent of ipsi- or contralateral reaches suggesting population activity occupies different subspaces therefore making ipsi- and contralateral arm reaches distinguishable.

Our results can be interpreted in line with existing literature that contralateral arm reaches have an increased neural activity compared to ipsilateral arm reaches during a 4-leg-stand. However, the missing selectivity for contralateral arm reaches cannot be explained by merely bimanual reaches during a 2-leg-stand as literature suggests we should still find a difference in neural activity between contra- and ipsilateral reaches. The existing literature has tested these

hypotheses while the monkeys were maintaining a sitting-pose. The role of pose in reach encoding remains an open question, which needs to be addressed in future studies.

Refinement of tracking methods

Our interaction and pose detection methods are based on single frame analysis. Depending on the behavior exposed, in some cases the information of a single frame can be ambiguous. Given the example frame for instance, we cannot assign whether the arm of the animal is going towards or away from the mouth or whether the monkey is reaching or starting to walk (Fig. 6). The way a human observer differentiates between two ambiguous possibilities is by looking at the behavior across time. Information about a few frames before and after this frame clarifies this ambiguous situation. This concept could be applied on our tracking methods by for instance adding a time criterion, which takes the information of x numbers of frames before and after the current frame into account to unambiguously assign the behavior or pose.

Depending on the scientific question that we want to address, in a few cases higher key-point precision might be necessary. If this is the case, the 2D and 3D tracking could be further improved by optimizing the camera views. Instead of using top view cameras only as shown in this study, we can use lower angle views mounted inside the ExR using custom-designed encasings (ExplorEye, Lacal and Gail, *in prep*) and more cameras as depicted in S-Fig.1.

Another possibility would be to increase the amount of manually labeled frames. For this, we trained the already pre-labeled MacaquePose (Labuguen et al., 2021) data set together with 300 manually labeled frames from the ExR. However, the combination of MacaquePose together with our labeled frames performs with less accuracy (train error 10.07, test error 13.57 after 1030000 training iterations) than a model trained solely on our labeled frames (train error 2.97, test error 5.71 after 50000 training iterations). We conclude this is based on the monkey size in each of the frames used in MacaquePose. Most of the labeled frames are cropped such that the monkey is covering the majority of the frame whereas in our recorded views the monkey is zoomed out and much smaller. Therefore, a key-point model heavily trained on MacaquePose does not generalize in the ExR sufficiently yet.

Technical implementations and their current limitations

We recorded this proof-of-concept study with a “true” wireless system, which means the recorded data was streamed in real-time. This can be advantageous for closed loop experiments as in BMI applications (Rajangam et al., 2016). However, the analogue system, which is suited for these types of large distances, can introduce additional noise problems during fast or sudden movements. Other systems, in which the signal is digitized immediately

on the headstage (Blackrock) face the challenge of antenna coverage in such a large space. For cases, in which closed loop implementation is not needed, data loggers can be used (e.g. Spike Gadget, Maisson et al., 2022 or Deuteron, Mao et al., 2020). These systems store the data on the SD card, which is directly placed on the headstage and therefore overcome the challenges of true wireless devices. However, real time implementations are not possible with these systems.

We implemented a custom written python software which is CPU based. This allowed us to record up to 70Hz with 8 cameras. However, when streaming from a higher count of, which could be needed to improve keypoint detection for instance, a GPU based streaming is better suited (e.g. JARVIS, https://jarvis-mocap.github.io/jarvis-docs/) allowing not only additional cameras but also higher frame rates and resolution.

Conclusion

In this study we showed the potential of large-scale experimental setups suited for systems neuroscience when investigating full-body movements beyond walking, with the goal of narrowing down the gap between systems neuroscience and field studies. We went one step further and provided, for the first time, concrete examples of how to extract relevant behaviors known from long-standing paradigms in conventional neuroscience to address specific and novel questions about the sensorimotor basis of action selection, specification and execution in freely moving conditions. In conclusion, the present study demonstrates that setups such as the ExR can substantially extend our possibilities in systems neuroscience as it allows studying neural correlates of complex, ecologically relevant full-body behaviors.

5.5 Methods

The Exploration Room

The Exploration Room (ExR) is a large-scale laboratory environment with the dimensions ~2-5 x 4.5 ~2.5 m^3 (L x W x H). The frame was custom constructed using Minitec profile systems (MiniTec, Schönenberg-Kübelberg, Germany). Its walls and floors consist of modular panels (858 x 928 mm, top row 858 x 600mm), which are held by thin metal stripes. This configuration allows us to exchange each of the panels individually to mount interactive devices. 8 LED panels illuminate the white room evenly to avoid shadows. The roof consists of 5 mesh stripes used for animal fencing. On the opposite side of the room two doors to allow human entrance were built in to allow access. The floor of the ExR is elevated by 28cm to allow wiring of floor mounted interactive devices. The overall room is designed such that it can be split into two

symmetrical halves using a motorized divider, where the lower half is transparent allowing the animals to see but not physically interact with each other.
To collect behavioral data, we implemented two types of camera mountings: 1) outside ExR mountings (used for data collection in this study) and 2) inside ExR mountings. The cameras were mounted in a custom printed encasing and covered by a UV filter to protect the camera lenses. The cameras were placed on a ball joint and a custom Minitec frame to allow adjusting of views and angles. For inside cage mounting, we used ExplorEyes, a new custom-designed camera encasing, in which the camera itself works like a ball-joint instead of using an external joint. This way interactions of monkeys cannot misplace the configured camera configuration.

We used a custom-written Python code to acquire images from up to 8 cameras using FLIR Chameleon 3 cameras. We recorded at 70 fps and a resolution of 1024x768. The software receives and stores all incoming TTL pulses received by our task controller (MoRoCo), which is written in C++, for later alignment.
For the proof-of-concept neural data recordings, we used a wireless system, which is suited to estimate and observe the data quality in real-time. For details, please see xxx. In summary, we used a 32ch TBSI headstage, which sends the neural broadband data to the TBSI receiver using 2 antennas. This receiver sends the signal via an amplifier to the neural signal processor which records the data on the PC. The identical TTL pulse, which is sent to the camera acquisition system, is also sent to the neural acquisition system for offline data alignment (Fig. 7).

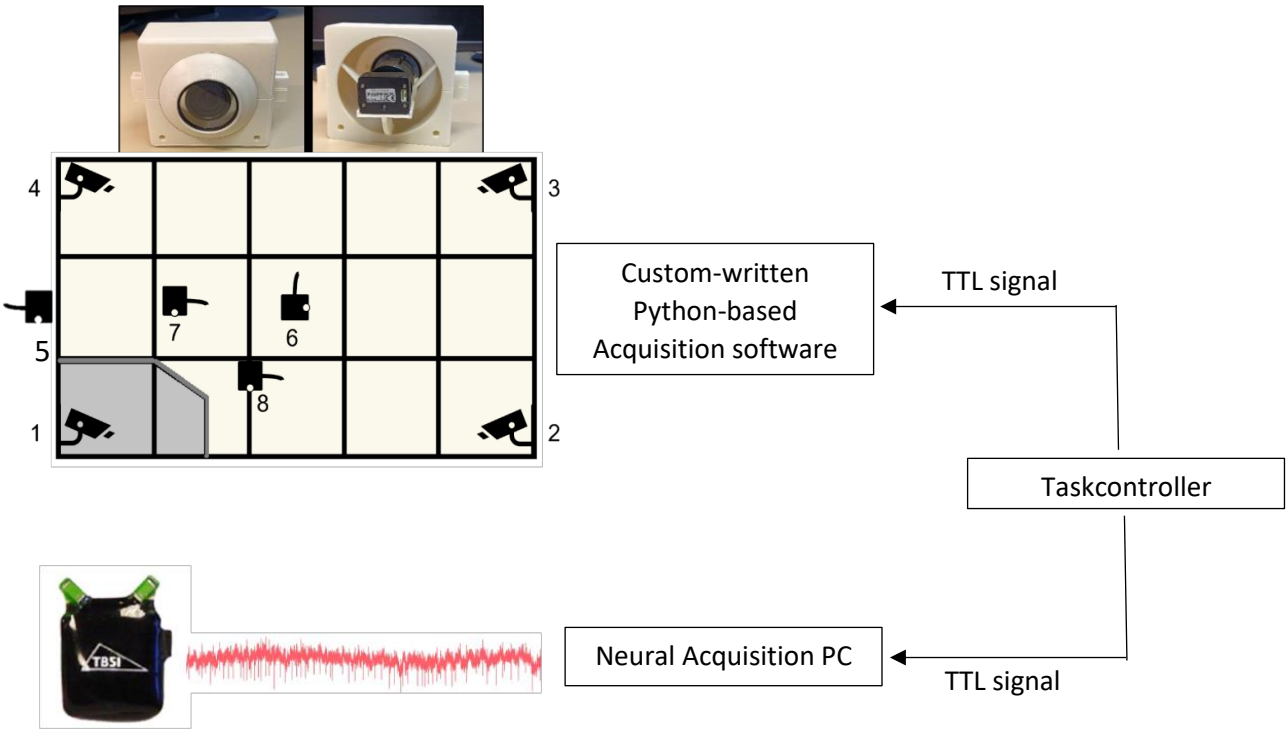

Figure 7: Overview of peripheral device communications for behavioral and neural recordings in the ExR. An external task controller PC sends a TTL signal to a) a custom-written python-based video acquisition software and b) to the neural data acquisition to collect wireless neural data.

The Playground Experiment

For the Playground Experiment we placed 32 potential food patches consisting of piles of wood chips along the floor, 2 elastic fitness bands with different tractions (nominal value by manufacturer 4.5kg and 13.7kg) as hanging branches in the center of the room, 2 interactive kiosk-systems for cognitive testing called XBISs (Calapai et al., 2017; Berger et al., 2018) and 2 hollow toys potentially filled with fruits. We habituated the animals to this new environment and trained them to go in and out of the ExR for 2-5 days. We then recorded 10 playground sessions with animal L and 6 each with animal H & K. While the animals were performing the task, we recorded their behavioral data with all 8 cameras simultaneously. In addition, we obtained neural data in the primary motor cortex (M1), parietal reach region (PRR) and dorsal premotor cortex (PMd) of animal L. In the scope of this study we used solely four top corner camera views, plus an additional lower view for monkey H and K, as they proved to be sufficient to achieve 2D tracking of actions and interactions and keypoint 3D reconstruction.

Animals and Surgery

All animals were housed in social groups with one to two male conspecifics in facilities of the German Primate Center. The facilities provide cage sizes exceeding the requirements by German and European regulations, and cages enriched with wooden structures, climbing and hanging structures, and a turnover of various toys and devices (Calapai et al., 2017; Berger et al., 2018). Monkeys L and H were implanted with multi-electrode chronical arrays and a customized recording chamber (Ahmed et al., 2022) during a single sterile surgery under deep gas anesthesia and analgesia via an intravenous catheter. Additionally, the animals receiving a craniotomy were prophylactically treated with systemic antibiotics cobactan, duphamox, or synulox 1 day pre surgery and 2–5 days post-surgery. Analgesia was refreshed on a 8- to 9-hours cycle continuously for up to three post-surgical days for non-craniotomy types of surgery (e.g., headpost implantation) and four to five postsurgical days for surgeries with craniotomies (e.g., chamber implantation) using levomethadone or rimadyl, depending on need.
All procedures have been approved by the responsible regional government office [Niedersächsisches Landesamt für Verbraucherschutz und Lebensmittelsicherheit (LAVES)] under permit numbers 3392 42502-04-13/1100 and 33.19-42502-04-18/2823 and comply with German Law and the European Directive 2010/63/EU regulating use of animals in research.

Deep Learning

Computer vision models based on deep learning architectures are able to learn a variety of different image and video related tasks. In this work we use architectures for action classification, object detection, tracking, pose estimation and interaction recognition (Fig.8).
We are using a modification of the multi-object tracking architecture FairMOT (Zhang et al., 2021) which is able to detect objects (in our case monkeys and patches) in every frame of a video and associate these detections across frames. We extend this architecture to classify poses of detected individuals, and to track all classes of interest in the video (monkey, wood piles, XBI, branches and kongs).
For interaction recognition between the monkey and the other objects in the room, we use the FCSGG architecture (Liu et al., 2021), which shares the same basic structure with FairMOT.
For key-point estimation, we use DeepLabCut (Mathis et al., 2018), a model which allows for key-point detection in laboratory environments.

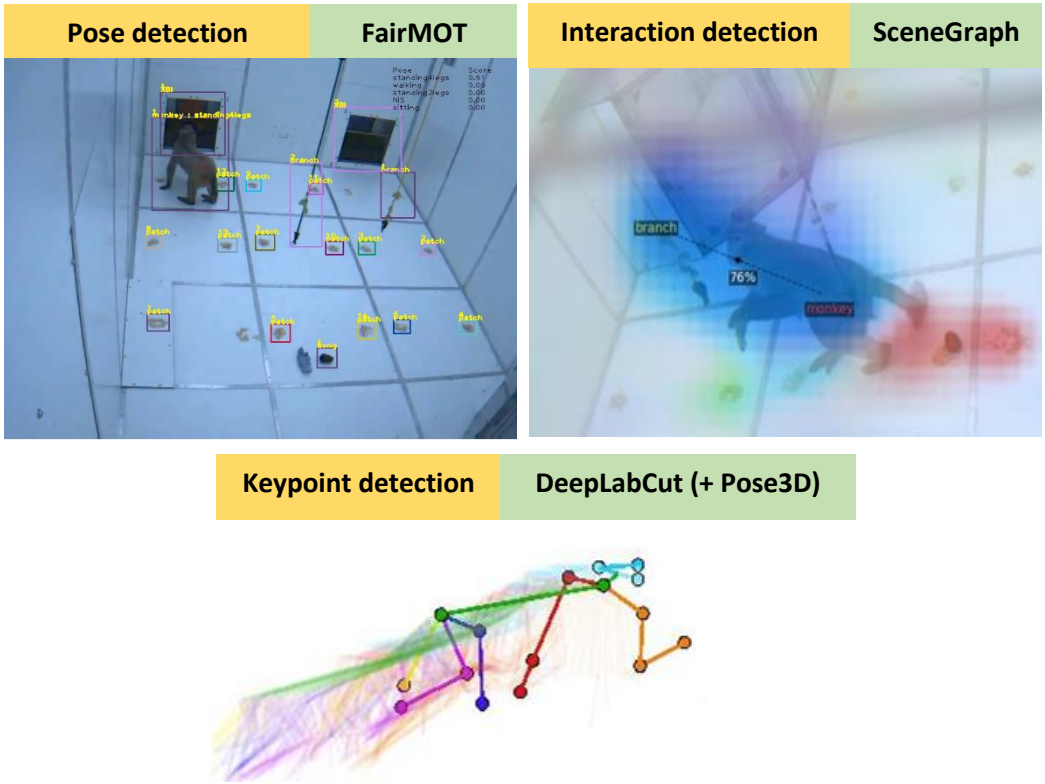

Figure 8: Overview of used tracking methods. We trained a FairMOT based model to predict the poses 'walking', 'sitting', '2-leg stand' and '4-leg stand'. We created a SceneGraph to predict interactions with 'branch', 'kong', 'XBI' and 'wood pile'. Keypoint tracking of individual limbs was performed by training DeepLabCut baked on 19 keypoints.

Multi-Object Tracking and Pose Classification

The task in Multi-Object Tracking is to detect all objects of interest in an image and associate the same individual across frames to form a trajectory. While many multi-object tracking architectures follow the tracking-by-detection paradigm (i.e., first get all detections and in a second step process the detections in order to get re-identification features for association), FairMOT yields detections and re-identification features simultaneously as proposed by (Wang et al., 2020) a neural network based on convolutions (CNN).

Given an input frame I $\in R^{\omega_0 \, x \, h_0 \, x 3}$ a convolutional backbone (e.g. Yu et al., 2018) creates a feature map (Fig.9). The width and height of the feature map are strided with a factor of 4 from the input frame, i.e. F $\in R^{\omega \, x \, h \, x \, C}$ where w = $\frac{\omega_0}{4}$, h=$\frac{h_0}{4}$ and C is the number of channels (in our case 512). The feature map is then used in parallel by several convolutional heads. We added a classification head for action recognition to the four heads present in FairMOT. Each one of the five heads is equipped with a loss function. We use the standard loss functions described in (Zhang et al., 2021; Zhou et al., 2019) for L_{heat} (focal loss), L_{size}, L_{off} (L1 loss) and L_{id} (cross

entropy). For the added classification head we add L_{pose} with cross entropy loss. Finally, we combine the five loss functions with a weighted sum and use the total loss for training the model. We pre-trained the tracking model with MacaquePose (Labuguen et al., 2021), a large annotated dataset with 13,000 images of macaques. We then fine tuned our model with 630 frames in total across all cameras from the Exploration room videos which were labeled with the open source software Visual Object Tracking Tool (VoTT, Microsoft, Albuquerque, New Mexico, U.S.). We used a self-made GUI (https://github.com/richardvogg/interaction-labelling-tool) to annotate four different actions: sitting, standing-4-legs, standing-2-legs and walking, as well as a placeholder action Not-in-Scene, which will be returned, if no monkey was detected in a frame.

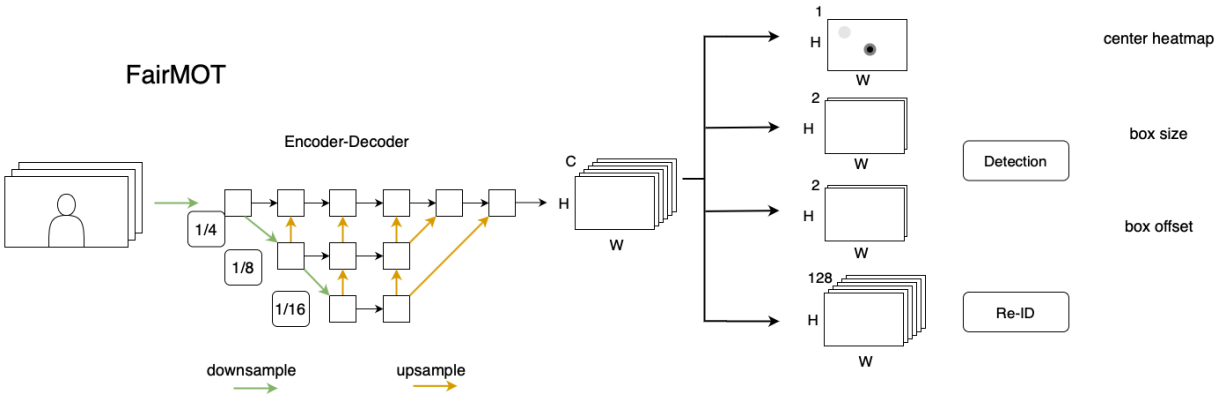

Figure 9: Our adaptation of the FairMOT architecture. We use DLA (Yu et al., 2018) as a backbone and the resulting feature map is processed by five parallel heads for center detection (heatmap), box offset, box size, re-identification features and pose classification.

Scene Graph Generation

The task of Scene Graph Generation consists in detecting all relevant objects in an image and understanding relationships between the objects. Formally, given an input image I as above, we expect the model to output a graph G = (V;E) where the vertices V are the detected objects and the edges E are possible interactions from a predefined list. For these experiments we only train one possible interaction, which we label as “interacts with” and learns which object the monkey is currently exploring. Similar to the tracking model FairMOT, the FCSGG model (Liu et al., 2021) for Scene Graph Generation bases its structure on CenterNet (Zhou et al., 2019). Instead of producing one feature map, FCSGG generates four feature maps for different resolutions which allows for more fine- and coarse-grained detections. Further, FCSGG extends Center-Net by one head which predicts Relationship Affinity Fields, by assigning each pixel in the image a two-dimensional vector which indicates whether there is a relationship between two objects and if yes, in which direction it goes.

Keypoint Tracking and 3D reconstruction

For keypoint body part tracking we used DeepLabCut (version 2.1.4; Mathis et al, 2018, Nath et al, 2019). Specifically, we labeled 300 frames taken from 4 videos (then 95% was used for training). The 19 annotated keypoints were left and right eyes, ears, shoulders, elbows, wrists, knees, ankles, head, neck, nose, start and end of tail. We used a ResNet-50-based neural network with default parameters for 50000 number of training iterations. We found the test error was: 5.71 pixels, train: 2.97 pixels (image size was 1024 by 768). We used a p-cutoff of 0.6 to condition the X and Y coordinates for future analysis. This network was then used to analyze videos from different Playground Experiment sessions.

We used Pose3D (Sheshadri et al., 2020), which is a wrapper around the standard Matlab stereo calibrator, for 3D projection of 2D tracked keypoints. Camera view 1 (Fig. 7) was used as the primary camera, all remaining cameras as Secondary. We first 3D reconstructed all keypoints using pairs of all cameras. We then calculate the average of the 3D reconstructed keypoints positions obtained from each camera pair to get the final 3D reconstruction.

Evaluation

In this section we will briefly evaluate the three tracking methods used in this study. First, we evaluated the FariMOT based pose tracking (Fig.10A). The tracking performance was calculated by randomly selecting 10 frames from each monkey and 4-5 different camera perspectives. The total of 140 frames (5 cameras for monkey H and K, 4 cameras for monkey L) is manually examined and we count true positive and false negative detections to calculate the sensitivity. We exclude false positives as the amount is negligibly small and there is almost no negative effect for the Scene Graph model. The class-specific results are reported in Table 1.

	Monkey	Patch	Screen	Cong	branch
Sensitivity	0.97	0.95	1.00	0.92	0.94

Table 1: Sensitivity (True Positive Rate) of the tracking model.

For the pose predictions/action classification, we create a validation set from 100 videos. These videos are each taken from one of five camera views and contain one of three monkeys. From each of these videos we sample 30 frames. We use a k-means clustering based method (proposed in Mathis et al., 2018) to automatically select frames with pairwise different characteristics for an optimal variety of scenes. These frames were labeled by hand. Afterwards, five labeled images were sampled per monkey, per camera perspective per pose to balance the validation set. Only for animal L there are no recordings from camera view 5 (Fig.7).

For the Scene Graph we randomly sampled 416 frames balanced by monkeys and camera views and predicted the object with the highest confidence as the object of interaction, if the confidence is above a threshold of 0.75. On the individual camera views, we obtain the confusion matrix displayed in Fig.10B. Patch interactions are the most misclassified interaction. We use post-processing ("Post processing of tracking") to improve the classification results.

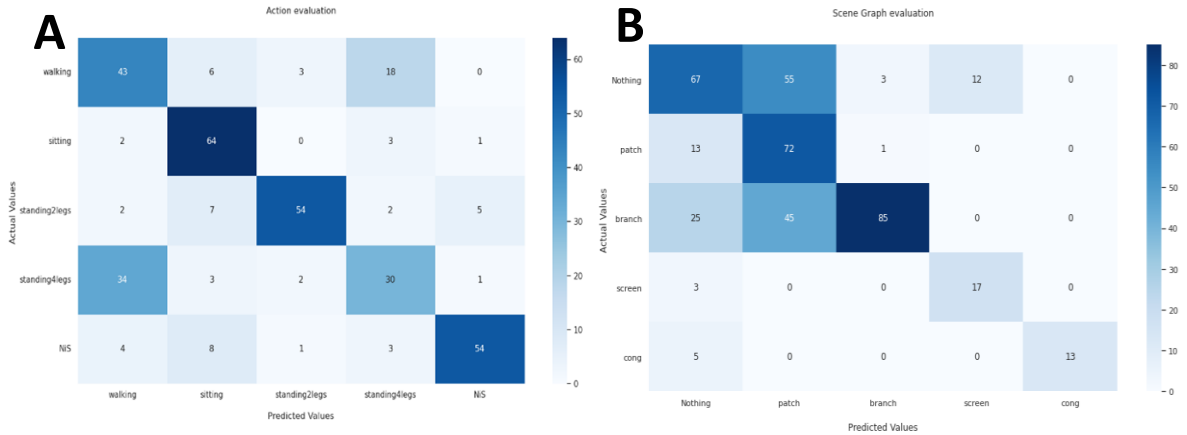

Figure 10: Results of tracking evaluations. A and B are the confusion matrices of the validation results for pose and interaction predictions respectively.

Behavioral data analysis

Post-processing of tracking

To improve tracking results, we applied the following post processing before analyzing the data. We set the confidence level to 0.9 for all detected pose outputs from FairMOT (sitting, walking, 2-leg-stand and 4-leg-stand) and checked, whether the detected poses were maintained for at least 70 frames (1s).

For SceneGraph we set the confidence level for all interactions except patches to 0.85; patch interaction's confidence level was set to 0.7. Additionally, whenever interactions with a branch and interactions with patches were detected within the same frame, we prioritized branch interaction and labeled that frame as such.

For 2D tracking we used only marker predictions which exceed the confidence interval of 0.9.

For 3D tracking we used a sliding window of 280 frames (4s) and removed jumping markers by means of an outlier detection algorithm, based on the assumption that physically the monkeys' body cannot jump across the room and back within a few frames. We replace those values with a linear interpolation from the last available value until the following, first available value for

each segment of missing data. To remove high-frequency noise from the tracked trajectories, which are caused by jittery marker placement during labelling, we additionally apply a 4th order Butterworth low-pass filter with a cutoff frequency of 0.5Hz.

Pose-Interaction effects

We calculated the proportions of session time in frames by extracting all frames, in which the monkey was either sitting, standing on 2 or 4 legs and walking based on FairMOT output. The proportions were calculated by taking the total amount of frames detecting a specific pose and dividing this by the total amount of frames recorded.

Next we took the information of pose behavior obtained from FairMOT and compared them to predictions of interactions using SceneGraph output, e.g. if frame 100 to 170 is predicting the monkey was sitting, we compare these frames to the interaction prediction, so in other words, in how many frames across the 70 frames (100 to 170) was the monkey interacting with a XBI, a kong, a branch or a wood pile. We calculated these proportions and visualized them to obtain the results across all 3 recorded monkeys.

Lastly we calculated the average firing rate across all extracted epochs, in which the specific poses were detected. Additionally, we calculated the correlations of neural activity across different pose behaviors. We used the Lilliefors-test to identify, whether our data is normally distributed. Whenever the null-hypothesis was rejected implying we do not have normally distributed data, we applied non parametric significance tests and correlations (Wilcoxon Rank sum test, Spearman correlation). When the test confirmed our null-hypothesis, we applied parametric tests (2-way ANOVA).

Single trial extraction and analysis in repetitive behavior

For the analysis of monkeys' behavior in the walk and reach task, we used synchronized timestamps for the start and end of each trial to crop the continuous video tracking data in discrete segments (trials). Full-body walking trajectories were extracted by averaging the position (preprocessed as described above) of keypoints outlining the monkey's torso (i.e., shoulders, neck, and start of tail), thus obtaining a geometrical estimation of the animal's center of mass. Finally, for a standardized representation across animals, we performed a rotation and normalization of all trajectories so that they lay on the horizontal plane and the distance from the average starting position and the average middle point between the two targets equals 1. A subset (about 30%) of all trajectories of successful trials is presented as an example (233 out of 778 trajectories from 7 sessions for K; 244 out of 808 from 16 sessions for H).

Single trial extraction and analysis in continuous behavior

To analyze between-patch behavior, we cut the trajectories following three criteria: (i) the walking pose (as detected by FairMOT) should be assigned with a confidence level equal or higher than 0.7 and (ii) maintained for at least 70 frames (1s); finally, the walking distance from the start to the end of the detected tracking segment should be of at least 1000 pixels. All obtained epoch-start and -end times were used to extract 3D reconstructed trajectories based on the keypoints shoulders, neck and base of the tail. These trajectories were then normalized to their starting position, in order to obtain a fan of traces unraveling for the center of the 3D coordinate system. The Cone Method (Ulbrich and Gail, 2021) was applied to these walking paths by setting the starting position at the origin and a virtual target of 100 pixels of radius for each trajectory end.

Reach detection extraction and analysis in continuous behavior

For at-station reach detection we first took all frames, in which the monkey is detected as "standing on 2 legs" and "standing on 4 legs". We then calculate the Euclidean distance between both arms' wrist and the head marker. We then calculated the slope (m) for both differences and defined: m>0, the reach going away from the mouth therefore a reach towards an object and m<0, the reach is going towards the mouth. To account for small marker jitters we defined, a point is only part of a reach, if it exceeds the averaged slope value by at least one standard deviation across the entire detected single epoch of the relevant behavior. To account for small single missing points between reaches and to not mistake one single reach as two short reaches we look at all start and end reach points. If the next reach is within 8 frames (<115ms), we merge them together as one reach. If the start and end position of a reach is within 3 frames (42ms), we exclude it from further analysis under the assumption full-arm reaches cannot be of such short durations.

For reaches during 4-leg-stand we additionally included all detected walking frames as walking and 4-stand-leg reaches can be mistaken by FairMOT based on single frame analysis. When analyzing walking behaviors, we added the criterion of leg distance. For this we calculated the velocity of both knee markers. If the velocity of one or the other knee exceeds 2 pix/s, we label this frame as walking and disregard the previously detected arm reach as it is considered as part of the walking movement.

In the session with recordings from area PMd, results were obtained unsupervised and did not require any additional human adjustments. The other two example sessions shown are with neural recordings in area M1 and PRR. In these two sessions reaches were detected first unsupervised. However, human supervision was necessary to add additional reaches, which could not be detected within the used camera view, as the reach was occluded by body parts.

Neural data analysis

Data acquisition

We used a 32-channel wireless TBSI headstage (W32, Triangle BioSystems International, Durham, USA) to record from a single 32-channel array per session. After amplification of the input voltage (gain 200) the analog signal was transmitted to the TBSI receiver (3.05GHz transmission frequency). The receiver then forwarded the signal to a 192ch Cerebus system (Blackrock Microsystems LLC, Salt Lake City, USA), which was connected via a HDMI wire and a Cereplex headstage (Cerebus input side) and an adapter (TBSI receiver output side). The Cerebus system digitized the incoming signal with 30 kHz. We set a threshold of -3.8 x RMS and recorded the raw signal as well as the thresholded signal.

Post-processing

The collected raw data was post processed as described in Dann et al., 2016. First, a 5000Hz low-pass using a zero—phase second order Butterworth filter. We then transformed the signal in PCA for each array separately and removed principal components that explain common signals. Then the signal was transformed back (Musial et al.,2002). At last, spikes were extracted by threshold crossing using a negative threshold defined by -3.8 x median (|signal|).

Averaged spiking frequencies

We calculated the spike density function from the spikes of each unit, which exceed the average firing rate of 2 Hz, by convoluting the spike trains (spike event times) with a Gaussian kernel (σ = 50 ms). Spike density functions (sampled at 200 Hz) were temporally aligned to the start frame of each extracted, relevant behavior of interest.

For neural data analysis of single trial trajectory analysis, we calculated the spike density and plot its mean per unit per occurrence. We used the Lilliefors-test to identify, whether our data is normally distributed. Whenever the null-hypothesis was rejected implying we do not have normally distributed data, we applied non parametric significance tests and correlations (Wilcoxon Rank sum test, Spearman correlation).

References

Aflalo, T.N, Graziano, S.A. (2007). Relationship between Unconstrained Arm Movements and Single-Neuron Firing in the Macaque Motor Cortex. *Journal of Neuroscience*, 27(11), 2760-2780. doi: 10.1523/JNEUROSCI.3147-06.2007.

Agetsuma N (1995) Dietary selection by yakushima macaques (*Macaca fuscata yakui*): The influence of food availability and temperature.*Int. J. Primatol* (16) 611–627. doi: 10.1007/BF02735284.

Ahmed, Z., Agha, N., Trunk, A., Berger, M., & Gail, A. (2022). Universal guide for skull extraction and custom-fitting of implants to continuous and discontinuous skulls. bioRxiv. doi: 10.1523/ENEURO.0028-22.2022.

Ames KC & Churchland MM (2019) Motor cortex signals for each arm are mixed across hemispheres and neurons yet partitioned within the population response. eLife 8:e46159. doi: 10.7554/eLife.46159.

Bala PC, Eisenreich BR, Yoo SBM, Hayden BY, Park HS & Zimmermann J (2020) Automated markerless pose estimation in freely moving macaques with OpenMonkeyStudio. Nat Comm (11) 4560. doi: 10.1038/s41467-020-18441-5.

Batista AP, Santhanam G, Yu BM, Ryu SI, Afshar A & Shenoy KV (2007) Reference frames or reach planning in macaque dorsal premotor cortex. J Neurophy (98-2) 966-983. doi: 10.1152/jn.00421.2006.

Berger M, Calapai A, Stephan V, Niessing M, Burchardt L, Gail A & Treue S (2018) Standardized automated training of rhesus monkeys for neuroscience research in their housing environment. J Neurophy (119-3) 796-807. doi: 10.1152/jn.00614.2017.

Berger M, Agha NS & Gail A (2020) Wireless recording from unrestrained monkeys reveals motor goal encoding beyond immediate reach in frontoparietal cortex *eLife* 9:e51322. doi: 10.7554/eLife.51322.

Buneo CA, Batista AP, Jarvis MR & Andersen RA (2008) Time-invariant reference frames for parietal reach activity. Exp brain Research (188) 77-89. doi: 10.1007/s00221-008-1340-x.

Calapai A, Berger M, Niessing M, Heisig K, Brockhausen R, Treue S & Gail A (2017) A cage-based training, cognitive testing and enrichment system optimized for rhesus macaques in neuroscience research. *Behav Res* Methods *49(1):35-45*. doi: 10.3758/s13428-016-0707-3.

Cisek P & Kalaska JF (2002) Simultaneous Encoding of Multiple Potential Reach Directions in Dorsal Premotor Cortex. J Neurophy (87-2) 1149-1154- doi: 10.1152/jn.00443.2001.

Cross KP, Heming EA, Cook DJ & Scott SH (2020) Maintained representations of the ipsilateral and contralateral limbs during bimanual control in primary motor cortex. J Neurosci (40-35) 6732-6747. doi:10.1523/JNEUROSCI.0730-20.2020.

Donchin O, Gribova A, Steinberg O, Bergman H & Vaadia E (1998) Primary motor cortex is involved in bimanual coordination. Nat (395) 274-278. doi: 10.1038/26220.

Dotan D, Meyniel F & Dehaene S (2018) On-line confidence monitoring during decision making. Cognition (171) 112-121. doi: 10.1016/j.cognition.2017.11.001.

Ferrari-Toniolo, S., Visco-Comandini, F., & Battaglia-Mayer, A. (2019). Two brains in action: joint-action coding in the primate frontal cortex. *Journal of Neuroscience*, *39*(18), 3514-3528. doi: 10.1523/JNEUROSCI.1512-18.2019.

Foster JD, Nuyujukian P, Freifeld O, Gao H, Walker R, Ryu SI, Meng TH, Murmann B, Black MJ & Shenoy KV (2014) A freely moving monkey treadmill model. J. Neural Eng (11-4). doi: 10.1209/0295-5075/109/27001.

Georgopoulos AP, Kalaska JF, Caminiti R & Massey JT (1982) On the relations between the direction of two-dimensional arm movements and cell discharge in primate motor cortex. J Neurosci (2-11) 1527-1537. doi: 10.1523/JNEUROSCI.02-11-01527.1982.

Georgopoulos, A. P., Schwartz, A. B. & Kettner, R. E. (1986). Neuronal population coding of movement direction. *Science*, *233*(4771), 1416-1419. doi: 10.1126/science.37498.

Georgopoulos, A. P. (1986). On reaching. *Annual review of neuroscience*, *9*(1), 147-170.

Voloh, B., Eisenreich, B. R., Maisson, D. J., Ebitz, R. B., Park, H. S., Hayden, B. Y. & Zimmermann, J. (2021). Hierarchical organization of rhesus macaque behavior. *bioRxiv*. doi: 10.1101/2021.11.15.468721.

Johnson, M. T. V. & Ebner, T. J. (2000). Processing of multiple kinematic signals in the cerebellum and motor cortices. *Brain Research Reviews*, *33*(2-3), 155-168. doi: 10.1016/S0165-0173(00)00027-8.

Kalaska, J. F., Caminiti, R. & Georgopoulos, A. P. (1983). Cortical mechanisms related to the direction of two-dimensional arm movements: relations in parietal area 5 and comparison with motor cortex. *Experimental Brain Research*, *51*(2), 247-260. doi: 10.1007/BF00237200.

Kazahari, N. & Agetsuma, N. (2008). Social factors enhancing foraging success of a wild group of Japanese macaques (Macaca fuscata) in a patchy food environment. *Behaviour*, *145*(6), 843-860. doi:10.1163/156853908783929188.

Klaes, C., Westendorff, S., Chakrabarti, S. & Gail, A. (2011). Choosing goals, not rules: deciding among rule-based action plans. *Neuron*, *70*(3), 536-548. doi:10.1016/j.neuron.2011.02.053.

Kuang, S., Morel, P. & Gail, A. (2016). Planning movements in visual and physical space in monkey posterior parietal cortex. *Cerebral cortex*, *26*(2), 731-747. doi: 10.1093/cercor/bhu312.

Labuguen, R., Matsumoto, J., Negrete, S. B., Nishimaru, H., Nishijo, H., Takada, M. & Shibata, T. (2021). MacaquePose: A novel "in the wild" macaque monkey pose dataset for markerless motion capture. *Frontiers in behavioral neuroscience*, *14*, 581154. doi:10.3389/fnbeh.2020.58115.

Lacal, I., Babicola, L., Caminiti, R., Ferrari-Toniolo, S., Schito, A., Nalbant, L. E. & Battaglia-Mayer, A. (2022). Evidence for a we-representation in monkeys when acting together. *Cortex*, *149*, 123-136. doi: 10.1016/j.cortex.2021.12.012.

Hengyue Liu, Ning Yan, Masood Mortazavi & Bir Bhanu. Fully convolutional scene graph generation. In *Proceedings of the IEEE/CVF Conference on Computer Vision and Pattern Recognition*, pages 11546–11556, 2021.

Maestripieri, D. (2005). Early experience affects the intergenerational transmission of infant abuse in rhesus monkeys. *Proceedings of the National Academy of Sciences*, *102*(27), 9726-9729. doi: 10.1073/pnas.0504122102.

Maisson DJN, Voloh B, Cervera RL, Conover I, Zambre M, Zimmermann J & Hayden BY (2022) Widespread coding of navigational variables in prefrontal cortex. biorxiv. doi: 10.1101/2022.10.13.512139.

Malaivijitnond, S., Lekprayoon, C., Tandavanittj, N., Panha, S., Cheewatham, C., & Hamada, Y. (2007). Stone-tool usage by Thai long-tailed macaques (Macaca fascicularis). *American Journal of Primatology: Official Journal of the American Society of Primatologists*, *69*(2), 227-233. doi: 10.1002/ajp.20342.

Mao D, Avila E, Caziot C, Laurens J, Dickman JD & Angelaki DE (2021) Spatial modulation of hippocampal activity in freely moving macaques. Neuron 109(21): 3521-3534. doi: 10.1016/j.neuron.2021.09.032.

Mathis, A., Mamidanna, P., Cury, K. M., Abe, T., Murthy, V. N., Mathis, M. W. & Bethge, M. (2018). DeepLabCut: markerless pose estimation of user-defined body parts with deep learning. *Nature neuroscience*, *21*(9), 1281-1289.doi: 10.1038/s41593-018-0209-y.

McCowan, B., Anderson, K., Heagarty, A. & Cameron, A. (2008). Utility of social network analysis for primate behavioral management and well-being. *Applied Animal Behaviour Science*, *109*(2-4), 396-405. doi: 10.1016/j.applanim.2007.02.009.

Möller S, Unakafov AM, Fischer J, Gail A, Treue S & Kagan I (2022) Human and macaque pairs employ different coordination strategies in a transparent decision game. biorxiv 2020.03.13.983551. doi: 10.1101/2020.03.13.983551.

Mooshagian, E., Wang, C., Holmes, C. D. & Snyder, L. H. (2018). Single units in the posterior parietal cortex encode patterns of bimanual coordination. *Cerebral Cortex*, *28*(5), 1549-1567. doi: 10.1093/cercor/bhx052.

Mooshagian, E. & Snyder, L. H. (2018). Spatial eye–hand coordination during bimanual reaching is not systematically coded in either LIP or PRR. *Proceedings of the National Academy of Sciences*, *115*(16), E3817-E3826. doi: 10.1073/pnas.1718267115.

Noel, J. P., Balzani, E., Avila, E., Lakshminarasimhan, K., Bruni, S., Alefantis, P. & Angelaki, D. (2022). Multiplexed and flexible neural coding in sensory, parietal, and frontal cortices during goal-directed virtual navigation. doi: 10.21203/rs.3.rs-1025042/v1.

Pesaran, B., Nelson, M. J. & Andersen, R. A. (2006). Dorsal premotor neurons encode the relative position of the hand, eye, and goal during reach planning. *Neuron*, *51*(1), 125-134. doi: 10.1016/j.neuron.2006.05.025.

Rajangam, S., Tseng, P. H., Yin, A., Lehew, G., Schwarz, D., Lebedev, M. A. & Nicolelis, M. A. (2016). Wireless cortical brain-machine interface for whole-body navigation in primates. *Scientific reports*, *6*(1), 1-13. doi: 10.1038/srep22170.

Rakhovskaya, M. V. (2013). Correlates of male consortship rate in free-ranging rhesus macaques (Macaca mulatta). *International Journal of Primatology*, *34*(4), 662-680. doi: 10.1007/s10764-013-9686-8.

Schwartz, A. B., Kettner, R. E. & Georgopoulos, A. P. (1988). Primate motor cortex and free arm movements to visual targets in three-dimensional space. I. Relations between single cell discharge and direction of movement. *Journal of Neuroscience*, *8*(8), 2913-2927. doi: 10.1523/JNEUROSCI.08-08-02913.1988.

Shahidi N, Parajuli A, Franch M, Schrater P, Wright A, Pitkow X & Dragoi V (2021) Population coding of strategic variables during foraging in freely-moving macaques. biorxiv. doi: 10.1101/811992.

Sheshadri, S., Dann, B., Hueser, T. & Scherberger, H. (2020). 3D reconstruction toolbox for behavior tracked with multiple cameras. *Journal of Open Source Software*, *5*(45), 1849. doi: 10.21105/joss.01849.

Silvernagel, M. P., Ling, A. S., Nuyujukian, P. & Brain Interfacing Laboratory. (2021). A markerless platform for ambulatory systems neuroscience. *Science Robotics*, *6*(58), eabj7045. doi: 10.1126/scirobotics.abj7045.

Suriya-Arunroj L & Gail A (2019) Complementary encoding of priors in monkey frontoparietal network supports a dual process of decision-making *eLife* 8:e47581. doi: 10.7554/eLife.47581.

Thura, D. & Cisek, P. (2014). Deliberation and commitment in the premotor and primary motor cortex during dynamic decision making. *Neuron*, *81*(6), 1401-1416. doi: 10.1016/j.neuron.2014.01.031.

Thura, D., Cos, I., Trung, J. & Cisek, P. (2014). Context-dependent urgency influences speed–accuracy trade-offs in decision-making and movement execution. *Journal of Neuroscience*, *34*(49), 16442-16454. doi: 10.1523/JNEUROSCI.0162-14.2014.

O'brien, T. G. & Kinnaird, M. F. (1997). Behavior, diet, and movements of the Sulawesi crested black macaque (Macaca nigra). *International Journal of Primatology*, *18*(3), 321-351. doi: 10.1023/A:1026330332061.

Ulbrich, P. & Gail, A. (2021). The cone method: Inferring decision times from single-trial 3D movement trajectories in choice behavior. *Behavior Research Methods*, *53*(6), 2456-2472. doi: 10.3758/s13428-021-01579-5.

Zhongdao Wang, Liang Zheng, Yixuan Liu, Yali Li & Shengjin Wang (2020) Towards real-time multi-object tracking. In *European Conference on Computer Vision*, pages 107–122. Springer.

Fisher Yu, Dequan Wang, Evan Shelhamer & Trevor Darrell (2018) Deep layer aggregation. In *Proceedings of the IEEE conference on computer vision and pattern recognition*, pages 2403–2412.

Yifu Zhang, Chunyu Wang, Xinggang Wang, Wen- jun Zeng & Wenyu Liu (2021) Fairmot: On the fair- ness of detection and re-identification in multiple object tracking. *International Journal of Computer Vision*, 129(11):3069–3087. doi: 10.48550/arXiv.2004.01888.

Xingyi Zhou, Dequan Wang, & Philipp Krähenbuühl (2019) Objects as points. *arXiv preprint arXiv:1904.07850*. doi: 10.48550/arXiv.1904.07850.

Supplementary

S-Fig.1: Left: Example frame of monkey L seemingly reaching towards the wood pile but actually continues his walking pattern. Right: Example frame of monkey H seemingly continuing to walk but actually reaches for the wood pile in front of him.

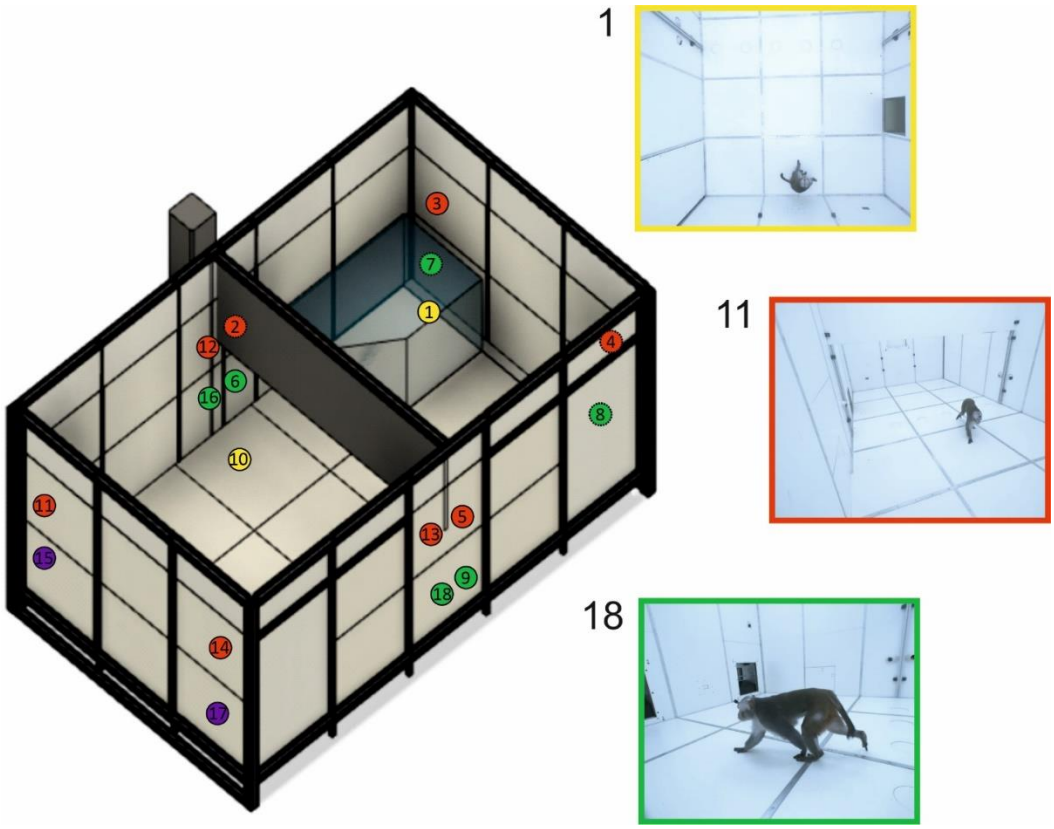

S-Fig.2: CAD rendering of the ExR with improved camera configuration. Yellow depicts the two top-view cameras, green and purple the low level cameras and red the positions of the second panel-row cameras.

Part III

General Discussion

Chapter 6

General Discussion

The main goal of this thesis was to understand action effect anticipation during action planning on a single neuron level while working towards ecologically relevant paradigms.

The five original manuscripts in this thesis contributed with the following findings:

First, we developed an openly accessible method to custom-fit cranial implants to individual skull and brain of animals to provide access to the brain for neural recordings. This tutorial is suited for users without any prior knowledge and enables scientists to design and custom fit their own implants independent of size and shape requirements.

Second, we developed a novel paradigm to address the question of action effect anticipation during action planning by linking the effects immediately to one's own actions. Our results provide first evidence that the frontoparietal reach network in the macaque's brain encodes action effect anticipation before action execution and is involved during internal simulation of the selected motor program prior to execution as well as in defining the goal for the action, which is in line with the ideomotor theory.

Third, we wanted to explore the mechanisms of action effect anticipation in a large-scale environment for free behaviors allowing a fuller repertoire of actions with their associated action effects. As existing setups are not able to address this question, we conceptualized and developed a novel, highly modular experimental setting for free behavior in rhesus macaques with markerless full-body motion capture and neural recordings. After overcoming technical challenges, we provide a first proof-of-concept study to demonstrate the suitability of large-scale environments in systems neuroscience with the focus of decision-making, action planning and execution therefore pushing existing limitations of systems neuroscience.

First single neuron evidence of action effect anticipation

With developing the novel AEA paradigm, we were able i) to dissociate physical action and action effect while maintaining the physical goal, and ii) to link actions to their effects immediately therefore demanding online control. The endogenously evoked action effects are considered to be involved in motor program selection either supporting (Paelecke and Kunde, 2007; Janczyk and M., Kunde, 2010; Wirth et al., 2015) or contradicting the concept of the ideomotor theory (Ziessler and Nattkemper, 2011; Ziessler et al., 2004) based on human

behavioral data. Neural evidence is sparse but suggests anticipated action effects might be involved in 'both' rather than 'in either or' one of them (Nikolaev et al., 2008). In rhesus macaque the frontoparietal reach network is known to be involved in motor planning and goal-definition (Crammond und Kalska, 1994, 2000, Wise und Mauritz 1985, Gail and Andersen, 2006) and suggested to be part of action effect anticipation (Kuang et al., 2016).

To provide the first neural evidence on a single neuron resolution, we recorded in the areas of the frontoparietal reach network including the dorsal premotor (PMd), primary motor cortex (M1) and the parietal reach region (PRR) in two rhesus macaques. Our results provide clear evidence for action effect encoding during planning before action execution in PMd and PRR, but not in M1. This allows us to revise the long-lasting debate of whether action effects are involved prior or after motor program selection. Our results confirm previous findings of Nikolaev and colleagues (2008) that neural encoding suggests a two-fold involvement of action effect anticipation: i) during a goal-definition stage, which implies the motor program is selected based on the to-be-expected action effects and ii) during internal simulation of the selected motor program, during which we compare the potential action effect to the desired action effect (Chapter 3, Fig. 3). We conclude, our findings suggest a 'AND' mechanism rather than a 'OR' mechanism therefore trying to reconcile the seemingly contradictory lines of research. These results led to the proposal of expanding the internal model towards the action planning phase and implementing the potential two-fold role in the theoretical framework of the internal model (Shadmehr and Krakauer, 2008).

As this study is the first and therefore only study on single neuron resolution to address the role of action effect anticipation and other existing neural evidence is sparse (Nikolaev et al., 2008; Pilacinski et al., 2018), additional studies are needed to understand the role of action effects during planning in more detail. Especially the question of which brain areas drive action effect anticipation and, if the proposed internal model is true, where the potential forward model would be generated, remains open.

Ecologically more relevant paradigm

Chapter 3 had a two-fold goal. First to close the gap in the long-standing literature of action effect anticipation and its role during planning by providing first single neuron level evidence. Second, to overcome shortcomings of existing paradigms, which are not considered as ecologically highly relevant.

We overcame limitations of existing studies, which were i) action and action effects are rather arbitrary associations not directly relevant for the action selection itself and ii) action effects are not time-continuous. We designed the novel AEA paradigms, which according to our understanding of current literature should evoke intrinsically motivated and therefore

endogenous action effects (Ziessler et al., 2012, Liu et al., 2019). To gain basic insights into the neural correlates of action effect anticipation, we recorded this study in chair seated rhesus macaques while they are interacting with the environment using one single arm. Additionally, the monkeys had to maintain eye- and head-fixation to provide full experimental control in our findings in line with conventions of systems neuroscience (Gail and Anderson, 2006; Kuang et al., 2016).

Motivated by the results of Chapter 2, we wanted to push existing limitations by one last step in the scope of this thesis. In natural environments monkeys as well as us humans are in many cases not only sitting and performing the same type of action (e.g. rotation movement with the arm) but the repertoire of interactions is broader implying action effect prediction of various types of behaviors (e.g. rotation direction, flexibility of branch). Current existing setups for free behaviors are not suited to address these questions as they are small-scaled (Berger et al., 2020; Shahidi et al., 2021). To overcome this limitation, we designed a novel, highly modular experimental setting called the Exploration Room. Not only did we physically build this setup but we also took the challenge upon us which comes with more naturalistic continuous behaviors of how to make sense of the data in such a free environment for systems neuroscience (Voloh et al., 2020, 2022). These challenges come along with two open questions to our understanding:

First, how can we make the animals elicit the behaviors we are interested in, repetitively but without human interaction. Second, how can we extract relevant information from a continuous behavioral stream, which then can be used for system neuroscience analysis allowing neural data analysis with established methods. After solving the technical challenges (e.g. synchronized video recordings for later markerless motion capture), we presented two examples of how to oversome the aforementioned two challenges. By establishing this novel setup, we enabled ourselves to investigate the role of action effect in a more complete repertoire therefore taking us a step closer towards enhancing our understanding of action effect anticipation closer to real-life.

Implications of enhanced understanding of action effect mechanisms

Action effect anticipation has been studied in this thesis not only to attempt to reconcile the contradicting parallel streams of studies. This thesis attempts to enhance our understanding of the role of action effect anticipation as action effect is understood to be involved in several mechanisms, which, once we understand the role better, can help to aid patients.

First, if the role of action effect is well-understood, this understanding could help towards improving BMI decoding. A line of research is focusing on providing patients control over a robotic arm by decoding the neural activity in the primary motor cortex (M1). This is then

provided as an input to the robotic device, which then enables us to control it. This concept has been successfully presented in literature (Hochberg et al., 2012; Gilja et al., 2012; Ifft et al., 2013; Collinger et al., 2013; Pandarinath et al, 2018; Wang et al., 2017; Penaloza and Nishio, 2018; Kyung-Hwan,2019). However, the application is not commercially available yet as, amongst others, the decoding remains counter-intuitive for patients. If action effect anticipation is an integral part of action planning, it could be additionally used to improve BMI decoders.

Clearly, the closer our basic research environment gets to real-life, the better the potential applications will be usable in a patient's natural home environment instead within a hospital based closed radius.

Second, an enhanced understanding of action effects can help us to understand patient conditions related to abnormalities in action control in neuropsychiatric patients. For instance, the phenomenon of delusional control, which is associated with schizophrenia patients, is believed to be related to missing action effect anticipations. Schizophrenia patients often report the experience of alien control implying the intended movement was not initiated by them but by an external force (Uhlmann et al., 2021; Rossetti et al., 2019; Mellors, 1970). These patients are believed to be aware of their movement goal, their intention to perform a movement and their movement actually happening but they are not aware of having the movement initiated and therefore report the movement was initiated by an external force.

Another example is the anarchic hand sign (Marchetti and Della Salla, 1998; Goldberg, 1981). Patients with this symptom report, again, that their hand performs actions independent from their intention. It was observed that in this case the discrepancy is between the desired goal and the movement. Patients seem to be unable to inhibit the activated motor program, which is initialized once an object (e.g. a pen) has been in sight.

It has been hypothesized (Blakemore et al., 2002) that in both cases the missing of action effect anticipation in a potential forward model before action execution could explain the phenomenon. The former could be potentially explained by an abnormality during the internal simulation of the selected motor program; the latter by an abnormality in goal-definition. Further advances in the understanding of action effects can help us to understand the mechanisms of these neuropsychiatric disorders.

Conclusion

In summary, this thesis intends to advance existing literature by filling the gap of neural evidence for action effect anticipation during action planning and therefore attempting to

reconcile the fields of psychology, action planning in systems neuroscience and the theoretical framework of the internal model. Additionally, this thesis provides new approaches to narrow the gap between highly constrained, therefore controlled experiments and an ecologically more relevant but less controlled environment by removing the necessary restraints step-by-step.

References

Abe, H., & Lee, D. (2011). Distributed coding of actual and hypothetical outcomes in the orbital and dorsolateral prefrontal cortex. Neuron, 70(4), 731-741. doi: 10.1016/j.neuron.2011.03.026.

Aflalo, T.N, Graziano, S.A. (2007). Relationship between Unconstrained Arm Movements and Single-Neuron Firing in the Macaque Motor Cortex. Journal of Neuroscience, 27(11), 2760-2780. doi: 10.1523/JNEUROSCI.3147-06.2007

Andersen, R. A. & Buneo, C. A. (2002). Intentional maps in posterior parietal cortex. Annual review of neuroscience, 25(1):189–220. doi: 10.1146/annurev.neuro.25.112701.142922.

Andersen, R. A., & Cui, H. (2009). Intention, action planning, and decision making in parietal-frontal circuits. Neuron, 63(5), 568-583. doi: 10.1016/j.neuron.2009.08.028

Bala PC, Eisenreich BR, Yoo SBM, Hayden BY, Park HS, & Zimmermann J (2020). Automated markerless pose estimation in freely moving macaques with OpenMonkeyStudio. Nat Comm (11) 4560. doi: 10.1038/s41467-020-18441-5.

Berger M, Agha NS, & Gail A (2020). Wireless recording from unrestrained monkeys reveals motor goal encoding beyond immediate reach in frontoparietal cortex eLife 9:e51322. doi: 10.7554/eLife.51322.

Blakemore, S. J., Wolpert, D. M., & Frith, C. D. (2002). Abnormalities in the awareness of action. Trends in cognitive sciences, 6(6), 237-242. doi: 10.1016/S1364-6613(02)01907-1.

Carpenter, W. B. (1852). On the influence of suggestion in modifying and directing muscular movement, independently of volition. Proceedings of the Royal Institution, 147–154.

Chase, S. M., Kass, R. E., & Schwartz, A. B. (2012). Behavioral and neural correlates of visuomotor adaptation observed through a brain-computer interface in primary motor cortex. Journal of neurophysiology, 108(2), 624-644. doi: 10.1152/jn.00371.2011.

Chowdhury, R. H., Glaser, J. I., & Miller, L. E. (2020). Area 2 of primary somatosensory cortex encodes kinematics of the whole arm. Elife, 9. doi: 10.7554/eLife.48198.

Cohen, Y. E. & Andersen, R. A. (2002). A common reference frame for movement plans in the posterior parietal cortex. Nature reviews. Neuroscience, 3(7):553–62. doi: 10.1038/nrn873.

Colby, C. L. & Goldberg, M. E. (1999). Space and attention in parietal cortex. Annual Review of Neuroscience, 22(1):319–349. doi: 10.1146/annurev.neuro.22.1.319

Collinger, J. L., Wodlinger, B., Downey, J. E., Wang, W., Tyler-Kabara, E. C., Weber, D. J., McMorland, A. J. C., Velliste, M., Boninger, M. L., & Schwartz, A. B. (2013). High-performance

neuroprosthetic control by an individual with tetraplegia. The Lancet, 381(9866):557–564. doi: 0.1016/S0140-6736(12)61816-9.

Crammond, D. J. & Kalaska, J. F. (2000). Prior information in motor and premotor cortex: activity during the delay period and effect on pre-movement activity. Journal of neurophysiology, 84(2):986–1005. doi: 10.1152/jn.2000.84.2.986.

Crammond, D. J. & Kalaska, J. F. (1994). Modulation of preparatory neuronal activity in dorsal premotor cortex due to stimulus-response compatibility. Journal of Neurophysiology, 71(3):1281–1284. doi: 10.1152/jn.1994.71.3.1281.

Crawford, J. D., Henriques, D. Y., & Medendorp, W. P. (2011). Three-dimensional transformations for goal-directed action. Annual Review of Neuroscience, 34(1):309–331. doi: 10.1146/annurev-neuro-061010-113749.

Desmurget, M., Reilly, K. T., Richard, N., Szathmari, A., Mottolese, C., & Sirigu, A. (2009). Movement intention after parietal cortex stimulation in humans. Science (New York, N.Y.), 324(811):811–813. doi: 10.1126/science.116989.

Eisenreich, B.R., Hayden, B.Y., & Zimmermann, J. Macaques are risk-averse in a freely moving foraging task (2009). Sci Rep 9, 15091 (2019). doi: 10.1038/s41598-019-51442-z.

Foster, Justin D., Paul Nuyujukian, Oren Freifeld, Hua Gao, Ross Walker, Stephen I. Ryu, Teresa H. Meng, Boris Murmann, Michael J. Black, & Krishna V. Shenoy (2014). A freely-moving monkey treadmill model. Journal of neural engineering 11 (4): 046020. doi: 10.1088/1741-2560/11/4/046020

Francis, B. A., & Wonham, W. M. (1976). The internal model principle of control theory. *Automatica*, *12*(5), 457-465. doi: 10.1016/0005-1098(76)90006-6.

Herbart, J. F. (1816). Lehrbuch zur Psychologie. Königsberg, Germany: Unzer.

Gail, A., & Andersen, R. A. (2006). Neural dynamics in monkey parietal reach region reflect context-specific sensorimotor transformations. *Journal of Neuroscience*, *26*(37), 9376-9384.doi: 10.1523/JNEUROSCI.1570-06.2006.

Georgopoulus, A. P., Schwartz, A. B., & Kettner, R. E. (1986). Neuronal population coding of movement direction. Science, 233(4771):1416–1419. doi: 10.1126/science.374988.

Georgopoulos, a. P., Kalaska, J. F., Caminiti, R., and Massey, J. T. (1982). On the relations between the direction of two-dimensional arm movements and cell discharge in primate motor cortex. J.Neurosci., 2(11)(11):1527–1537. doi: 10.1523/JNEUROSCI.02-11-01527.1982.

Goldberg, G., Mayer, N. H., & Toglia, J. U. (1981). Medial frontal cortex infarction and the alien hand sign. Archives of Neurology, 38(11), 683-686. doi: 10.1001/archneur.1981.00510110043004.

Golub, M. D., Byron, M. Y., & Chase, S. M. (2015). Internal models for interpreting neural population activity during sensorimotor control. *Elife*, *4*, e10015.doi: 10.7554/eLife.10015.

Greenwald, A. G. (1970). Sensory feedback mechanisms in performance control: With special reference to the ideo-motor mechanism. Psychological Review, 77, 73–99. doi: 10.1037/h0028689.

Harless, E. (1861). Der Apparat des Willens. In I. H. Fichte, H. Ulrici, & I. U. Wirth (Eds.), Zeitschrift für Philosophie und philosophische Kritik: Vol. 38 (pp. 50–73). Halle, Germany: Pfeffer.

Hughes, G., & Waszak, F. (2011). ERP correlates of action effect prediction and visual sensory attenuation in voluntary action. Neuroimage, 56(3), 1632-1640. doi: 10.1016/j.neuroimage.2011.02.057.

James, W. (1890). The principles of psychology (2 vols.). New York: Holt

Janczyk, M. & Kunde, W (2010). Does dorsal processing require central capacity? More evidence from the PRP paradigm. *Exp Brain Res* 203,89–100. doi: 10.1007/s00221-010-2211-9.

Johnson, P. B., Ferraina, S., Bianchi, L., & Caminiti, R. (1996). Cortical networks for visual reaching: Physiological and anatomical organization of frontal and parietal lobe arm regions. Cerebral Cortex, 6(2):102–119. doi: 10.1093/cercor/6.2.102.

Kalaska, J. F. & Crammond, D. J. (1992). Cerebral cortical mechanisms of reaching movements. Science, 255(5051):1517–1523. doi: 10.1126/science.1549781.

Kalaska, J. F., Caminiti, R., & Georgopoulos, A. P. (1983). Cortical mechanisms related to the direction of two-dimensional arm movements: relations in parietal area 5 and comparison with motor cortex. Experimental Brain Research, 51(2):247–260. doi: 10.1007/BF00237200.

Kok, P., & Lange, F. P. D. (2015). Predictive coding in sensory cortex. *An introduction to model-based cognitive neuroscience* (pp. 221-244). Springer, New York, NY. doi: 10.1007/978-1-4939-2236-9_11.

Kuang, S., Morel, P., & Gail, A. (2016). Planning movements in visual and physical space in monkey posterior parietal cortex. *Cerebral cortex*, *26*(2), 731-747. doi: 10.1093/cercor/bhu312.

Kurata, K. (1991). Corticocortical inputs to the dorsal and ventral aspects of the premotor cortex of macaque monkeys. Neuroscience Research, 12(1):263–280. doi: 10.1016/0168-0102(91)90116-G.

Shim, K. H., Jeong, J. H., Kwon, B. H., Lee, B. H., & Lee, S. W. (2019). Assistive robotic arm control based on brain-machine interface with vision guidance using convolution neural network. In 2019 IEEE International Conference on Systems, Man and Cybernetics (SMC) (pp. 2785-2790). IEEE. doi: 10.1109/SMC.2019.8914058.

Laycock, T. (1876). Reflex, automatic, and unconscious cerebration: A history and a criticism. The Journal of Mental Science, 21, 477–498. doi: 10.1192/bjp.21.96.477.

Liu, K., Hu, W., & Chen, Y. (2019). Encoding of Stimulus-driven and Intention-driven Actions in Monkey's Primary Motor Cortex. In *Proceedings of the 2019 6th International Conference on Biomedical and Bioinformatics Engineering* (pp. 99-106). doi: 10.1145/3375923.3375945.

Lotze, R. H. (1852). Medizinische Psychologie oder Physiologie der Seele (pp. 287–325). Leipzig, Germany: Weidmann'sche Buchhandlung.

Maisson DJN, Voloh B, Cervera RL, Conover I, Zambre M, Zimmermann J & Hayden BY (2022). Widespread coding of navigational variables in prefrontal cortex. biorxiv. doi: 10.1101/2022.10.13.512139.

Mandelblat-Cerf, Y., Paz, R., & Vaadia, E. (2009). Trial-to-trial variability of single cells in motor cortices is dynamically modified during visuomotor adaptation. *Journal of Neuroscience*, *29*(48), 15053-15062. doi: 10.1523/JNEUROSCI.3011-09.2009.

Mao D, Avila E, Caziot C, Laurens J, Dickman JD & Angelaki DE (2021). Spatial modulation of hippocampal activity in freely moving macaques. Neuron 109(21): 3521-3534. doi: 10.1016/j.neuron.2021.09.032.

Marchetti, C. & Della Salla, S. (1998) Disentangling the alien and anarchic hand. Cogn. Neuropsychiatry 3, 191–208. doi: 10.1080/135468098396143.

Marconi, B., Genovesio, A., Battaglia-Mayer, A., Ferraina, S., Squatrito, S., Molinari, M., Lacquaniti, F., & Caminiti, R. (2001). Eye-hand coordination during reaching. i. anatomical relationships between parietal and frontal cortex. Cerebral Cortex, 11(6):513–527. doi: 10.1093/cercor/11.6.528.

Matsumoto, M., Matsumoto, K., Abe, H., & Tanaka, K. (2007). Medial prefrontal cell activity signaling prediction errors of action values. Nature neuroscience, 10(5), 647-656. doi: https://doi.org/10.1038/nn1890.

Mellor, C. S. (1970). First rank symptoms of schizophrenia: I. the frequency in schizophrenics on admission to hospital II. Differences between individual first rank symptoms. The British Journal of Psychiatry, 117(536), 15-23. doi: 10.1002/14651858.CD010653.pub2.

Nikolaev, A. R., Ziessler, M., Dimova, K., & van Leeuwen, C. (2008). Anticipated action consequences as a nexus between action and perception: evidence from event-related potentials. *Biological Psychology*, *78*(1), 53-65. doi: 10.1016/j.biopsycho.2007.12.010.

O'Neill, M., & Schultz, W. (2018). Predictive coding of the statistical parameters of uncertain rewards by orbitofrontal neurons. *Behavioural brain research*, *355*, 90-94. doi: 10.1016/j.bbr.2018.04.041.

Ohbayashi, X. M., Picard, N., and Strick, P. L. (2016). Inactivation of the dorsal premotor area disrupts internally generated, but not visually guided, sequential movements. The Journal of Neuroscience, 36(6):1971–1976. doi: 10.1523/JNEUROSCI.2356-15.2016.

Paelecke, M., & Kunde, W. (2007). Action-effect codes in and before the central bottleneck: evidence from the psychological refractory period paradigm. *Journal of Experimental Psychology: Human Perception and Performance*, *33*(3), 627. doi: 10.1037/0096-1523.33.3.627.

Penaloza, C. I., & Nishio, S. (2018). BMI control of a third arm for multitasking. Science Robotics, 3(20), eaat1228. doi: 10.1126/scirobotics.aat122.

Pfister, R., Kiesel, A. & Hoffmann, J (2011). Learning at any rate: action–effect learning for stimulus-based actions. *Psychological Research* 75, 61–65. doi: 10.1007/s00426-010-0288-1.

Pilacinski, A., Wallscheid, M., & Lindner, A. (2018). Human posterior parietal and dorsal premotor cortex encode the visual properties of an upcoming action. PloS one, 13(10), e0198051. doi: 10.1371/journal.pone.0198051.

Pandya, D. N. & Kuypers, H. G. J. M. (1969). Cortico-cortical connections in the rhesus monkey. Brain research, 13(1):13–36. doi: 10.1016/0006-8993(69)90141-3.

Rajangam, S., Tseng, P.-H., Yin, A., Lehew, G., Schwarz, D., Lebedev, M. A., a&nd Nicolelis, M. A. L. (2016). Wireless cortical brain-machine interface for whole-body navigation in primates. Scientific Reports, 6:22170. doi: 10.1038/srep22170.

Rizzolatti, G. & Luppino, G. (2001). The cortical motor system. Neuron, 31(6):889–901. doi: 10.1016/S0896-6273(01)00423-8.

Shadmehr, R. & Krakauer, J.W. (2008). A computational neuroanatomy for motor control. *Exp Brain Res* 185, 359–381. doi: 10.1007/s00221-008-1280-5.

Shahidi N, Parajuli A, Franch M, Schrater P, Wright A, Pitkow X, & Dragoi V (2021). Population coding of strategic variables during foraging in freely-moving macaques. biorxiv. doi: 10.1101/811992.

Shin, Y. K., Proctor, R. W., & Capaldi, E. J. (2010). A review of contemporary ideomotor theory. Psychological bulletin, 136(6), 943. doi: 10.1037/a0020541.

Snyder, L. H., Batista, A. P., & Andersen, R. A. (1997). Coding of intention in the posterior parietal cortex. Nature, 386(6621):167–170. doi: 10.1038/386167a0.

Snyder, L. H., Batista, A. P., & Andersen, R. A. (2000). Intention-related activity in the posterior parietal cortex: A review. Vision Research, 40(10–12):1433–1441. doi: 10.1016/S0042-6989(00)00052-3.

Stavisky, S. D., Kao, J. C., Ryu, S. I., & Shenoy, K. V. (2017). Trial-by-trial motor cortical correlates of a rapidly adapting visuomotor internal model. Journal of Neuroscience, 37(7), 1721-1732. doi: 10.1523/JNEUROSCI.1091-16.2016.

Thorndike, E. L. (1913). Ideo-motor action. Psychological Review, 20(2), 91. doi: 10.1037/h0072027.

Velliste, M., Perel, S., Spalding, M. C., Whitford, a. S., & Schwartz, a. B. (2008). Cortical control of a robotic arm for self-feeding. Nature, 453(June):1098–1101. doi: Cortical control of a robotic arm for self-feeding.

Voloh, B., Maisson, D., Cervera, R.L., Conover, I., Zambre, M., Hayden, B.Y.,& Zimmermann, J. (2022). Prefrontal control of actions in freely moving macaques. bioRxiv 2022.10.26.513892; doi: 10.1101/2022.10.26.513892.

Voloh, B., Eisenreich B.R., Maisson J-N D., Ebitz, R.B., Park, H. S., Hayden, B.Y., & Zimmermann, J.(2021). Hierarchical organization of rhesus macaque behavior. bioRxiv 2021.11.15.468721. doi: 10.1101/2021.11.15.468721.

Wang, Y., Zeng, H., Song, A., Xu, B., Li, H., Zhu, L., ... & Liu, J. (2017). Robotic arm control using hybrid brain-machine interface and augmented reality feedback. In 2017 8th International IEEE/EMBS Conference on Neural Engineering (NER) (pp. 411-414). IEEE. doi: 10.1109/NER.2017.8008377.

Wirth, R., Pfister, R., Janczyk, M., & Kunde, W. (2015). Through the portal: Effect anticipation in the central bottleneck. *Acta Psychologica*, *160*, 141-151. doi: 10.1016/j.actpsy.2015.07.007.

Wise, S. P., Boussaoud, D., Johnson, P. B., & Caminiti, R. (1997). Premotor and parietal cortex: Corticocortical connectivity and combinatorial computations 1. Annu. Rev. Neurosci, 20:25–42. doi: 10.1146/annurev.neuro.20.1.25.

Wise, S. P. & Mauritz, K. H. (1985). Set-related neuronal activity in the premotor cortex of rhesus monkeys: effects of changes in motor set. Proceedings of the Royal Society of London. Series B, Biological sciences, 223(1232):331–354. doi: 10.1098/rspb.1985.0005.

Wodlinger, B., Downey, J. E., Tyler-Kabara, E. C., Schwartz, a. B., Boninger, M. L., & Collinger, J. L. (2014). Ten dimensional anthropomorphic arm control in a human brain- machine interface:

Difficulties, solutions, and limitations. J Neural Eng, In Press(1):16011. doi: 10.1088/1741-2560/12/1/016011.

Wolpert, D. M., & Kawato, M. (1998). Multiple paired forward and inverse models for motor control. *Neural networks*, *11*(7-8), 1317-1329.doi: 10.1016/S0893-6080(98)00066-5.

Zarr, N., & Brown, J. W. (2016). Hierarchical error representation in medial prefrontal cortex. NeuroImage, 124, 238-247. doi: 10.1016/j.neuroimage.2015.08.063.

Zhang, M., Barash, S. (2000). Neuronal switching of sensorimotor transformations for antisaccades. Nature 408, 971–975. doi: 10.1038/35050097.

Ziessler, M., Nattkemper, D., & Vogt, S. (2012). The activation of effect codes in response preparation: new evidence from an indirect priming paradigm. Frontiers in psychology, 3, 585. doi: 10.3389/fpsyg.2012.00585. doi: 10.3389/fpsyg.2012.00585.

Ziessler, M., & Nattkemper, D. (2011). The temporal dynamics of effect anticipation in course of action planning. Quarterly Journal of Experimental Psychology, 64(7), 1305-1326. doi: 10.1080/17470218.2011.553067.

Ziessler, M., Nattkemper, D. & Frensch, P.A .(2004). The role of anticipation and intention in the learning of effects of self-performed actions. Psychological Research 68, 163–175. doi: 10.1007/s00426-003-0153-6.

Supplementary Chapter 1: Switch from egocentric to allocentric reference frame during ecologically more relevant interactions in rhesus macaque

S1.1 Abstract

In our daily life we produce desired changes in our environment by performing voluntary actions, which go beyond simple touchscreen or keyboard. Which role these action effects play especially during action planning remains up to debate. They have been studied extensively s in humans. When similar concepts are studied in rhesus macaques, existing neural and behavioral data was mainly obtained from highly constrained experimental settings including head-fixation, sometimes additionally eye-fixation.

Rhesus macaques as well humans interact with their natural environment by performing movements, which go beyond simple touches and involve haptic interactions. How existing concepts of action effect anticipation can be generalized towards these scenarios closer to real-life still remains an open question.

To provide a first piece of evidence, we developed a haptic device called the B-PRIME. It consists of two rotating barrels. The inner barrel is motorized and computer controlled and the outer barrel is freely rotatable by the monkey. Depending on the task condition the inner barrel either follows the rotation direction of the outer barrel or moves in the opposite direction.

Our results provide evidence that monkeys tend to adjust their behavior to a probe-before-you-know strategy when placed in a less constrained environment. They adopt their movements such that a two-step rotation is necessary even when it is not enforced by the task design. Our findings demonstrate that the first rotation is performed in an egocentric reference frame, while the second is completed in an allocentric reference frame potentially to reduce the cognitive demand.

S1.2 Introduction

Action effects are assumed to play an integral part during action planning. Vast literature exists providing evidence how the prediction of action effect could be involved during motor program selection (Stock and Stock, 2004; Paelecke and Kunde, 2007) or during the internal simulation of the selected motor program before execution (Ziessler and Nattkemper, 2011; Ziessler et al., 2004, Pfister et al., 2010). It has been criticized that existing tasks use rather unintuitive paradigms, in which action effects are not directly linked to actions and have no influence on whether or not the subject will perform the action correctly.

Ahmed and colleagues (Chapter 3) presented a novel paradigm, which links action effects directly to the action in real-time. Neural data was recorded in the frontoparietal reach region providing first neural evidence of action effect encoding during action planning.

However, the experimental setting was still highly constrained as it was recorded with chair-seated monkeys while maintaining head- and eye-fixation. This is the state-of-the-art in systems neuroscience when studying decision-making and action planning in rhesus macaques.

With recent technological advances however, it is now possible to conduct neurophysiological experiments in less constrained experimental environments, e.g. without eye- and head-fixation. Berger and colleagues (2020) provided a first evidence for neural encoding of reaches in a walk and reach task. Mao and colleagues (2021) provided an extensive study about the underlying neural mechanisms for navigation. Voloh and colleagues (2022) recently presented neural data for transition behaviors between actions (e.g. jumping).

Most importantly, these advances allow us to understand how the findings obtained in highly controlled setups can be generalized towards ecologically more relevant behaviors. The questions remain open, whether the findings of highly constrained paradigms are general findings invariant to environment restraints or whether they might be partially adapted due to the experimental design itself. Aflalo and Graziani (2007) recorded neural activity in the primary motor cortex while the monkey was chair seated but performing free arm reaches in 3D space.

When attempting to explain the variance in the data based on the physical arm movement direction, which is known to be present from earlier studies (Georgopoulos, 1982;1986; Kalaska et al., 1983), they find only 8% could be explained in free reaches. When they calculated the explained variance using a subset of the 3D arm reaches, which are more similar to a center-out reach task (Zhang and Barash, 2000; Gail and Andersen, 2006), the variance increased to 42%. Another interesting finding by Eisenreich and colleagues (2019) presented two animals with a reward-based decision-making task, in which the monkey decides when to leave a current food source to get to the next. Results obtained in a conventional setup provide evidence that monkeys show a risk-affine behavior in line with existing literature (Sleezer et al., 2016; Wang et al., 2017). When the same monkeys are placed in a large-scale environment, in which the monkeys can walk freely, they show clear risk-averse strategies. These findings have been discussed in the context of when presented with a less restrictive environment, monkeys tend to apply different strategies as compared to a highly constrained, static environment. The simplification and abstraction of task might motivate the animals to apply different strategies than they would in a more dynamic environment.

Along this line of research, we wanted to conduct an experiment allowing us to investigate the encoding of action effect anticipation in a less constrained environment without eye- and head-fixation while the monkey is interacting with a haptic device instead of a screen with abstract symbols. We developed a novel haptic device called the B-PRIME (Ahmed et al., Chapter 4), which allows us to translate the AEA paradigm (Ahmed et al., Chapter 3) directly. We mounted the B PRIME in the ReachCage (Berger et al., 2020), which is an experimental setup enabling us to record wireless neural data and behavior. For improved comparison, amongst the two rhesus macaques trained, we trained one, who had performed the AEA task in a conventional setting earlier.

Our findings suggest that monkeys, when interacting with a haptic device in a less constrained environment, adopt their solving strategy. Instead of anticipating the action effect based on an abstract stimulus they adopt a probe-before-you-know strategy, in which they match their arm movements such that the barrel is rotated in a 2-step reach even though it is not enforced by task design. Our preliminary results provide evidence that reaches during first rotations are performed in an egocentric reference frame encoding the physical arm movement whereas the second rotation is performed in an allocentric reference frame encoding the action effects

S1.3 Results

We implemented the AEA paradigm as presented in Ahmed et al. (Chapter 3). This paradigm allows to link actions with their action effects on a continuous basis therefore overcoming the criticism of existing paradigms using rather arbitrary (non-linked) effects. It additionally allows to dissociate between the action effect direction (visual consequence direction), visual goal (goal location) and motor goal (endpoint of physical arm movement). With this paradigm we tested the hypothesis that neurons in the primary motor (M1) and dorsal premotor (PMd) cortices encode action effects.

We trained two adult rhesus macaques to perform the AEA task using the B-PRIME (Chapter 4) on in total 4 conditions The goal of the task is to rotate the outer barrel such, that the indicated active reward pocket, which is either on the left or right side relative to the monkey in the beginning of the trial, turns to the center and therefore becomes accessible to the monkey. The monkey can rotate the outer barrel either to the left or to the right. Depending on the action effect stimulus, the inner barrel will either follow the rotation direction of the outer barrel (non-inverse condition) or go in the opposite direction (inverse condition).

We recorded simultaneously in the dorsal premotor cortex (PMd), primary motor cortex (M1) and parietal reach region (PRR). The latter only in animal L, as animal B's signal quality was insufficient.

Fig. 1A shows spike densities averaged across trials for each of the four conditions (Chapter 3, Methods) from example neurons. The vertical line at timepoint 0 indicates the Go-Cue, after which the monkeys are allowed to interact with the B-PRIME. Time before 0 is considered as the planning phase, in which the animals are provided with all information necessary to prepare the upcoming movement. We do not see any action effect related preparatory activity but mainly an arm related preparation (light blue and dark green vs dark green and light blue).

Animal L takes on average 1200ms to complete the first rotation (RT not excluded) whereas animal B needs around 1500ms. The example neurons show that during the first rotation we see a clear separation (light green and dark blue vs dark green and light blue) for arm rotation direction (physical action) especially in areas PMd and M1 across both animals. After the first rotation, this separation switches to either action effect encoding (light green and light blue vs dark green and dark blue) or to a mixed selectivity thus splitting in all four conditions. This is specifically evident in areas PMd and PRR. Surprisingly also in area M1 the tuning for physical action disappears.

Panel B and C present the results of a general linear model (GLM) with stepwise regression, which was trained on calculating the percentage of tuned neurons for either action effect

direction (Fig. 1B, purple), physical action (turquoise) or their combinations and interactions for the time epochs ‘baseline’, ‘first rotation’ and ‘second rotation’.

In area PRR for animal L (Fig.1B) we find 18% of neurons are tuned for physical action (predictable as block wise task design) and 1 % for action effect during the baseline period. During the first rotation, 42% of neurons are tuned for physical action, which is reduced during the second rotation to only 33%. During the second rotation we find additional tuned neurons with 11% tuned for effects only and 16% presenting a mixed selectivity for action effect and physical action. In area PMd in animal L (Fig.1C) we find 5% of neurons are tuned for physical action, 6% for action effects and 1% for physical action and action effect during baseline period. Once the rotation is initiated, we report 23% of neurons are tuned for physical action, 1% each for action effect and their combination. During the second rotation however we report 19% of neurons are tuned for physical action, 8% for action effect and 2% for their combination.

For animal B we find a similar trend. During baseline we report 23% of neurons are tuned for physical action and 1% for action effect. Once the first rotation starts, we see 50% of neurons are tuned for physical action, 5% for action effects and 3% for their combination. Interestingly during the second rotation this trend switches. 23% of neurons are tuned for physical action, 15% for action effects and 19% for action effect and physical action.

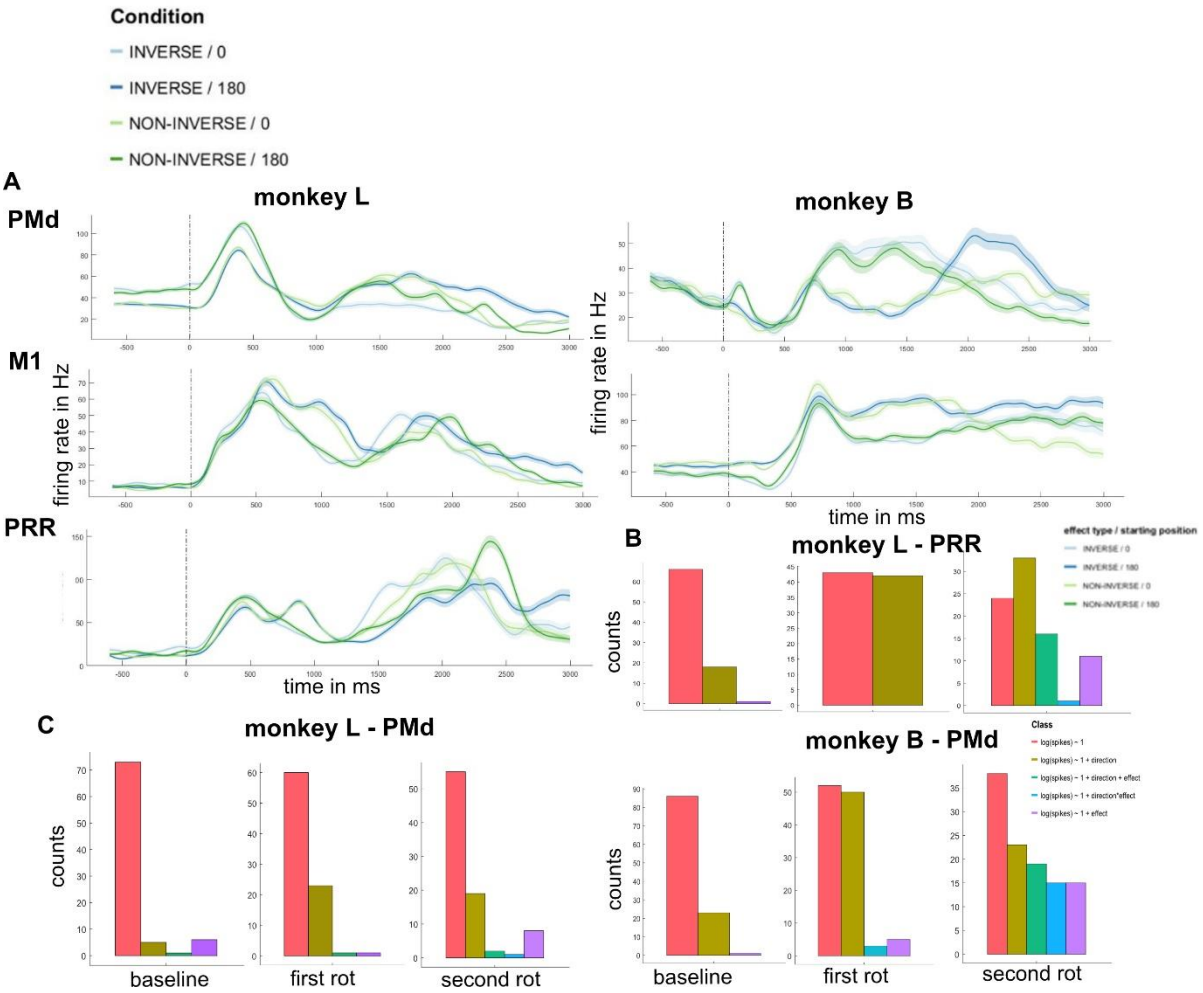

Figure 1: A. Averaged spike densities with standard error of mean across the four conditions for areas PMd and M1 in animal L and B and area PRR in animal L. B. We trained a general linear model (GLM) with stepwise regression to calculate the percentage of tuned neurons for action effects, physical movement, combination or interaction of these. The model was applied on the epochs 'baseline', 'planning' and 'first rotation' and 'second rotation'.

Next we performed population analysis. First we calculated the principal components (PC) of each brain area per monkey separately for the time period of 500 ms before until 3000 ms after Go-cue (vertical line). In Fig.2 we present the second and third principle component since the first was mostly modulated by the trial structure. The vertical line at timepoint 0 again indicates the Go-Cue, after which the monkeys are allowed to interact with the B-PRIME The second and third PC and the third PC in animal L and B respectively show a separation in action effects (light green and blue vs dark green and blue) in PMd and PRR but only after the first rotation was completed (1200 and 1500ms after Go cue). Surprisingly, in area M1 we see a similar behavior for animal L for the presented session, but not in animal B.

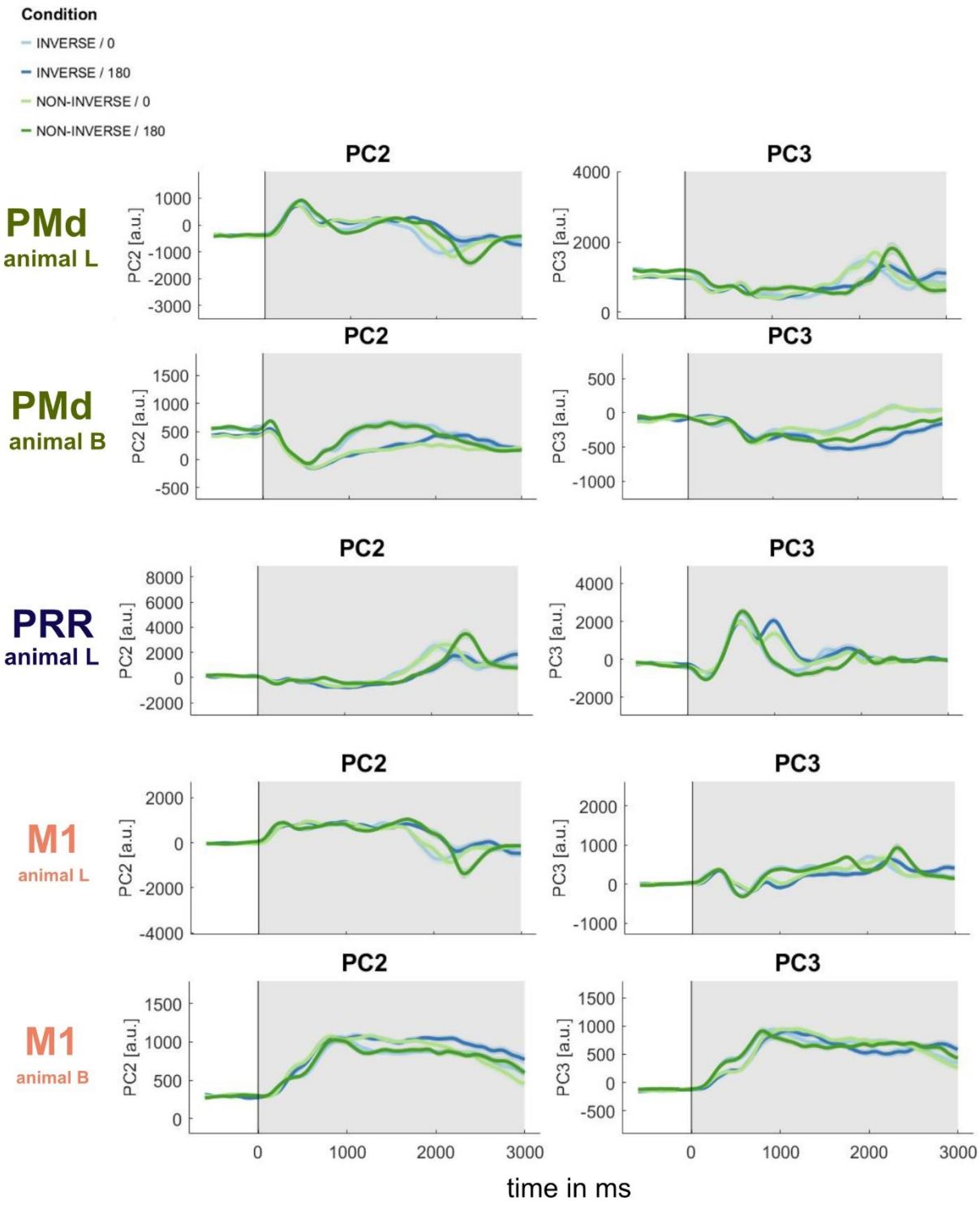

Figure 2: Second and third principal components for areas PMd, M1 in both animals and PRR in animal L aligned to Go-cue.As the single unit activity demonstrates neurons with mixed selectivity, we wanted to disentangle the signal by applying a demixed PCA. Fig. 3 shows a simplified version of the dPCA results for better overview. Each panel (A to C) consists of two rows. The upper row shows components

with the highest variance explained based on the action effect and the lower panel shows components with the highest variance explained based on the physical movement direction. The bar plot presents each of the total 20 components and is color-coded by whether it explains the variance based on task irrelevant components (gray), action effect (turquoise), physical movement (yellow) or interactions between effect and physical movement (red). Our preliminary dPCA results suggest that the individual components could be demixed well for animal B (bar plots mostly in one color) whereas in animal L the demixing does not results in single components explaining the variance based on one of the tested task parameters.

We report in total around 20.4 variance is explained by action effect in PMd in monkey L and 5.3% in monkey B in this example session. 10.7 % and 11.3% is explained based on the physical action in monkey L and b respectively. In area M1 we find 7.2% and 2% of variance explained based on action effect and 9% and 4% based on physical action for monkey L and B, respectively. 8.9% of variance is explained based on action effect in area PRR and 9.1% based on physical action. Interestingly, the time course of variance explained based on action effects is similar across both animals. The variance can only be explained starting after 1200ms after go cue (vertical line) so only after the first rotation is completed.

We next calculated the averaged explained variance based on action effects and physical action and compared these within the epochs during first and during second rotation (Fig.3D). We report the median of explained variance based on the physical action during the first rotation is 19% and during the second rotation is 18 % across 14 sessions with monkey L. The variance explained across sessions during the first rotation is 10% and significantly increased with 23% during the second rotation ($p<0.0001$, Wilcoxon Rank sum test). For monkey B we report the median of explained variance based on the physical action at 31% during the first and at 40% during the second rotation. The explained variance based on action effects is 2% during the first and 19 % during the second rotation. In summary, we see a similar trend of increase in explained variance based on action effect during the second rotation. However, this effect is not significant. We calculated the average across 6 sessions for monkey B. Including additional sessions will be required before a final observation can be made.

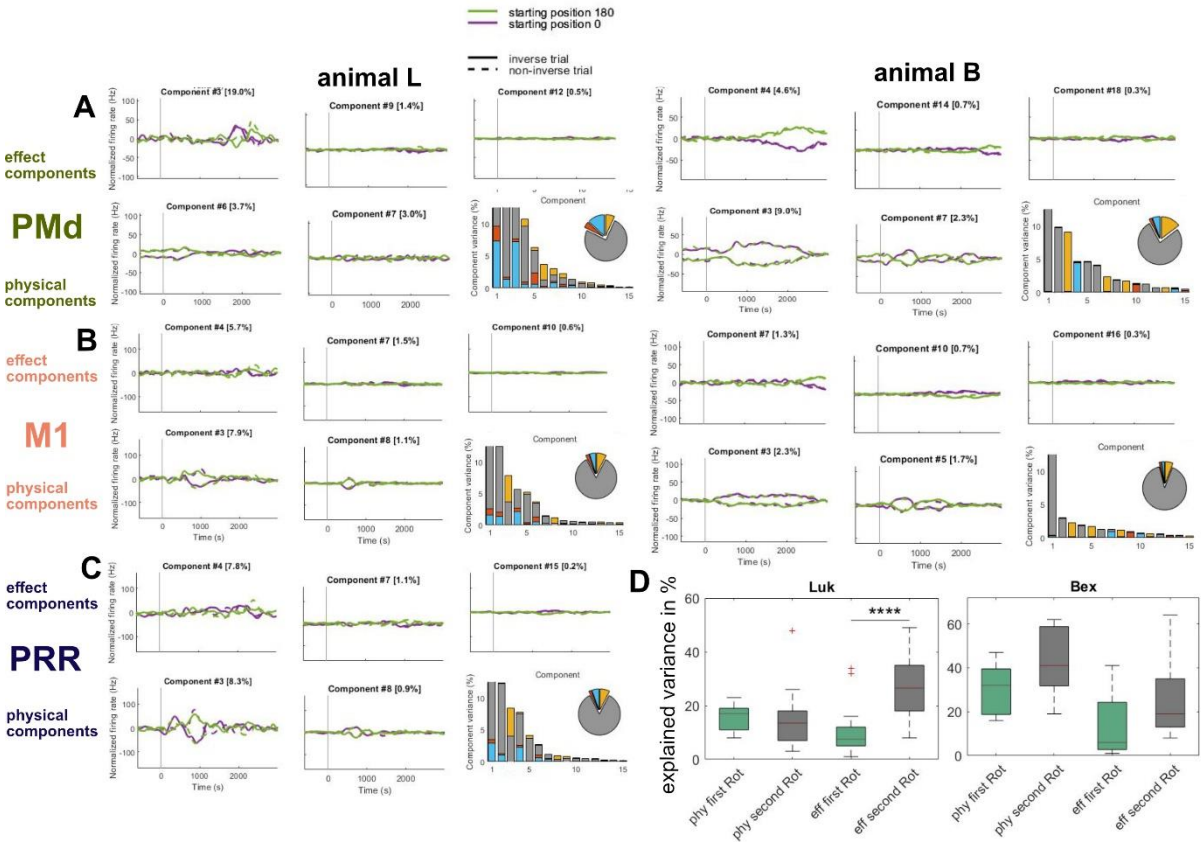

Figure 3: *Simplified dPCA results of AEA task. Panel A to C depict the demixed PCA components, which explain the variance based on action effects (upper panel) and physical arm movement direction (lower panel) for the time window 500 before go cue until 3000ms after. The bar and pie charts provide an overview of the explained variance by components. Panel D summarizes the percentage of explained variance based on action effect or based on physical arm movement in monkey L (left panel) across 14 and in monkey B (right panel) across 6 sessions.*

The dPCA results for animal B suggest, the physical encoding is present throughout the rotation time (first and second rotation of the outer barrel) but the encoding of the action effects, which is the rotation direction of the inner barrel, becomes only evident during the second rotation. As these results are not consistent between both animals at the current state of our analysis, we next we trained a SVM decoder to investigate at which stage the encoding of action effects and for the physical arm movement is present during both rotations.

For this, we first trained the decoder on the physical action of the non-inverse condition. We then test this decoder on the inverse conditions.

We expect the decoder to perform below chance level during the first rotation, as the direction of arm movement is the opposite between the inverse and non-inverse conditions. The performance should stay below chance level for the second rotation, if the neural activity for arm movement direction is the determining one during the second rotation. If however, neural

activity is mainly correlated with the action effect direction, the performance during the second rotation should increase above chance level, as the action effect directions are identical in the inverse and non-inverse conditions.

Our results (Fig.4) for one session of each monkey demonstrates the decoders performance drops below chance level during the first rotation but increased to up to 70% for animal L and 75% for animal B during the second rotation.

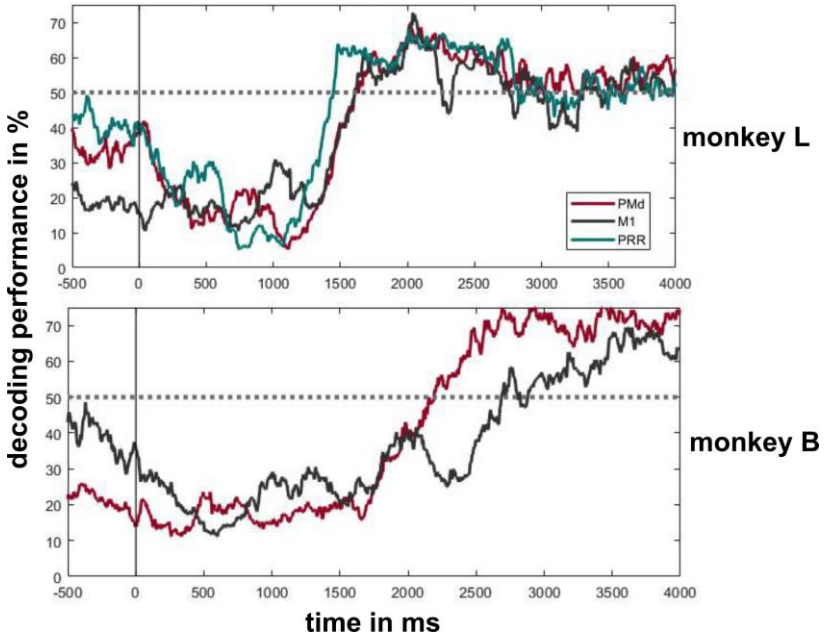

Figure 4: Decoding performance of trans-conditional decoding trained on physical action of non-inverse trial types and tested on action effects of inverse trial types.

S1.4 Discussion

We implemented an ecologically more relevant version of the previously developed AEA paradigm (Ahmed et al., *Chapter 3*). Our preliminary findings suggest that monkeys adopt a probe-before-you-know paradigm when interacting with a haptic device. Both monkeys waited until the Go-cue to then adjust their arm movements such that the entire movement becomes a 2-rotational arm reach even though it was not demanded by task design. During the first and shorter rotation the monkeys act accordingly to their egocentric reference frame as they encode and prepare the physical action. The egocentric reference frame (body-centered) is considered as the 'default' reference frame when we interact with our environment (Wang et

al., 2016, Tversky & Hard, 2009). Only when demanded by the task, we switch to an allocentric reference frame (world-centered) as it is associated with potentially increased cognitive demand (Epley et al., 2004), in our case the reference frame of action effects. Both monkeys do not prepare their movements in an allocentric reference frame prior to execution as observed in the conventional setting (Ahmed et al., Chapter 3) but we see preparatory activity across all brain areas of the frontoparietal reach network for the physical action. As monkey B was familiar with the AEA paradigm and presented a different strategy in the conventional setup, we can conclude the differences are not individual-specific but rather task-specific.

New solving strategy or simply ignoring the stimuli?

Based on these preliminary results one possible interpretation can be that the monkeys simply ignoring the stimuli. We exclude this interpretation based on three arguments. First, we observed when the monkeys miscalculated their arm movement and rotated the B-PRIME more than usual, the monkeys present a freezing behavior as we would expect from a mismatch in intended behavior. They do not complete the taskdespite having the reward pocket right in front of them, which led to error trials instead of simply completing the trial by reaching inside the reward pocket.

Second, we adjusted the translational gain between the outer and inner barrel, which means a shorter rotation of the outer barrel results in a bigger rotation in the inner barrel. Both monkeys adjust their arm movement such that even in trials, in which a short arm movement would be sufficient to rotate the barrel entirely, they still make a two-step rotation.

Third, with animal L we implemented the task such that instead of an LED cue as the spatial cue, which indicated the relevant reward pocket, we physically decentralize the inner barrel making the relevant reward pocket visible but not reachable. This decentralization comes along with a sound, which makes the indication of the activated reward pocket difficult to miss. From the observed monkey behavior, we can conclude this was a highly relevant. Again, by adopting his arm movements such that a 2-step rotation was needed.

Implication of differences in strategies in conventional versus free behaviors

In this study we implemented the AEA task in both experimental settings, conventional setting with chair-seated, eye- and head-fixated monkey and in a less constrained environment, in which the monkey could move with his entire body without any head- or eye-fixation. Additionally, we recorded from one identical animal in both setups for maximal comparison. Our results nevertheless suggest the monkeys apply a different strategy when placed in a ecologically relevant and less constrained environment. This finding is very much in line with

recent studies (Aflalo et al., 2007; Eisenreich et al., 2019; Yin et al., 2018). If we focus on the latest two studies, Yin and colleagues (2018) presented that we find navigational related neural signals in the primary and premotor cortex, which are very similar to the ones found in hippocampus; an area highly related to navigation. Eisenreich and colleagues (2019) performed a similar comparison study to ours and found that when monkeys are playing a foraging game in a conventional setup, in which they have to decide when to leave the current patch in order to forage in the next one. The monkeys present a risk-affine behavior, which has been shown in other studies conducted in conventional setups (Strait et al., 2004; Heilbronner and Hayden,2013). When the same monkeys are placed in a free experimental setup, their behavior changes to risk-adversity, the opposite of what has been found before.

Therefore, we can interpret the preliminary results with caution suggesting that in a dynamic, more complex environment monkeys tend to optimize their cognitive demand and prefer to rather act on the fly than planning beforehand, which is a luxury provided in a more restrained environment.

This hypothesis needs to be investigated in detail in future studies. While conventional experimental setups provide us excellent opportunities to understand basic concepts of the brain and therefor are extremely valuable, efforts towards –by now technologically possible - less constrained environments should be made in an attempt to understand the underlying mechanisms of action planning and decision-making..

Refinements

As this study presents only preliminary results, in the next step we will analyze the video based recorded data with markerless motion capture to identify behavioral parameters, which can help to understand the provided concepts in detail. Additionally, more recorded sessions should be included and tested systematically.

S1.5 Methods

Experimental setting

Task design

We designed a novel AEA task, which allows to dissociate between the action effect direction (visual consequence direction), visual goal (goal location) and motor goal (endpoint of physical arm movement). Details can be read in Ahmed et al. (Chapter 3). We developed a novel interactive device called the B-PRIME which allows interactions beyond touches on a

touchscreen (Ahmed et al., Chapter 5). In summary, the monkey had to rotate the outer barrel of the B PRIME in a given direction such that one of the two relevant reward pockets face the monkey. Then the monkey reaches inside the reward pocket similar to behaviors observed in the wild, which activates a reward system (Fig.5).

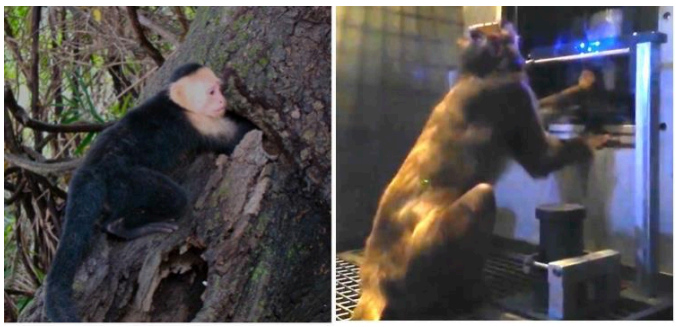

Figure 5: Monkeys interacting with their environment; left: searching for food in a tree cavitiy, right: placing the hand in the B PRIME cavity (reward pocket) to get fluid reward.

We mounted the B PRIME in the ReachCage (Berger et al., 2020), which enables us to record video data and wireless neural data (Fig.6).

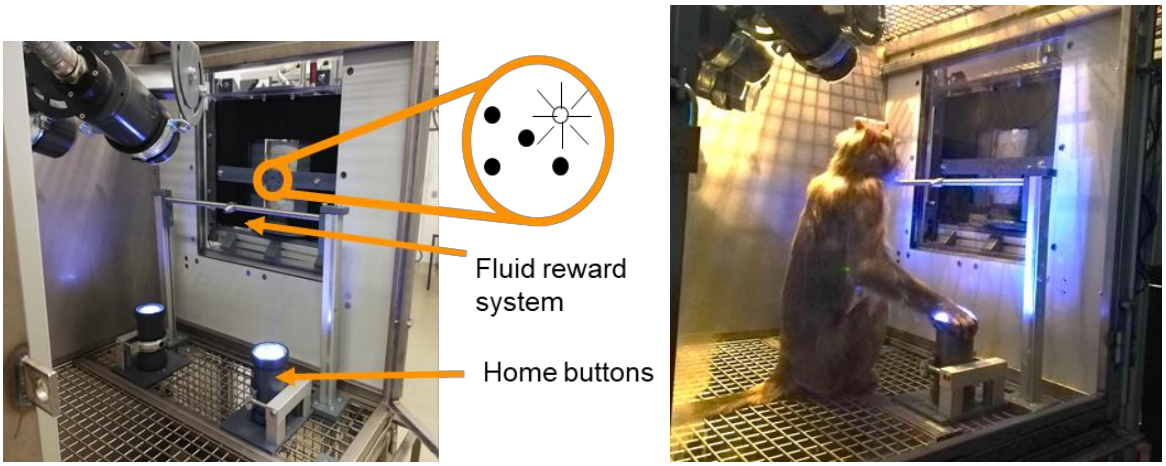

Figure 6: B PRIME mounted in the Reachcage. Left: Home buttons, which need to be fixated with both hand to initialize the trial. 5 LEDs on the B PRIME indicate different trial stages and conditions, a mouthpiece for fluid reward after each successful trial. Right. Monkey L initiating a trial.

Task timeline

The monkeys initiated the trials by placing both their hand onto the two home buttons (Fig.6, 7), which have a proximity sensor and therefore can detect the hands. Then the action effect was indicated either by turning all LEDs on in green (non-inverse) or in blue (inverse) for 500ms.

The LEDs were turned off for 600 to 900ms and then turned on again in white. Either the two left LEDs lid up indicating the starting position of the relevant reward pocket is on the left or the two right ones indicating the rewarded pocket is on the right. All LEDs tuned off again for 1000 to 1500ms in which the monkey could prepare his upcoming activity. If the monkey looked away during the time period,in which the stimuli are provided, the trial was aborted by the experimentor.A yellow central LED lid up and presented the Go-cue, after which the monkey was free to rotate the outer barrel in the correct direction. Rotations in the wrong directions aborted the trial. We trained the monkeys on this task in a block wise manner with block size of 10 hits.

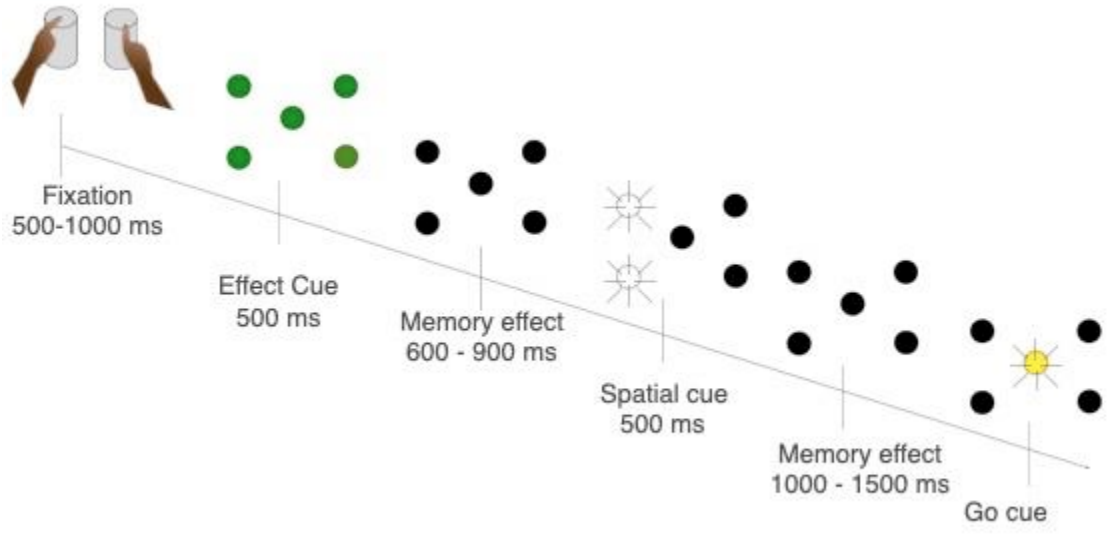

Figure 7: Complete timeline of one trial.

Animals and Surgery

We trained two adult male rhesus macaques (monkey L 8.3 kg and monkey B 16 kg) on the AEA task using the B PRIME. Monkey L had prior experience with a variety of tasks in previous projects but was naïve to the AEA paradigm and the B PRIME. Monkey B had experience with the AEA paradigm in a conventional setting (Chapter 3) but was naïve to the B PRIME. Both animals were implanted with custom designed and fitted implants (Berger et al., 2020; Ahmed et al., 2022). Monkey L was implanted on the right hemisphere in areas PMd, M1 and PRR with 2 floating microwire arrays, 32 electrodes each (250 micro electrode separation, impedance 0.1 to 0.4 MOhm, Microprobes for LifeScience, Gaithersburg, Maryland, USA). Monkey B was

implanted on the left hemisphere in areas PMd, M1, PRR and S1 with 2 floating microwire arrays, 32 electrodes each. Further details are provided in Chapter 3.

Neural data analysis

Data acquisition

We recorded from all six 32-channel arrays simultaneously using digital wireless Exilis Blackrock headstages (Blackrock Microsystems LLC, Salt Lake City, USA) to record from two arrays per brain area (PMd, M1, PRR) per session with a sampling rate of 30kHz. The single was digitalized at 16-bit amplitude and wirelessly transmitted to the signal processor (Cereplex Direct) at 3.05 and 3.375GHz. Details have been described previously in Berger et al. (2020).

Single unit analysis

We recorded in total 31 sessions with monkey L and 19 sessions with monkey B.For single unit analysis we spike sorted 1 session of monkey L and B using the Plexon Offline Spikesorter (Plexon, Inc, Dallas, Texas, USA). Further details are provided in *Chapter 3*.

Population analysis

PCA and dPCA were described in *Chapter 3* and applied identically except for the time course. We calculated the principle components of PCA and dPCA for the time epoch 500ms before (planning period, in which the monkey can prepare his upcoming action but is not allowed to execute it) until 3000ms after Go cue (movement period, in which both monkeys have completed both rotations of the barrel).

SVM decoding

In order to test if physical movement or action effect is encoded in the brain areas throughout the time course of a trial, we used support vector machine (SVM) to classify the corresponding direction (i.e. left or right for physical movement or action effects) using the Scikit-learn module (Pedregosa et al., 2011). In the process, SMVs find a hyperplane that maximizes the margin between data points of different categories for accurate classification.

We used neural firing rates as input. To determine the decoding performance over the time course of a trial, we selected firing rates from a sliding window of 100 ms that was shifted by 10 ms and trained individual SVMs for each interval. Accuracy was computed by dividing number of correctly classified directions by number of all trials in the test set. To validate classification results we performed 10-fold cross-validation for each trained model.

References

Aflalo, T.N, Graziano, S.A. (2007). Relationship between Unconstrained Arm Movements and Single-Neuron Firing in the Macaque Motor Cortex. *Journal of Neuroscience*, 27(11), 2760-2780. doi: 10.1523/JNEUROSCI.3147-06.2007.

Andersen, R. A., Asanuma, C., Essick, G., and Siegel, R. M. (1990). Corticocortical connections of anatomically and physiologically defined subdivisions within the inferior parietal lobule. *Journal of Comparative Neurology*, 296(1):65–113. doi: 10.1002/cne.902960106.

Berger M, Agha NS & Gail A (2020) Wireless recording from unrestrained monkeys reveals motor goal encoding beyond immediate reach in frontoparietal cortex. *eLife* 9:e51322. doi: 10.7554/eLife.51322.

Colby, C. L. and Duhamel, J. R. (1991). Heterogeneity of extrastriate visual areas and multiple parietal areas in the macaque monkey. *Neuropsychologia*, 29(6):517–537. doi: 10.1016/0028-3932(91)90008-v.

Collinger, J.L., Wodlinger, B., Downey, J.E., Wang, W., Tyler-Kabara, E.C., Weber, D.J., McMorland, A.J.C., Velliste, M., Boninger, M.L., Schwartz, A.B.(2013). High-performance neuroprosthetic control by an individual with tetraplegia. *Lancet*. 381(9866), 557–564. doi: 10.1016/S0140-6736(12)61816-9.

Eisenreich, B.R., Hayden, B.Y., & Zimmermann, J. Macaques are risk-averse in a freely moving foraging task. *Sci Rep* 9, 15091 (2019). doi: 10.1038/s41598-019-51442-z

Epley, N., Morewedge, C. K., & Keysar, B. (2004). Perspective taking in children and adults: Equivalent egocentrism but differential correction. *Journal of Experimental Social Psychology*, 40(6), 760–768. doi: 10.1016/j.jesp.2004.02.002.

Felleman, D. J. and Van Essen, D. C. (1991). Distributed hierachical processing in the primate cerebral cortex. *Cerebral Cortex*, 1(1):1–47. doi: 0.1093/cercor/1.1.1-a.

Gail, A., & Andersen, R. A. (2006). Neural dynamics in monkey parietal reach region reflect context-specific sensorimotor transformations. *Journal of Neuroscience*, 26(37), 9376-9384.doi: 10.1523/JNEUROSCI.1570-06.2006

Georgopoulos, A. P., Kalaska, J. F., Caminiti, R., & Massey, J. T. (1982). On the relations between the direction of two-dimensional arm movements and cell discharge in primate motor cortex. *Journal of Neuroscience*, 2(11), 1527-1537. doi: 10.1523/JNEUROSCI.02-11-01527.1982

Georgopoulos, A. P., Schwartz, A. B., & Kettner, R. E. (1986). Neuronal population coding of movement direction. *Science*, 233(4771), 1416-1419. doi: 10.1126/science.3749885

Gilja, V., Nuyujukian, P., Chestek, C.A., Cunningham, J.P., Yu, B.M., Fan, J.M., Churchland, M.M., Kaufman, M.T., Kao, J.C., Ryu, S.I., Shenoy, K.V. (2012). A high-performance neural prosthesis enabled by control algorithm design. *Nat. Neurosci.* 15(12), 1752–1757. doi: 10.1038/nn.3265.

Graziano, M. S. A. and Cooke, D. F. (2006). Parieto-frontal interactions, personal space, and defensive behavior. *Neuropsychologia*, 44(13):2621–2635. doi: 10.1016/j.neuropsychologia.2005.09.009.

Heilbronner, S. R. & Hayden, B. Y. (2013). Contextual factors explain risk-seeking preferences in rhesus monkeys*. Front. Neurosci*. 7, 1–7. doi: 10.3389/fnins.2013.00007.

Hochberg, L.R., Bacher, D., Jarosiewicz, B., Masse, N.Y., Simeral, J.D., Vogel, J., Haddadin, S., Liu, J., Cash, S.S., Smagt, P.V.D., Donoghue, J.P., van der Smagt, P. (2012). Reach and grasp by people with tetraplegia using a neurally controlled robotic arm. *Nature*. 485(7398), 1–17. doi: 10.1038/nature11076.

Ifft, P.J., Shokur, S., Li, Z., Lebedev, M.A., Nicolelis, M.A. (2013). A brain-machine interface enables bimanual arm movements in monkeys. *Sci. Transl. Med*. 5(210), 210ra154. doi: 10.1126/scitranslmed.3006159.

Kalaska, J. F., Caminiti, R. & Georgopoulos, A. P. (1983). Cortical mechanisms related to the direction of two-dimensional arm movements: relations in parietal area 5 and comparison with motor cortex. *Experimental Brain Research*, 51(2), 247-260.doi: 10.1007/BF00237200.

Manea, A., Zilvestand, A., Hayden, B., Zimmermann, J (2023). Neural timescales reflect behavioral demands in freely moving rhesus macaques. *biorxiv*. doi: 10.1101/2023.03.27.534470.

Mao D, Avila E, Caziot C, Laurens J, Dickman JD & Angelaki DE (2021) Spatial modulation of hippocampal activity in freely moving macaques. *Neuron* 109(21): 3521-3534. doi: 10.1016/j.neuron.2021.09.032.

Nikolaev, A. R., Ziessler, M., Dimova, K., & van Leeuwen, C. (2008). Anticipated action consequences as a nexus between action and perception: evidence from event-related potentials. *Biological Psychology*, *78*(1), 53-65.doi: 10.1016/j.biopsycho.2007.12.010.

Paelecke, M., & Kunde, W. (2007). Action-effect codes in and before the central bottleneck: evidence from the psychological refractory period paradigm. *Journal of Experimental Psychology: Human Perception and Performance*, *33*(3), 627. doi: 10.1037/0096-1523.33.3.627.

Pandarinath, C., Ames, K.C., Russo, A.A., Farshchian, A., Miller, L.E., Dyer, E.L., Kao, J.C. (2018). Latent factors and dynamics in motor cortex and their application to brain-machine interfaces. *J. Neurosci.* 38 (44), 9390–9401. doi: 10.1523/JNEUROSCI.1669-18.2018.

Pedregosa, F., Varoquaux, G., Gramfort, A., Michel, V., Thirion, B., Grisel, O., Blondel, M., Prettenhofer, P., Weiss, R., Dubourg, V., et al. (2011). Scikit-learn: Machine Learning in Python. J. Mach. Learn. Res. 12, 2825−2830.

Pfister, R., Kiesel, A. & Hoffmann, J.(2011) Learning at any rate: action–effect learning for stimulus-based actions. *Psychological Research* 75, 61–65. doi: 10.1007/s00426-010-0288-1

Pilacinski, A., Wallscheid, M., & Lindner, A. (2018). Human posterior parietal and dorsal premotor cortex encode the visual properties of an upcoming action. *PloS one*, 13(10), e0198051. doi: 10.1371/journal.pone.0198051

Rizzolatti, G. and Luppino, G. (2001). The cortical motor system. *Neuron*, 31(6):889–901. doi: 10.1016/s0896-6273(01)00423-8.

Rossetti, I., Romano, D., Florio, V., Doria, S., Nistico, V., Conca, A., Mencacci, C., Maravita, A. (2020). Defective Embodiment of Alien Hand Uncovers Altered Sensorimotor Integration in Schizophrenia. *Schizophrenia Bulletin*, 46 (2), 294–302. doi: 10.1093/schbul/sbz050.

Sleezer, B. J., Castagno, M. D. & Hayden, B. Y. Rule encoding in orbitofrontal cortex and striatum guides selection. *J. Neurosci*. doi: 10.1523/JNEUROSCI.1766-16.2016.

Stock, A., Stock, C. A short history of ideo-motor action. *Psychological Research* 68, 176–188 (2004). doi: 10.1007/s00426-003-0154-5.

Strait, C. E., Blanchard, T. C. & Hayden, B. Y. (2014). Reward value comparison via mutual inhibition in ventromedial prefrontal cortex. *Neuron* 82, 1357–1366. doi: .1016/j.neuron.2014.04.032.

Testard, C., Tremblay, S, Parodi, F., DiTullio, R.W., Acevedo-Ithier, A. (2023). Neural signatures of natural behavior in socializing macaques. *biorxviv*. doi: 10.1101/2023.07.05.547833.

Tversky, B., & Hard, B. M. (2009). Embodied and disembodied cognition: Spatial perspective-taking. *Cognition*, 110(1), 124–129. doi: 10.1016/j.cognition.2008.10.008

Uhmann, L., Pazen, M., van Kemenade, B. M., Kircher, T., Straube, B.(2021). Neural Correlates of Self-other Distinction in Patients with Schizophrenia Spectrum Disorders: The Roles of Agency and Hand Identity. *Schizophrenia Bulletin*, Volume 47 (5), 1399–1408. doi: 10.1093/schbul/sbaa186.

Voloh, B., Maisson, D., Cervera, RL., Conover, I., Zambre, M., Hayden, B., Zimmermann, J (2022). Prefrontal control of actions in freely moving macaques. *bioRxiv* 2022.10.26.513892; doi: 10.1101/2022.10.26.513892.

Wang, H., Liu, N., Zou, G. (2016) et al. The Simon effect based on the egocentric and allocentric reference frame. *Atten Percept Psychophys* 78, 427–436. doi: 10.3758/s13414-015-1032-0.

Wang, M. Z. & Hayden, B. Y. (2017) Reactivation of associative structure specific outcome responses during prospective evaluation in reward-based choices. *Nat. Commun*. 8, 1–13. doi: 10.1038/ncomms15821.

Yin, A., Tseng, P.H., Rajangam, S. et al. Place Cell-Like Activity in the Primary Sensorimotor and Premotor Cortex During Monkey Whole-Body Navigation. *Sci Rep* 8, 9184 (2018). doi: 10.1038/s41598-018-27472-4.

Zhang, M., Barash, S. Neuronal switching of sensorimotor transformations for antisaccades. *Nature* 408, 971–975 (2000). doi: 10.1038/35050097.

Ziessler, M., & Nattkemper, D. (2011). The temporal dynamics of effect anticipation in course of action planning. *Quarterly Journal of Experimental Psychology*, *64*(7), 1305-1326. doi:10.1080/17470218.2011.553067.

Ziessler, M., Nattkemper, D. & Frensch, P.A. The role of anticipation and intention in the learning of effects of self-performed actions. *Psychological Research* 68, 163–175 (2004). doi: 10.1007/s00426-003-0153-6.

Ziessler, M., Nattkemper, D., & Vogt, S. (2012). The activation of effect codes in response preparation: new evidence from an indirect priming paradigm. *Frontiers in psychology*, *3*, 585. doi: 10.3389/fpsyg.2012.00585.

Curriculum Vitae

Professional experience

Researcher, PhD Student
German Primate Center, Sensorimotor Group of Prof. Dr. Alexander Gail
Göttingen, Germany
August 2018 - December 2022

Project 1:
- Led the project “Constructing a novel environment for freely moving rhesus macaques," advancing current limitations of systems neuroscience.
- Designed and implemented an in-house camera acquisition system using Python for synchronised recordings.
- Seamlessly integrated diverse recording systems into laboratory software.
- Led a dynamic team of 7 scientists within a larger cross-functional team of 15 experts.
- Created scientific and technical content for grant applications securing €12.5 million in funding.

Project 2:
- Led the project “Neural correlates of action effect anticipation” and development of a novel paradigm for chair-seated rhesus macaques.
- Developed a specialised software solution for touchscreens and conducted data analysis with Matlab.
- Trained rhesus macaques and conducted 256-channel electrophysiological recordings.
- Wrote detailed written reports of research findings and conclusions

Project 3:
- Led research, development, and construction of an innovative haptic device for freely moving rhesus macaques
- Designed and programmed an innovative task for a European project with €4.2 million in funding.
- Led an interdisciplinary team of 4, spanning various fields and skills.
- Trained rhesus macaques and conducted wireless neural recordings with 192 channels.
- Conducted data analysis and wrote detailed written reports of research findings and conclusions
- Created scientific and technical content for grant applications

Project 4:
- Part of the interdisciplinary and European project “Deep Movement Diagnostics (DeMoDiag)” developing computer vision-based diagnostic tools for movement disorders.
- Designed a modular experimental room with synchronised cameras for precise marker-less tracking.
- Conducted a pilot study involving 13 human subjects validating the diagnostic tools.
- Utilised Python-based machine learning algorithms for data analysis.
- Conducted data analysis and wrote detailed written reports of research findings and conclusions
- Created scientific and technical content for grant applications

Internship
German Primate Center, Sensorimotor Group of Prof. Dr. Alexander Gail
Göttingen, Germany
October 2017 - August 2018

- Developed a novel method for custom-fitting and designing cranial implants used in systems neuroscience.
- Created an open-source pipeline for custom design and fitting of implants.
- Published research in a peer-reviewed journal and provided a comprehensive GitHub repository.

Quality and Project Manager
H+H Maslanka
Tuttlingen, Germany
March 2015 - September 2015

- Conducted quality assessment and improvement for process engineering methods.
- Gained hands-on experience in precision mechanics, soldering, and lathe work.
- Executed endurance tests and analysed results for endoscope components.
- Conducted research and testing of novel materials for endoscopy quality improvement.

Project Manager
Karl Storz Endoscopy
Tuttlingen, Germany
September 2013 - February 2014

- Conducted market analysis for competitive products
- Designed and executed experiments using novel materials.
- Analysed data and wrote comprehensive reports

Product Manager
Karl Storz Endoscopy
Schaffhausen, Switzerland
March 2013 - September 2013

- Developed an application tip for a holmium laser light guide for use in Otorhinolaryngology.
- Designed and executed experiments using novel materials.
- Analysed data and wrote comprehensive reports

Education

PhD Candidate
German Primate Center, Sensorimotor Group of Prof. Dr. Alexander Gail
Göttingen, Germany
August 2018 - December 2022

- Degree: Dr. rer. nat.
- Thesis Title: "Neural correlates of action effect anticipation - towards ecologically more relevant paradigms."

M.Sc. in Neuroscience
University of Oldenburg, Lab of Prof. Dr. Jutta Kretzberg
Oldenburg, Germany
October 2015 - September 2017

- Thesis Title: "Intracellular Recordings and Hodgkin-Huxley Model simulation of leech neurons."

B.Sc. in Medical Engineering
Hochschule Furtwangen
Villingen-Schwenningen, Germany
March 2011 - February 2015

- Degree: Ing.(FH)
- Thesis Title: "Development of an application tip for a holmium laser light guide for applications in Otorhinolaryngology."

Computer Skills

- Matlab: Excellent
- Python: Good
- SciLab: Good
- C++: Basic knowledge
- Arduino: Excellent
- Microsoft Office: Excellent
- Fusion 360: Excellent
- Rhino: Very good
- SolidWorks: Very good
- ProEngineer: Basic knowledge

Languages

- English: Fluent in speaking and writing (C1)
- German: Fluent in speaking and writing (Native language)
- Urdu: Fluent in speaking (Native language)
- Hindi: Fluent in speaking
- Italian: Level A2

Awards

- DPZ “Promotionspreis 2022” for the best PhD thesis in 2022, Göttingen, Germany
- Young Investigator Award at Neurizons Conference, Göttingen, Germany

Extracurricular Activities*

- Chair of Organization Team of the Women Career and Networks Symposium
- Team member of sub-team Finances of Women Careers and Networks Symposium
- Participant of the Margaret-Maltby Mentoring Program
- PhD Representative at the DPZ
- Member of Leibniz PhD Network

- Member of GGNB Times
- Co-Chair of Neuroscience Student Body Council at the University of Oldenburg
- Member of the Admission Committee of Master's Program 'Neuroscience' at the University of Oldenburg
- Member of Career Day Neuroscience organization team at the University of Oldenburg
- Member of Department Council at University of Oldenburg
- Member of the Faculty Council at Hochschule Furtwangen
- Member of Buddy Program at Hochschule Furtwangen
- Participation at Dundee Youth Festival
- Teaching Urban Dance

Invited and conference Talks

- Various invited talks and conference presentations at international events *

Outreach / Science Communication

- Active involvement in public engagement and science communication efforts*

Publications

- Authored papers and conference posters in various scientific journals and conferences*

**(details available on webpage zurnaahmed.com or upon request)*